Univerzita Karlova

Přírodovědecká fakulta

Studijní program: Biologie

Studijní obor: Imunologie

Bc. Alois Zdrha

Vliv endosymbiontů na složení a vlastnosti exosomů *Trichomonas vaginalis*

Effect of endosymbionts on composition and properties of *Trichomonas vaginalis* exosomes

Typ závěrečné práce:

Diplomová práce

Vedoucí práce/Školitel:

prof. RNDr. Jan Tachezy, Ph.D.

Praha, 2022

Prohlášení

Prohlašuji, že jsem závěrečnou práci zpracoval samostatně a že jsem uvedl všechny použité informační zdroje a literaturu. Tato práce ani její podstatná část nebyla předložena k získání jiného nebo stejného akademického titulu.

V Praze, 11. 8. 2022

.....

Alois Zdrha

Poděkování

Zejména bych chtěl poděkovat svému školiteli prof. RNDr. Janu Tachezymu, Ph.D. za jeho čas, vedení a výbornou zpětnou vazbu. Speciálně bych chtěl poděkovat Petru Radovi za izolaci exosomů, Ravimu Kumarovi Narayanasamymu za provedení PCR, Tamaře Smutné za pomoc s detekcí cytokinů, Marianovi Novotnému za pomoc při modelování proteinů a Martinovi Zoltnerovi, Karlu Harantovi a Vojtěchovi Žárskému za pomoc s analýzou proteomických dat. Také děkuji svým kolegům z laboratoře Zdeňku Vernerovi, Nadine Zimmann a Ivanu Hrdému za cenné rady a podporu.

Acronyms

AGO	argonaute
AP	activator protein
ATF	activating transcription factor
BP	biological process
CC	cellular compartment
CCL	C-C motive ligand
COG	cluster of orthologous group
CP	cysteine proteases
CST	community state type
ERAP	endoplasmic reticulum aminopeptidase
ESCRT	endosomal sorting complex required for transport
EV	extracellular vesicle
FPLC	fast protein liquid chromatography
GM-CSF	granulocyte macrophage-colony stimulating factor
GO	gene ontology
GPR	G protein-coupled receptor
HCV	hepatitis C virus
IL	interleukin
INF	interferon
LG	lipoglycans
LPS	lipopolysaccharide
LRV	leishmania virus
MF	molecular function
MIF	macrophage migration inhibitory factor
MP	metallopeptidase
MSA	multiple sequence alignment
MVB	multivesicular body
NET	neutrophil extracellular trap
OD	optical density
ORF	open reading frame
PBMC	peripheral blood mononuclear cell
PC	principle component
PCA	principle component analysis
PDGF-BB	platelet-derived growth factor-BB
PI3K	phosphatidylinositol 3-kinase
PRR	pathogen recognition receptor
RdRp	RNA dependent RNA polymerase
RIC	repair of iron centres
RISC	RNA-induced silencing complex
ROS	reactive oxygen species
rpm	reads per million
SHIP	SH2 domain-containing inositol 5'-phosphatase
SMAD	mothers against decapentaplegic homolog
SNARE	soluble NSF (N-ethylmaleimide-sensitive factor) attachment protein receptor
ST	Sucrose-Tris
STAT	signal transducer and activator of transcription
sTNF RI	soluble TNF receptor I
SYK	spleen tyrosine kinase
TLR	toll like receptor
TNF	tumour necrosis factor
tRF	tRNA fragment
Tsp	tetraspanin
TVV	*Trichomonas vaginalis* virus
TYM	tryptone-yeast extract-maltose
VEC	vaginal epithelial cell
VPS	vacuolar protein sorting-associated protein
2CMC	2'-C-methylcytidine
2CMA	2'-C-methyladenine

Abstrakt

Trichomonas vaginalis je parazit lidského reprodukčního systému a je původcem nejrozšířenější nevirové sexuálně přenosné nemoci trichomoniázy. Tato nemoc má většinou mírný průběh, ačkoli dokáže způsobit i závažné zdravotní komplikace. Průběh onemocnění je závislý na imunitním systému pacienta, mikrobiomu a virulenci parazita. Je však důležité, že virulence *T. vaginalis* je značně variabilní a je závislá na sekretovaných a povrchových molekulách. Mezi ně patří proteázy a adheziny, které mohou být sekretované v sekretomu nebo v extracelulární váčcích (EV). Dalšími potenciálními faktory virulence jsou: *Trichomonas vaginalis* virus (TVV) a *Mycoplasma hominis*. Ačkoliv se vlivem TVV na virulenci *T. vaginalis* zabývalo mnoho studií, vědci se dosud neshodli. Tato práce analyzuje vliv TVV na složení proteinů a RNA v exosomech a dopad TVV na sekreci cytokinů.

Klíčová slova

endosymbionti, dsRNA virus, TVV, exosomy, paraziti, *Trichomonas vaginalis*, bioinformatika

Abstract

Trichomonas vaginalis is a parasite of the human reproductive tract and the causative agent of trichomoniasis, the most spread non-viral sexually transmitted disease. Although trichomoniasis usually has mild symptoms, it can lead to serious adverse effects. The course of the disease is influenced by the host immune system, microbiome and virulence of the parasite. Importantly, the virulence of *T. vaginalis* is extremely variable, and it depends on secreted and surface molecules. Among these are proteases and adhesins, which can be secreted as part of the secretome or through extracellular vesicles (EVs). Further potential virulence factors are the endosymbionts of *T. vaginalis*: *Trichomonas vaginalis* virus (TVV) and *Mycoplasma hominis*. Although extensively studied, no consensus on whether TVV exacerbates trichomoniasis has been reached. The aim of this thesis is to analyse the effect of TVV on the protein and RNA exosomal cargo and to assess the cytokines induced by exosomes of TVV-positive *T. vaginalis*.

Key words

endosymbionts, dsRNA virus, TVV, exosome, parasite, *Trichomonas vaginalis*, bioinformatics

Contents

1. Introduction

Trichomonas vaginalis is the causative agent of trichomoniasis, a sexually transmitted disease of the human reproductive tract.[1] It afflicts both females and males, although to a different extent. Long-term chronic infection with no symptoms is the most common course of trichomoniasis in many individuals. Nonetheless, ∼30% of infected individuals develop symptoms. These symptom are usually mild but rare cases of trichomoniasis with severe symptoms also appear.[2] *T. vaginalis* infection is commonly cured by metronidazole, but resistant strains of *T. vaginalis* are on the rise.[3]

The hallmark of *T. vaginalis* infection is purulent discharge in women.[2] The inflammation caused by *T. vaginalis* is reflected by the secretion of interleukin 8 (IL-8) by vaginal epithelial cells (VECs). This secretion has been attributed to the sensing of *T. vaginalis* by toll-like receptors (TLRs) and *T. vaginalis* has been shown to modulate the IL-8 secretion by different mechanisms. IL-8 plays a crucial role in the immune reaction against *T. vaginalis* because it attracts neutrophils, which is the main cell type involved in *T. vaginalis* killing. Interestingly, many cytokines, which are produced during *T. vaginalis* infection, including IL-8, have been attributed not to the sensing of *T. vaginalis* per se, but to its endosymbionts: *Trichomonas vaginalis* virus (TVV) and *Mycoplasma hominis*. Nevertheless, the impact of these endosymbionts on clinical outcomes is still a matter of debate and no clear consensus has been reached.[2][3]

Due to the potent pro-inflammatory response to TVV, the virus has been considered one of the *T. vaginalis* virulence factors.[4] Other important factors of *T. vaginalis* virulence are adhesive molecules, proteases and extracellular vesicles (EVs). Adherence is critical for *T. vaginalis* survival in the vaginal tract, as it prevents the expulsion of *T. vaginalis* from the vaginal tract and enables contact-dependent host cell cytolysis. Its importance is shown by the redundancy of different kinds of adherent molecules ranging from lipoglycans (LG) to distinct families of adhesive proteins, exemplified by the BspA family.[2][5] Similarly, many paralogues of different kinds of proteases are found in *T. vaginalis*, for instance, cysteine proteases (CPs) have around ∼150 paralogues [5] and certain CPs are known to play a pivotal role in the *T. vaginalis* pathogenicity.[3]

Furthermore, *T. vaginalis* releases two types of EVs: exosomes and ectosomes (microvesicles). The cargo of these EVs has been shown to contain both adhesive proteins (e.g. BspA) and peptidases (e.g. metallopeptidases (MPs)). Moreover, exosomes appear to be able to increase the adherence of low adherent strains of *T. vaginalis* and modulate the host immune response. Lately, EVs of *T. vaginalis* were found to carry a specific cargo of small RNAs.[3][5] Among those small RNA molecules are tRNA fragments, which are nowadays recognized as a means of host-pathogen interactions.[6]

It has been recently shown that TVV appears to modulate exosomal cargo and exosome-induced cytokine production.[7] Furthermore, it is well established from studies on different organisms that viruses are able to hijack the exosomal pathway for their own spreading.[8] In this work, we have decided to further analyse the effect of TVV on the *T. vaginalis* exosomal cargo and the exosome-induced cytokines in order to elucidate the role of TVV in *T. vaginalis* virulence. Testing several nucleoside analogs, we have discovered that 2'-C-methylcytidine (2CMC) is a potent inhibitor of the TVV RNA dependent RNA polymerases (RdRps).[9] Thus, we have derived TVV-positive and TVV-negative isogenic clone of *T. vaginalis*. Exosomes from these clones were purified and subjected to a proteomic analysis and sequencing of short RNA molecules. Lastly, the potential of the exosomes to elicit an immune response was tested in HaCaT cells through measurement of cytokine secretion.

2. *Trichomonas vaginalis*

T. vaginalis is an anaerobic protist, which causes trichomoniasis, the most prevalent curable non-viral sexually transmitted disease with a global prevalence of ∼5%.[1] Most cases of trichomoniasis in both males and females are asymptomatic. However, owing to the extreme variability in the virulence of different strains of *T. vaginalis* [10] and diverse reactions of hosts to *T. vaginalis* infection [11], cases of symptomatic infections also appear.[11][12][13] Over 75% of males infected with *T. vaginalis* do not typically exhibit any symptoms. Hence, they serve as asymptomatic carriers of the disease. Nonetheless, instances of urethritis and prostate inflammation occur.[2] In comparison to males, women suffer from symptomatic trichomoniasis in ∼50% of cases. The symptoms can be mild as, for instance, vaginal discharge or dysuria [13], but the infection can lead to severe adverse effects as well. Among those are pelvic inflammatory disease or adverse pregnancy outcomes. Moreover, the infection with *T. vaginalis* is associated with a higher risk of cervical cancer and HIV transmission. Metronidazole is the primary remedy used for trichomoniasis treatment, although the rising metronidazole resistance among different *T. vaginalis* strains is of great concern.[14]

During infection, *T. vaginalis* undergoes dramatic morphological changes. The infective form of *T. vaginalis* is a free swimming drop-like trofozoite with four anterior and one recurrent flagella.[15] When *T. vaginalis* comes into contact with host cells, it rapidly reorganizes its cytoskeleton and spreads over the host cells in an amoebic-like form.[16] Furthermore, *T. vaginalis* can also form clumps of parasites [17], whose function is unknown, and cysts-like structures (pseudocysts).[18] The pseudocysts can be induced by low pH [18] or iron depletion.[19] However, similarly to the clumps of parasites, their importance in *T. vaginalis* infection remains to be elucidated.

T. vaginalis infects the lower part of the woman reproductive tract. As such, it inevitably interacts with the local microbiome. The vaginal microbiome is clustered into five community state types (CST-I, -II, -III, -IV, -V). CST-I, -II, -III and -V are associated with more acidic pH as a result of the presence of lactobacilli. On the contrary, CST-IV is associated with higher pH due to the absence of lactobacillus species, the presence of anaerobic bacteria like *Gardnerella vaginalis* and *T. vaginalis*.[20] *T. vaginalis* may promote CST-IV by directly killing lactobacillus species [21], but CST-IV is also present without *T. vaginalis* infection.[20] The competitive relationship between *T. vaginalis* and lactobacillus species is further supported by the fact that lactobacillus species compete with *T. vaginalis* over VEC attachment unlike the anaerobic bacterial species, such as *G. vaginalis*.[22] Moreover, it has been shown that *Lactobacillus gasseri* is able to displace *T. vaginalis* from VECs in a contact-dependent manner using, among others, aggregation-promoting factors 2.[23] On the other hand, *T. vaginalis* together with

anaerobic bacteria, like the aforementioned *G. vaginalis*, disrupt the tight junctions between human ectocervical cells *in vitro* in a cumulative manner.[24] Furthermore, co-incubation of *G. vaginalis*, *T vaginalis* and ectocervical cells increases the ability of *T vaginalis* to attach to the ectocervical cells by 3 folds.[25] This suggests a delicate interplay between *T. vaginalis* and the vaginal microbiota, which can suppress or enhance *T. vaginalis* infection.

2.1 Immune reaction

Apart from the vaginal microbiome, *T. vaginalis* interacts with the host immune system. IL-8 was detected to be among the significantly elevated cytokines during *T. vaginalis* infection.[26][22] This cytokine stands out as an important cytokine in the *T. vaginalis* immune response. The reason is, that IL-8 attracts neutrophils, which are the major effector cells responsible for *T. vaginalis* killing. Neutrophils eliminate pathogens via phagocytosis or by releasing neutrophil extracellular traps (NETs).[27] *T. vaginalis* triggers the release of NETs in neutrophils [28], but its elimination was shown to be independent of NETs, since blocking of NETosis had no effect on *T. vaginalis* killing.[27] Similarly, phagocytosis does not play a role in *T. vaginalis* killing since neutrophils are much smaller than *T. vaginalis*, and, therefore, are unable to fully engulf it.[27] Instead, neutrophils seem to kill *T. vaginalis* within minutes by trogocytosis, which is a phenomenon in which a cell nibbles fragments from another cell in a contact-dependent manner. This trogocytic killing of *T. vaginalis* was shown to be dependent on opsonization and neutrophil serine proteases.[27]

Several other cytokines have been attributed to *T. vaginalis* infection. IL-17 and IL-22 have been found to be significantly increased in cervicovaginal lavage during *T. vaginalis* infection.[29] However, in another study of cervicovaginal lavage, IL-17 was not significantly elevated in *T. vaginalis* infection despite using similar methods.[30] This discrepancy might be caused by differences in selected cohorts. In one case the samples were taken from symptomatic individuals [29], whereas in the other, symptoms were not evaluated.[30] Furthermore, experimental *T. vaginalis* infections in an estrogenized mouse model have shown increased levels of IL-2, 4 and interferon gamma (INF-γ) from vaginal washes.[31] *In vitro* experiments have shown increased levels of IL-1β, IL-6, IL-8, C-C motive ligand 5 (CCL5), INF-γ, tumour necrosis factor-α (TNF-α), macrophage inflammatory protein-α (MIP-α) in different immune or epithelial cell lines upon interaction with *T. vaginalis*.[22][32][33][34][35]

Cytokines are produced in response to an infection when pathogen recognition receptors (PRRs) are stimulated. It has been shown in VECs that specific PRRs, TLR2 and TLR3, are up-regulated in VECs upon co-incubation with *T. vaginalis*.[32] Similarly, TLR2 expression together with TLR4 were also increased in prostate epithelial cells after

T. vaginalis infection.[36] The importance of TLR2 for sensing *T. vaginalis* has been further indicated in macrophages, where the deletion of TLR2 led to a complete loss of IL-6, 8 and TNF-α secretion after the stimulation with *T. vaginalis*, probably due to lower phosphorylation of two kinases: p38 and extracellular signal-regulated kinase (ERK).[33] Almost identical results were obtained in prostate epithelial cells, where a TLR2 or TLR4 antibody treatment led to lower IL-6 expression due to the lower phosphorylation of, among other signaling molecules, p38 and ERK.[36]

Apart from TLRs, other signaling molecules have been implicated in the sensing of *T. vaginalis* infection. Galectins recognize β-galactosides and poly-N-acetyl-lactosamine repeats, which are part of *T. vaginalis* LGs. LGs are recognized by both galecin-1 and -3, but with a different outcome. Stimulation of galectin-1 leads to lower IL-8 secretion, while stimulation of galectin-3 leads to higher secretion, which suggests galectin-1 binding being beneficial for the *T. vaginalis* survival.[34] Interestingly, many of the aforementioned cytokines are attributed to the sensing of *T. vaginalis* endosymbionts and not *T. vaginalis* itself. The isogenic strain *T. vaginalis* G3 with intracellular *M. hominis* induced higher levels of IL-8, IL-6, IL-1β and TNF-α in human monocytes than *M. hominis* free *T. vaginalis* G3.[35][37] Similarly, TVV-positive strains of *T. vaginalis* induce higher levels of IL-6, IL-8 and CCL5 than TVV free trichomonads.[32] TVV effect will be discussed in more detail further in the text.

2.2 Virulence factors

T. vaginalis needs to acquire nutrients from the host environment in order to establish infection and persist in hosts. *T. vaginalis* is cytotoxic towards many kinds of host cells [10][37][38] and it is able to phagocytose them.[21] Similarly, the vaginal bacteria, such as lactobacilli, are frequently phagocytosed by *T. vaginalis*.[21] Furthermore, *T vaginalis* uptakes molecules like glucose [39] or iron from the environment.[19] All of this is achieved by *T. vaginalis* virulence factors, which are present on its surface [17][40] or actively secreted.[41][42]

Nevertheless, these abilities are not equivalent among distinct *T. vaginalis* strains. Indeed, individual strains isolated from patients may differ in their properties, which is reflected in their virulence. This was shown in a study of 26 *T. vaginalis* strains, where their ability to lyse ectocervical and benign hyperplasia prostate cells was assessed. The 26 strains were divided into low adherent and high adherent strains and a clear correlation between adhesion and cytolysis was shown. Since the cytotoxicity was strictly contact-dependent, it implied that adherence is very important for the virulence of *T. vaginalis*.[10] Furthermore, *T. vaginalis* is able to lyse not only epithelial cells but also various immune cells. B cells are killed preferentially by *T. vaginalis* rather than T cells and the killing appears to be both contact-dependent and independent.[37] To

a lower degree, also monocytes and macrophages can be killed by *T. vaginalis*. In macrophages, the cell death occurs partially through the highly inflammatory pathway of pyroptosis.[37][38] Conversely, *T. vaginalis* induces immunologically silent death, apoptosis, in neutrophils.[43] How apoptosis by *T. vaginalis* is triggered has been recently studied in a cervical cancer cell line. *T. vaginalis* appears to cause high ROS mitochondrial production and endoplasmatic reticulum stress through activation of a JNK kinase. Interestingly, apoptosis could be triggered by the excretory/secretory products alone.[44]

The *T. vaginalis* cytotoxic effect is in many cases contact-dependent, which implies the importance of various adhesive molecules in the pathology of *T. vaginalis*. Indeed, *T. vaginalis* possesses high number of sometimes extremely large families of adhesive molecules. One of those is the BspA family with ∼900 putative proteins [45] and until now ∼500 of them have been shown to be transcribed.[46] BspA proteins were mainly found on the cell surface [17][47] and in EVs.[42][48] However, proteomic analyses generally include only a few specific BspA proteins.[42][47][48] Similarly, only a few BspA proteins are up-regulated upon contact with host cells.[45] This implies that the proteins of this large family have different functions as suggested by their presence in distinct cell compartments and distinct expression patterns in the morphological stages of free swimming trofozoites, amoebic-like forms and pseudocysts.[42][46][47][49]

Apart from BspA, many other proteins have been proposed to play a role in *T. vaginalis* adherence. *T. vaginalis* tetraspanins are up-regulated upon contact with host cells [45] and tetraspanin 8 increases adherence of *T. vaginalis* to both host cells and *T. vaginalis*. Adherence to other trichomonads is a common feature of highly adhesive strains, as they often form clumps of parasites. Furthermore, it was shown that palmitoylation of tetraspanin 8 and protein palmitoylation, in general, are important for *T. vaginalis* adherence.[17] Additionally to tetraspanins and BspA, cadherin-like protein and triosephosphate isomerase have been detected on the surface of *T. vaginalis* and suggested to play an important role in the adherence of *T. vaginalis*. The cadherin-like protein directly increased the adherence of *T. vaginalis* to ectocervical cells, and, as a result, host cell killing was also more efficient.[50] The triosephosphate isomerase was shown to bind laminin and fibronectin, which are important components of the extracellular matrix.[51] Besides, another extracellular matrix and membrane cell component, heparan sulfate, was found to be bound by a *T. vaginalis* hypothetical protein and it also increased the *T. vaginalis* adhesion to host cells.[52]

Even though cytolysis is very often contact-dependent, the above-mentioned adhesive molecules alone are not able to mediate the host cell lysis. The important factors involved in cytotoxicity are *T. vaginalis* proteases that are coded by ∼300 genes. Of those, the most prominent are the CPs and MPs with ∼150 and ∼90 members, respectively.[53] Members of both protein classes are actively secreted by *T. vaginalis* [41] and some CPs are up-regulated upon contact with host cells.[45]

From the ∼300 *T. vaginalis* proteases, several are present in the *T. vaginalis* secretome. Among those are CPs: TvCP2, TvCP3, TvCP4, TvCPT and TvLEGU, MPs: TvMP50 and different leishmanolysin-like (GP63-like) peptidases.[41][54][55][56] They are secreted via the classical ER-Golgi-secretory pathway or lysosomal pathway as shown for TvCP2.[57] Furthermore, proteases are also part of the exosomal cargo [42] and they are present on the surface of *T. vaginalis*, exemplified by TvROM1, TvCP39 and some GP63-like peptidases.[40][58][59]

Since different proteases are up-regulated upon contact with host cells and are found in secretome [41], EVs [42] and on the *T. vaginalis* surface [59], it can be expected that they play a crucial role in *T. vaginalis* virulence. Surprisingly, they do not mediate only cytotoxicity of *T. vaginalis* but they also contribute to adherence, as was found for TvLEGU and TvROM1. Involvement of TvLEGU was suggested based on the observation that a specific antibody against TvLEGU decreases adherence to HeLa cells.[54] In the case of TvROM1, its overexpression led to higher adherence and cytotoxicity towards ectocervical cells. Interestingly, two *T. vaginalis* proteins, TVAG_166850 and TVAG_280090 were found to be cleaved by TvROM1 and mutation of the putative TvROM1 cleavage site of TVAG_166850 led to higher retention of the protein on the parasite surface and higher adherence to ectocervical cells.[40] Further studies have found that inhibitors of cysteine/serine and GP63-like proteases decrease the killing of VECs and HeLa cells, respectively.[56][58] Furthermore, inhibition of TvMP50 by specific antibodies was able to partially abolish the killing of prostate cells when the cells were co-incubated with *T. vaginalis*.[55] Similarly, HeLa cells were partially protected from the *T. vaginalis* cytotoxic effect when a non-functional recombinant protein, TvCP39, was added to the co-incubation of HeLa cells and *T. vaginalis*.[59]

Peptidases also play a major role in immune evasion. As already stated, *T. vaginalis* is able to kill many different immune cells. This is probably peptidase dependent, as it can be estimated from the mentioned studies conducted on epithelial cells.[10] Interestingly, pore-forming saposin-like proteins are coded in the *T. vaginalis* genome and one of these saposin-like proteins, TvSaplip12, has been shown to exert antibacterial activity.[60] Furthermore, TvSaplip6 and 8 were identified in *T. vaginalis secretome* [41], but further studies are needed to elucidate the importance of the saposin-like proteins in *T. vaginalis* virulence towards different epithelial and immune cells. Additionally, *T. vaginalis* is able to degrade IgA, IgG and C3 by the secreted and surface localized CPs, thereby avoiding opsonization and complement-dependent lysis.[61][62] Moreover, *T. vaginalis* appears to be able to acquire CD59, a factor restricting the formation of the membrane attack complex, from the host, which increases its protection against the complement-dependent lysis.[63]

Apart from the activities of secreted proteases, *T. vaginalis* can manipulate the immune system with other secreted components. Dendritic cells treated with granulocyte

macrophage-colony stimulating factor (GM-CSF) are activated and strongly express the markers of activation like MHCII and co-stimulatory molecules. However, the combined exposure to GM-CSF and the secretome of *T. vaginalis* leads to unchanged or even lower expression of these markers.[64] Furthermore, incubation of *T. vaginalis* secretome and lipopolysaccharide (LPS) stimulated dendritic cells results in higher secretion of IL-10 by the dendritic cells when compared to denritic cells, which were stimulated with LPS alone.[64] This effect might be attributed to the secreted α-tubulin2, but it requires further validation.[65] Furthermore, secreted molecules from the co-incubation of prostate epithelial cells and *T. vaginalis* induce the M2 tolerogenic phenotype in macrophages.[66] *T. vaginalis* also secretes leukotriene B4 and a homolog of the human macrophage migration inhibitory factor (TvMIF) both of which stimulate secretion of IL-8 from neutrophils and monocytes, respectively.[67][68] TvMIF appears to have the same function as the human MIF as it readily binds its receptors and is able to repel macrophages. In addition, TvMIF benefits *T. vaginalis* by increasing its survival under stress conditions.[69]

3. *Trichomonasvirus*

TVV is a non-segmented double-stranded (ds)RNA virus, which is commonly found in *T. vaginalis*.[70] It was discovered in 1985 [71] and since then, it has been extensively studied, mainly in order to ascertain its role in the virulence of *T. vaginalis*.[72][73][74][75] TVV comprises 4 different species: TVV1, TVV2, TVV3 and TVV4, which together form the *Trichomonasvirus* genus in the *Totiviridae* family. Recently, the existence of a new species, TVV5, has been proposed on the account of *de novo* sequence assembly.[70] The new TVV5 has only 42% nucleotide identity with its closest relative (TVV2) [70], which is below the 60% cutoff proposed for distinguishing different TVV species.[76]

Even though the sequence identity among distinct TVV species can be very low, the genome structure and length have not undergone dramatic changes. The TVV dsRNA ranges from 4.5 to 5.5 kb in length and it contains 2 open reading frames (ORF).[70][76][77] The first ORF encodes the viral capsid protein and the second RdRp. The capsid protein has its own translation initiation and termination. Hence, it is translated as a single protein. In contrast, the RdRp has no initiation codon and its translation is achieved through a polymerase frameshift on a slippery sequence located between the two ORFs. As a result, the RdRp is translated only as a fusion protein of the capsid protein and the RdRp.[76]

RdRps are indispensable molecules for RNA viruses due to their involvement in viral genome replication. All of the RdRps possess seven conserved structural/sequential motives A-G.[78] Due to this structural conservation, RdRps are targets of viral inhibition. Nucleoside analogs are often used as such inhibitors. According to their effect, we divide these analogs into mutation agents, obligatory terminators and non-obligatory terminators. 2'C methyl nucleoside analogs belong to the non-obligatory terminators, whose mechanism of action is not completely understood. However, they seem to terminate the synthesis, albeit in a different manner than the obliged terminators.[79] 2'-C-methyladenine (2CMA) was found to be a potent inhibitor of leishmania virus 1 (LRV1) [80], but no similar studies were conducted on TVV. Until now TVV free isogenic strains have been derived only via prolonged *in vitro* cultivation.[75]

3.1 *Trichomonasvirus*: a virulence factor

Prevalence of TVV in *T. vaginalis* ranges from low (∼20%) [81][82][83], over medium (40-50%) [12][74][84][85][86][87][88][89], to high (∼90%).[90] These differences can be explained by small sample sizes, geographical differences or distinct methods of TVV detection. Despite these differences, it seems that usually around 50% of *T. vaginalis* are infected with TVV, which makes it a highly prevalent *T. vaginalis* endosymbiont.

The most prevalent TVV species is TVV1 followed by TVV2 and TVV3 and the least prevalent is TVV4.[72] A single *T. vaginalis* strain can be infected with one of those species or with multiple TVV species simultaneously.[76][87][91]

Due to the high prevalence of TVV, many studies have tried to find a correlation between TVV infected *T. vaginalis* and clinical symptoms or metronidazole resistance. Despite extensive research, consensus on whether TVV causes more severe symptoms of trichomoniasis has not been reached. Several studies have found that the presence of TVV in *T. vaginalis* correlates with vaginal discharge [11][12][13][85], dysuria [12][13][85], pruritus and erythema of different parts of the female reproductive tract.[85] Interestingly, in two studies symptoms were not directly correlated to the TVV presence, but to *T. vaginalis* genotypes. In spite of using different approaches to genotype *T. vaginalis*, both studies have concurred that there are two major *T. vaginalis* genotypes and one of those genotypes is more likely to be TVV positive and to cause symptomatic infections.[11][85] Contrary to symptomatic infection, where the presence of TVV was correlated with more severe symptoms, metronidazole resistance was connected with the absence of TVV.[74][75]

In contrast to the aforementioned studies, other laboratories did not observe the correlation between TVV presence and a more aggressive infection [75][87][89][90] or metronidazole resistance.[86][90] There are several reasons which may explain these contradictory results. Firstly, most studies had only a very small sample size of *T. vaginalis* and hence even a smaller sample size of TVV-positive *T. vaginalis*. The number of *T. vaginalis* samples included rarely surpassed 50.[12][13][75][85][87][90] In two cases the number of *T. vaginalis* samples was over 100. A positive correlation between TVV infection of *T. vaginalis* and symptomatic trichomoniasis was found in a study in which 119 clinical isolates were included.[11] However, in another study, 355 samples of *T. vaginalis* were studied and no correlation between TVV and symptoms, nor metronidazole resistance was found.[89] Secondly, there is evidence of *T. vaginalis* forming two genotype groups, which appear to correlate with symptoms severity and the metronidazole resistance.[92] However, only two studies used *T. vaginalis* genotyping and found that TVV is more often associated with *T. vaginalis* isolates from more symptomatic individuals.[11][85] Thirdly, only one study accounted for the presence of other *T. vaginalis* endosymbionts. In this study, *T. vaginalis* was also screened for *M. hominis* and no correlation was found between TVV and the metronidazole resistance, nor between *M. hominis* and the metronidazole resistance.[86] All of this indicates the need for future studies to use large samples, to genotype *T. vaginalis* and screen for all of the *T. vaginalis* endosymbionts.

Several experimental studies have shown that the presence of TVV affects protein expression in *T. vaginalis* and the cytokine profile of host cells, and, therefore, suggested the possible impact of TVV on the course of *T. vaginalis* infection. Proteomic analyses of *T. vaginalis* cells revealed that TVV causes a change in *T. vaginalis* protein expression in

the whole cell [93][94] and the exosomal cargo.[7] In a cell proteomic analysis employing 2D-SDS-PAGE, several proteins were found to be differentially expressed between the TVV-positive and TVV-negative isogenic strains of *T. vaginalis*. The TVV-negative strains were derived through long-term (over 6 months) cultivation.[93] Interestingly, CPs were found to be up-regulated in the TVV-positive strains.[93] Nevertheless, the possibility of the protein expression being influenced by prolonged cultivation was not addressed. Therefore, these results need to be interpreted with caution. Apart from proteases, adhesive molecules may be also influenced by TVV presence as it was suggested by one study in which higher adherence of *T. vaginalis* infected with TVV2 and TVV3 was found.[88]

Furthermore, P270 is a major *T. vaginalis* immunogen and its surface protein levels and mRNA were shown to be up-regulated in TVV-positive *T. vaginalis* strains.[73][77] However, neither of the proteomic studies confirmed the higher presence of P270 in TVV infected *T. vaginalis*.[7][93][94]

A single study tried to elucidate whether the presence of TVV in *T. vaginalis* had any impact on the protein cargo of released exosomes. In this study, proteomic analysis was performed using exosomes released from the same *T. vaginalis* isogenic strains with or without TVV. The TVV free strain was derived through long-term cultivation.[7] Seven proteins were identified to be significantly differentially expressed and two of them were found to be putative human homologs of maltase-glucoamylase and keratine 1. Maltase-glucoamylase plays an important role in neutrophil degranulation [7], and thus its presence and function in exosomes ought to be further studied.

TVV also appears to affect the host cell cytokine production. It was shown that VECs secreted IL-8 and CCL5 when stimulated with *T. vaginalis* and this secretion was shown to be elicitable by the TVV virion particles alone.[22] A further study showed that VECs reacted to the co-incubation with TVV-positive strains with higher IL-8, IL-6, INF-β and CCL5 secretion in comparison to the co-incubation with TVV-negative strains. Since metronidazole kills *T. vaginalis* and thus mediates TVV release, the ability of metronidazole treated trichomonads to stimulate the cytokine release from VECs was tested. The VECs reacted to the treated TVV-positive strains with much higher secretion of IL-6, IL-8 and CCL5, when compared to the treated TVV-negative strains. Importantly, identical results were obtained when isolated TVV virions or poly(I:C), a dsRNA mimicking molecule, were used for the VECs stimulation.[32]

The increased IL-8, IL-6 and CCL5 secretion was dependent on the dsRNA sensing by TLR3.[32] Similar TLR3 dependent cytokine secretion was found in leishmania strains harboring LRV1. Moreover, TLR3 deletion in mice led to lower parasitemia when infected with a virus-positive leishmania strain.[95] Conversely, exosomes from TVV-negative strains, but not from TVV-positive strains, caused up-regulation of IL-8 and CCL5 in the VEC cell line.[7]

The above mentioned LRV1 belongs to the same *Totiviridae* family as TVV, and it appears to influence the immune reaction similarly to TVV. In *Leishmania guyanensis* LRV1 positive strains induce higher levels of IL-6, CCL5, INF-β and TNF-α than LRV-negative strains [95], comparably to TVV.[32] In addition, LRV1 is present in the lesihmania exosomes and co-injection of exosomes from an LRV-positive strain with LRV-negative strains into mice leads to exacerbation of leishmaniasis when compared to mice co-injected with LRV-negative strains and their own exosomes.[96] Comparably, *L. guyanensis* positive strains, but not their isogenic LRV-negative counterpart, were shown to cause more severe disease in mice. The disease exacerbation was related to the LRV stimulated INF-β secretion, which in turn promoted autophagy of nucleotide-binding oligomerization domain, leucine rich repeat and pyrin domain containing 3 (NLRP3) protein and apoptosis-associated speck-like protein containing a CARD (ASC). This caused lower caspase-1 activation in macrophages, and, therefore, promoted leishmania survival.[97] Although *T. vaginalis* is not an intracellular parasite like leishmania [96], TVV causes a similar cytokine response as LRV.[32][95] Therefore, TVV might influence inflammation in a similar manner.

4. Parasite extracellular vesicles

EVs are extracellular structures with unique biogenesis, which are enclosed by a single membrane. According to their size and origin, we can discriminate three types of EVs: exosomes (∼50∼150 nm), derived from an intracellular compartment known as multivesicular body (MVB), ectosomes, also known as microvesicles (∼100∼1000 nm), budding from the cell membrane, and apoptotic bodies (∼100∼5000 nm), formed during cell apoptosis.[98] Recently, a new type of extracellular nanoparticles, termed exomeres (∼30∼50 nm), without a lipid bilayer was identified in an exosomal fraction from human tumour tissues.[99] However, their importance in parasitic infections has not been addressed yet.

EVs of distinct sizes and content from *T. vaginalis* have been implicated to play a crucial role in host-parasite interactions.[42][100] *T. vaginalis* exosomes are of the expected size ranging from ∼50 to ∼100 nm in diameter.[7][42] Similarly, microvesicles are in the expected size range: ∼200∼800 nm in diameter.[48][101] EVs of comparable sizes have been identified in many other parasitic organisms as, for instance, exosomes of *Leishmania donovani* (∼50∼150 nm) [102] and *Entamoeba histolytica* (∼50∼150 nm) [103] or microvesicles of *Giardia intestinalis* (∼100∼450 nm).[104] Interestingly, EVs larger than 1000 nm were detected in *T. vaginalis*, but their function is unknown.[48]

The generation of EVs is dependent on a protein family known as the endosomal sorting complex required for transport (ESCRT). ESCRT facilitates EV biogenesis and also influences EV cargo selection. However, ESCRT independent EV formation is also possible through other proteins, like tetraspanins, or lipids, like ceramide, which due to its cone shape naturally induces membrane budding. Furthermore, EV biogenesis requires cytoskeletal proteins, small GTPases of the Rab family and many other proteins and molecules as shown in Fig. 1.[98][105] Molecules involved in EV biogenesis are rarely studied in parasites. Nevertheless, the importance of vacuolar protein sorting-associated protein 32 (VPS32), an ESCRT protein, for EV biogenesis has been recently shown in *T. vaginalis*. VPS32 overexpression in *T. vaginalis* led to increased secretion of EVs (exosomes and ectosomes) and these EVs were able to increase the adherence of the low adherent strain G3 when compared to the control expressing normal level of VPS32. Proteomic analysis of the EVs identified several distinctly expressed proteins. Among those were Rab and clathrin related proteins and *T. vaginalis* virulence factors like BspA, a GP63-like protein and MP20, which are important for adherence and cytotoxicity.[101]

Importance of other proteins in the parasite EV biogenesis has been shown in *G. intestinalis*. It possesses peripheral vacuoles, which are vesicles located under the its membrane, whose subsets are equivalent to MVB. This MVB-like subset contains intraluminal vesicles, which are under normal conditions secreted as exosomes. The

formation of these exosomes, termed small exosome-like vesicles, is dependent on VPS4 and Rab11 since mutation of VPS4 or suppression of Rab11 leads to a complete loss of intraluminal vesicles in peripheral vacuoles.[106] *G. intestinalis* is also able to shed large ectosome-like vesicles from its surface and this large vesicle biogenesis was shown to be dependent on peptidylarginine deiminase.[107] Furthermore, Ca^{2+} was found to be important for the ectosome-like vesicles release in *G. intestinalis* [104] as well as in *T. vaginalis*.[48] Apart from the proteins and ions, ceramide was found to be associated with peripheral vacuoles and intraluminal vesicles, suggesting its involvement in the small vesicle biogenesis of *G. intestinalis*.[106]

Interestingly, exosomal release independent of MVB from membrane protrusions, named membrane nanotubes, was observed in *Trypanosoma brucei*.[108] The release of these membrane nanotube exosomes was found to be VPS36 independent in contrast to the usual MVB exosomal release.[109] It is obvious that there are large gaps in our knowledge of the EV biogenesis in parasites and further studies are required to fully understand their complex formation.

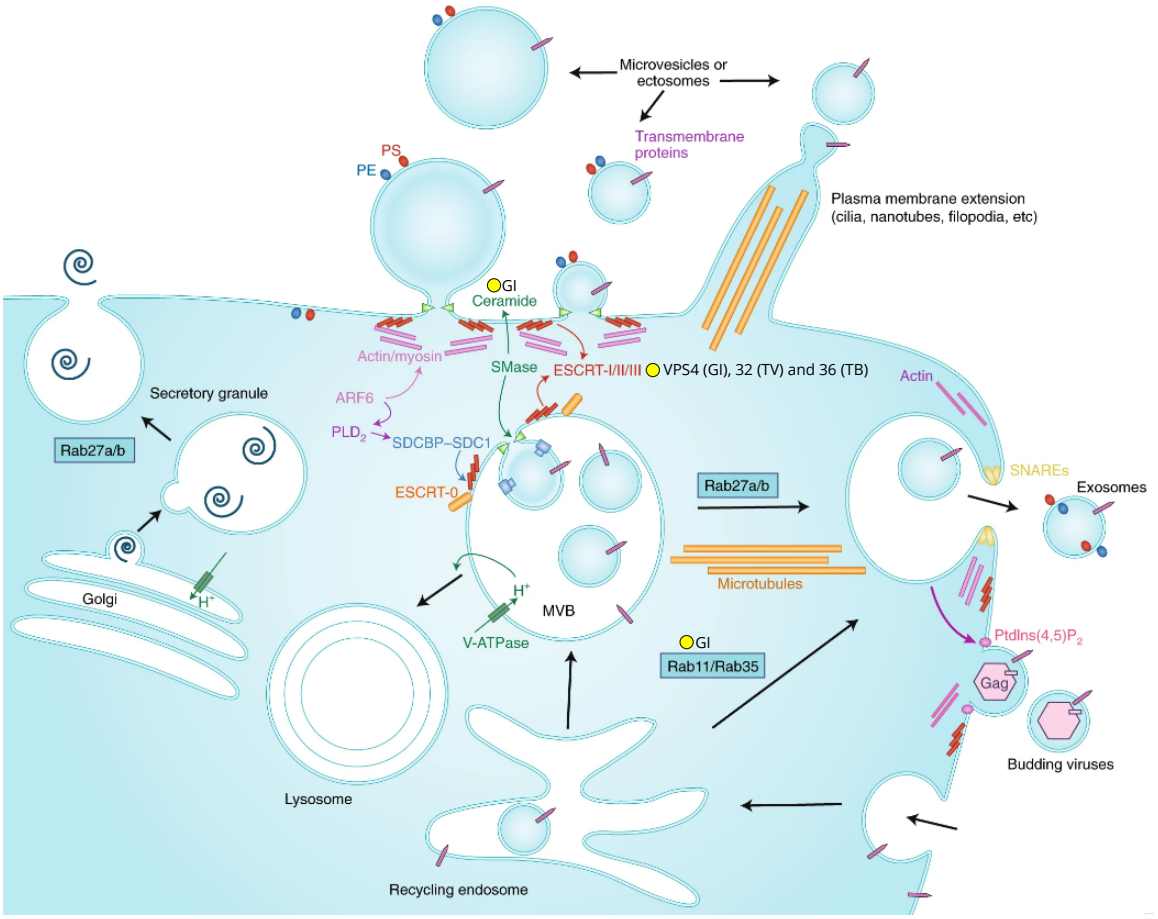

Figure 1: Proteins and molecules involved in EV biogenesis. Components involved in the mammalian EV biogenesis are shown. Proteins and molecules known to play a role in the EV biogenesis of parasites are highlighted with yellow dots. ARF6: ADP ribosylation factor 6; GI: *G. intestinalis*; PE: phosphatidylethanolamine; PLD2: phospholipase D2; PS: phosphatidylserine; PtdIns(4,5)P_2: phosphatidylinositol 4,5-bisphosphate; SDCBP: syndecan binding protein; SDC1: Syndecan 1; SMase: sphingomyelinase; SNARE: soluble NSF (N-ethylmaleimide-sensitive factor) attachment protein receptor; TB: *T. brucei*; TV: *T. vaginalis* (adapted from [98])

Upon the release of EVs, they are taken up by target cells. The uptake proceeds via immediate membrane fusion, which results in the release of the EV cargo into the cell cytosol, or endosomal uptake. In the endosomal compartment, exosomes can be either recycled and released from the cells, degraded in lysosome, or their cargo can be released into the cell cytosol through fusion with the endosomal membrane.[98] In parasites, both membrane fusion [110][111] and endosomal uptake have been suggested for EV uptake.[109][112] However, only in *T. vaginalis*, the mechanism of EV uptake was studied.

In general, uptake of cargo can be mediated through several mechanisms: pinocytosis, phagocytosis and clathrin or caveolin dependent endocytosis. From these, only the suppression of caveolin endocytosis led to a ∼90% decrease in the uptake of *T. vaginalis* EVs by benign hyperplasia prostate cells. Similarly, depletion of cholesterol, which is indispensable for caveolin rafts, and, therefore, caveolin dependent endocytosis, also led to a ∼90% reduction of the EV uptake by the same cell line. The uptake of *T. vaginalis* EVs was also found to be dependent on glycosaminoglycans and heparan sulfate, as their loss in the recipient cells led to a ∼70% and ∼45% decrease in the uptake, respectively.[113] Until now, the mechanism of uptake of other parasite EVs has not been addressed.

4.1 EV content

Taking into account that biogenesis of EVs results from extensive molecular trafficking within the endo-lysosome compartment, it is not surprising that EVs contain proteins connected with vesicular or protein transport and cytoskeletal proteins in *T. vaginalis* [42][48] and other parasite.[103][114][115] Furthermore, EVs mediate host-parasite interactions, and, therefore, presence of distinct virulence factors is expected. *T. vaginalis* exosomes have been found to contain BspA as well as a number of different peptidases and even proteins mimicking the host cell proteins like TvMIF.[17][42][101]

Furthermore, argonaute (AGO) proteins have been identified in exosomes of *E. histolytica* [103] and *T. brucei*.[109] Proteins of AGO family together with miRNA and other proteins form RNA-induced silencing complex (RISC), which can induce gene silencing by RNA interference pathways.[116] However, *T. vaginalis* appears to possess only ∼ 20 putative miRNA genes [117], some of which might be missannotated.[118] Some of these putative *T. vaginalis* miRNA molecules are derived from tRNA.[117] Indeed, EVs in *T. vaginalis* and many other parasites contain, apart from mRNA and rRNA, large amount of tRNA fragments (tRFs).[102][110][111][119] These fragments can be bound by AGO proteins, and thus potentially function as miRNAs.[120][121]

tRFs are generated from mature tRNA with RNases and they can be separated into halves (31-40 nt long) and fragments (14-30 nt long). The two categories can be further divided into five subcategories: 5' tRNA halve, 3' tRNA halve, 5' tRNA frament

(tRF-5), 3' tRNA fragment (tRF-3) and internal fragment (internal tRF).[116][122] The halves span the entire length from one end of tRNA up to the anticodon, whereas the fragments can start at any location at either end of tRNA, but they do not reach the anticodon. Internal tRFs are an exception when compared to tRF-3 and tRF-5, since they can begin and end almost anywhere in the tRNA molecule and they usually span the anticodon loop (Fig. 2).[116][122] tRFs have been found to exert AGO independent functions, for instance, global transcriptional repression, or AGO dependent functions, where tRFs 20-30 nt long are bound by an AGO protein and mediate repression of target genes.[116] *T. vaginalis* has two AGO paralogues with a PIWI domain, which usually binds 25-30 nt long RNA molecules.[123] However, none of these proteins have been identified in exosomes nor ectosomes of *T. vaginalis* [7][42][48][101], but one of the AGO paralogues (TVAG_453810) has been identified in the *T. vaginalis* secretome.[41] The secreted AGO could potentially be taken up by host cells, where it could mediate RISC dependent gene silencing.[124]

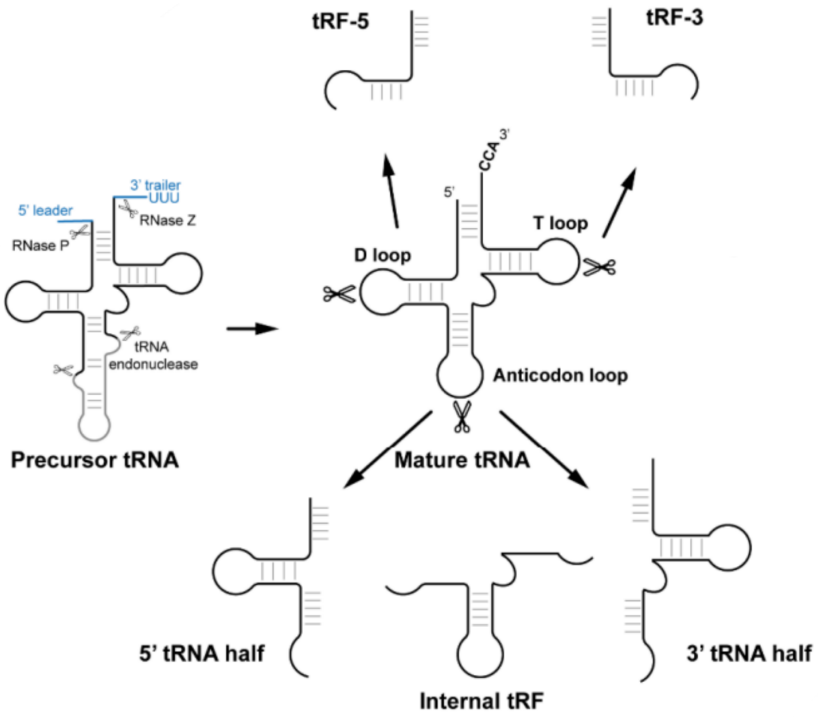

Figure 2: tRFs generation and categories. The picture shows the generation of tRFs from mature tRNA and regions of mature tRNA to which each tRF or tRNA halve corresponds. (adapted from [122])

4.2 Modulatory effects of parasite EVs

EVs have numerous functions in host-parasite interaction. Exosomes from high adherent *T. vaginalis* strains are able to increase the adherence of low adherent strains. Interestingly, pretreatment of either host cells or low adherent *T. vaginalis* strains with the exosomes from the high adherent strains both leads to increased adherence of the

low adherent strains.[42] Besides *T. vaginalis*, there are other parasitic species, which can increase adhesiveness through their EVs. For instance, pretreatment of host cells with large ectosome-like vesicles, but not small exosome-like vesicles, from *G. intestinalis* increases the adhesiveness of *G. intestinalis* to host cells.[104] This implies that exosomes and ectosomes have their specific cargo, and, therefore, different roles in host-parasite interactions. Similarly, *T. vaginalis* exosomes and ectosomes seem to contain distinct cargo. Although, overlaps between their content have been reported.[42][48] These overlaps can be either due to the actual content similarity or technical limitations, which preclude complete separation of the exosomal and ectosomal fractions.[125]

The increased adhesiveness of virulent *T. vaginalis* strains could be attributed either to the ability of *T. vaginalis* to transform into the amoebic-like form or to higher amount of adhesive molecules.[21][42][101] When co-cultured with VECs, virulent *T vaginalis* strains transform from the swimming drop-like trofozoite into a stable amoebic-like shape within 15 min while avirulent strains have unstable amoebic-like state and the transformation takes them longer.[21]

Virulent *T. vaginalis* are usually highly adherent [10] and these strains seem to have differential expression of several membrane proteins when compared to avirulent strains. Among these are adhesive polymorphic membrane proteins, a serine protease and several hypothetical proteins.[47] Importantly, overexpression of genes coding two hypothetical proteins (TVAG_244130 or TVAG_166850) of high adherent *T. vaginalis* strains in low adherent strains led to their increased adherence to VECs.[47] Interestingly, a serine/threonine protein phosphatase was also up-regulated in the high adherent strains.[47] Phosphatases have been found to play a role in *Trypanosoma cruzi* EV dependent adherence as their inhibition decreased the EV mediated adherence of the parasite.[126]

The effects of *T. vaginalis* exosomes can be dependent on proteases as, for instance, GP63-like proteases, which were found to be part of the exosomal proteome [42][101] and are involved in the *T. vaginalis* cytotoxicity.[58] Albeit, their presence in exosomes might have another function as it can be hypothesised from *L. donovani* exosomes. *L. donovani* is an intracellular parasite which infects spleen and liver, where it resides in monocytes or macrophages. During the *L. donovani* infection serum cholesterol levels continuously drop, which is connected with accumulation of a precursor of miR-122 in hepatic cells. This miRNA controls lipid metabolism and its maturation requires processing with Dicer1. When the hepatic cells where transfected with miR-122, which did not require processing with Dicer1, the exosomal inhibition of miR-122 activity was lost. The Dicer1 itself was regulated via the activity of a GP63 protease that was shown to cleave it, thereby inhibiting the Dicer1 function.[127] This suggests that proteases can have distinct functions and targets. Hence, further investigations of GP63-like proteases and other exosomal proteases are required to gain insight into their function in *T. vaginalis*

exosomes.

Aside from proteins, *T. vaginalis* EVs also contain tRFs, which appear to be preferentially packed as ∼88% of all RNA reads belong to tRNA genes. The most abundant types of the tRFs are derived from: tRNA-Glu, tRNA-Gly, tRNA-Phe and tRNA-Lys.[119] The abundance and types of the tRFs in EVs is similar to that of the whole *T. vaginalis* cells, in which they account for ∼39% (tRNA-Glu), ∼12% (tRNA-Glu), ∼12% (tRNA-Phe) and ∼5% (tRNA-Lys).[118]

Both in whole cells and exosomes, most of the tRFs are derived from the 5' end of tRNA molecules and they are usually 5' tRNA halves.[118][119] The exact function of tRFs in the host-parasite interaction has not been addressed in *T. vaginalis* yet. This type of interaction was investigated only in *T. cruzi*, from which the two most abundant tRFs, derived from tRNA-Thr and tRNA-Leu, were transfected with lipofectamines into HeLa cells. The transfection with tRNA-Thr and tRNA-Leu led to a change in expression of 20 and 3 genes, respectively. Among the 20 proteins there were, for instance, activating transcription factor 3 (ATF3), which is an important transcription regulator of many immune related genes. However, the concentration of the tRFs used did not mimic the one found in the *T. cruzi* EVs and the uptake of the used lipofectamines might differ from the EV uptake. Therefore further experiments are required to confirm the function of these tRFs.[110]

EVs modulate many aspects of host cell physiology, including the immune system, as it can be seen in the example of *Helicobacter pylori*. Outer membrane vesicles of this bacterium induce IL-8 secretion in gastric epithelial cells and this IL-8 release was found to be down-regulated by a tRF from tRNA-Met.[128]

Similarly, EVs of *T. vaginalis* stimulate the secretion of IL-8, IL-6 and CCL5 from VECs.[7][42] However, when the VECs were preincubated with exosomes the secretion of IL-8 in reaction to subsequent co-incubation with trichomonads was lower.[42] Similarly, peripheral blood mononuclear cells (PBMCs) have been shown to react to *T. vaginalis* EV stimulation by IL-6, IL-8 and TNF-α secretion [7] but when the PMBCs were stimulated by EVs collected from VECs co-cultured with *T. vaginalis*, the IL-8 secretion was decreased.[7] Furthermore, macrophages are activated by *T. vaginalis* EVs. However, they also exhibit high IL-10 mRNA levels.[129] These experiments suggest that EVs of *T. vaginalis* are immunosuppressive. Indeed, an experiment in a special mouse model pretreated with estradiol valerate and norethisterone enanthate, in order for the mouse to be susceptible to the *T. vaginalis* infection, showed that EV pretreatment led to lower physical signs of inflammation.[129]

5. Materials

5.1 Tools and instruments

A list of specific tools and instruments, which were used in all of the experiments:

- Beckman centrifuge (Beckman Coulter Inc., Brea, United States)
- Beckman Fraction recovery system (Beckman Coulter Inc., Brea, United States)
- Beckman SW 41 swing-out rotor (Beckman Coulter Inc., Brea, United States)
- Beckman ultracentrifuge (Beckman Coulter Inc., Brea, United States)
- Fast protein liquid chromatography (FPLC) pump (KNAUER, Berlin, Germany)
- Fraction collector (ThermoFisher Scientific, Waltham, Unites States)
- Illumina sequencer MiSeq (Illumina, San Diego, USA)
- Orbitrap Fusion Tribrid mass spectrometer (ThermoFisher Scientific, Waltham, Unites States)
- RNA Nano 6000 Assay Kit of the Bioanalyzer 2100 system (Agilent Technologies, Santa Clara, USA)
- UV-Vis flow spectrophotometer (ThermoFisher Scientific, Waltham, Unites States)
- Vivaflow 200 system with 100 000 MWCO PES membrane (Sartorius, Göttingen, Germany)

5.2 Bioinformatics

5.2.1 Databases, sequences and data sets

All utilized databases together with the hyperlinks of the sites, from which they were downloaded, are provided. Further, if any sequence or data set were downloaded from a given database, the IDs of the sequences and the names of the data sets are provided.

- ImmPort (https://www.immport.org/home) [130]
  - Immune system related genes – GeneList.txt

- InnateDB (https://www.innatedb.com/) [131]
  - Innate immunity related genes – InnateDB_genes.txt
- miRable (http://bioinfo.univ-rouen.fr/mirabel/index.php?page=mir)[132]
- miRbase (https://www.mirbase.org/) [133]
  - Database of mature miRNA molecules – mature.fa
- NCBI (https://ncbi.nlm.nih.gov/) [134]
  - non-redundant protein database
  - GenBank sequences for RNA-seq analysis: TVV1 (NC_027701.1), TVV2 (NC_003873.1), TVV3 (NC_004034.1), TVV4 (NC_038700.1)
  - GenBank sequences for modeling: TVV1 (AAA62868.1), LRV1 (APT68186.1)
- PDB (https://www.rcsb.org/) [135]
  - PDB IDs: 1KHW, 1RA7, 1XR7, 2B43, 2CKW, 2E9R, 2E9Z, 2EC0, 2ILY, 2ILZ, 2IM0, 2IM1, 2IM2, 2UUT, 3BSN, 3DDK, 3H5X, 3H5Y, 3KOA, 3N6M, 3N6N, 3OLB, 3UQS, 4K4Y, 4K50, 4LQ9, 4NRT, 4NRU, 4NZ0, 4O4R, 4WTI, 4WYW, 4Y2A, 4Y34, 5F8I, 5XE0, 5ZIT, 6KWR, 6L4R
- Pfam database v. 35.0 [136]
- TargetScan v. 8.0 (https://www.targetscan.org/vert_80/) [137]
  - 3' UTR database – UTR Sequences.txt
- TrichDB database release 52 (https://trichdb.org/trichdb/app/record/gene/TVAG_373240) [138]
  - Annotated proteins – TrichDB-52_TvaginalisG3_AnnotatedProteins.fasta
  - Annotated transcripts – TrichDB-52_TvaginalisG3_AnnotatedTranscripts.fasta
  - Reference genome – TrichDB-52_TvaginalisG3_Genome.fasta
  - GFF file – TrichDB-52_TvaginalisG3.gff
- Uniprot (https://www.uniprot.org/) [139]
  - Mapping service – Retrieve/ID mapping
  - Human proteins – UP000005640_9606.fasta
- UniRef/Uniclust (http://wwwuser.gwdg.de/~compbiol/uniclust/2020_06/) [140]
  - UniRef clustered database – UniRef30_2020_06_hhsuite.tar.gz

5.2.2 Software

All of the used programs and their version are listed. Programs used on websites have url included.

- BBmap v. 38.96 [141]
- BLAST v. 2.13.0 (https://blast.ncbi.nlm.nih.gov/Blast.cgi) [142]
- Bowtie2 v. 2.4.4 [143]
- coverageBed v. 2.30.0 [144]
- cutadapt v. 1.8.3 [145]
- eggnog mapper v. 2.1.7 [146]
- Fiji 2.5.0 [147]
- GraphPad Prism 7 (La Jolla, California, USA)
- hhblits v. 3.3.0 [148]
- HMMER v. 3.3.2 [149]
- locPREFMD (http://feig.bch.msu.edu/locprefmd/) [150]
- MAFFT v. 7 (https://mafft.cbrc.jp/alignment/server/) [151]
- MaxQuant LFQ v. 1.6.2.0 [152]
- Microsoft Excel v. 17 [153]
- miRanda v. 3.3a [154]
- molprobity (http://molprobity.manchester.ac.uk/) [155]
- Outlier calculator (https://www.graphpad.com/quickcalcs/Grubbs1.cfm)
- PfamScan v. 1.6.4 [136]
- PHYRE2 (http://www.sbg.bio.ic.ac.uk/~phyre2/html/page.cgi?id=index) [156]
- PyMOL 2.5.2 [157]
- P2rank (https://prankweb.cz/) [158]

- Rstudio 4.1.2 [159]
  - artMS [160]
  - DESeg2 [161]
  - gprofiler2 [162]
  - MSstats [163]
  - Rsubread [164]
  - VennDiagram [165]
- samtools v. 1.7 [166]
- TargetP v. 2.0 (https://services.healthtech.dtu.dk/service.php) [167]
- TMHMM v. 2.0 (https://services.healthtech.dtu.dk/service.php?TMHMM-2.0) [168]
- tRNAscan-SE v. 2.0 (http://lowelab.ucsc.edu/tRNAscan-SE/index.html) [169]

5.3 Kits

The purchased kits together with their specifications, provided materials and chemicals are shown. The composition of the chemicals is listed, if available.

- ELISA kits (Thermo Fisher Scientific, Waltham, USA)

  Common chemicals:

  - Standards – IL-1β, IL-6, IL-8, CCL2, CCL5
  - Stop solution – 1M H_3PO_4
  - Substrate – tetramethylbenzidine
  - Wash Buffer – 1X PBS, 0.05 Tween^{TM}-20
  - 1X Coating Buffer – 1X PBS
  - 100X Streptavidin-HRP
  - 250X Capture Antibody – anti-IL-1β, anti-IL-6, anti-IL-8, anti-CCL2, CCL5
  - 250X Detection Antibody – biotin conjugated anti human IL-1β, IL-6, IL-8, CCL2, CCL5

  Common materials:

  - ELISA plates – IL-1β, IL-6, IL-8, CCL2, CCL5

Specific chemicals (CCL5):

- Assay Buffer A (20X)
- Blocking Buffer – 2X Assay Buffer A

Specific chemicals (IL-1β, IL-6, IL-8, CCL2):

- ELISA/ELISPOT Diluent (5X)

- Highpure RNA isolation kit (Roche Diagnostics, Mannheim, Germany)
- Human inflammation antibody array (Abcam, Cambridge, UK)

Chemicals:

- Detection Buffer C
- Detection Buffer D
- 1X Blocking Buffer
- 20X Wash Buffers I
- 20X Wash Buffers II
- 1000X HRP-Conjugated Streptavidin
- 2000X Biotin-Conjugated Anti-Cytokines

Materials:

- 8-well tray

- Kapa SYBR FAST one-step Universal kit (Sigma-Aldrich, Missouri, USA)
- NEXTFLEX® Small RNA-Seq Kit v3 for Illumina® Platforms (Perkin Elmer, Waltham, USA)
- Qubit® RNA Assay Kit in Qubit® 2.0 Flurometer (Life Technologies, Carlsbad, USA)

5.4 Cell lines and animals

The cell lines used in this work together with their specifications are listed.

- HaCaT

Description: Human spontaneously transformed aneuploid immortal keratinocyte cells

Origin: Provided from the Institute of Hematology and Blood Transfusion located in Prague, from V. Vonka, RRID:CVCL_0038 [170]

- TV79-49c1^{+}

  Description: A *T. vaginalis* strain containing TVV1, TVV2 and TVV3

  Origin: Isolated from a patient [171]

- TV79-49c1^{-}

  Description: A *T. vaginalis* strain cured from the TVV infection with 2CMC

  Origin: Derived in our laboratory [9]

5.5 Chemicals and other material

All the necessary chemicals and materials, which were not provided as a part of the purchased kits, are listed together with their composition.

- Chloroform (Sigma, Kawasaki, Japan)
- Fetal bovine serum (Sigma, Kawasaki, Japan)
- IgG-peroxidase anti-rat antibody (Sigma-Aldrich, Burlington, USA)
- Methanol (Sigma, Kawasaki, Japan)
- $NaHCO_3$ (Sigma, Kawasaki, Japan)
- OptiPrep (Axis-Shield PoC AS, Dundee, Scotland)

  composition (5%):

  - 250 mM Sucrose
  - 1 mM EDTA
  - 10 mM Tris
  - pH 7.4

  composition (50%):

  - 250 mM Sucrose
  - 6 mM EDTA
  - 60 mM Tris
  - pH 7.4

- PCR primers – see Table_S7_PCR_primers.xlsx (Sigma-Aldrich, Missouri, USA)
- Penicillin (Sigma, Kawasaki, Japan)
- Polyclonal rat anti Tsp1 antibody (Antibody Registry RRID:AB 2910119) – provided by Petr Rada [172]
- RPMI 1640 complete medium (ThermoFisher Scientific, Waltham, Unites States)
- Streptomycin (Sigma, Kawasaki, Japan)
- Sucrose-Tris (ST) buffer (Sigma, Kawasaki, Japan)

  composition:

  - 250 mM sucrose
  - 10 mM Tris
  - 0.5 mM KCl
  - pH 7.2
- Trizol reagent (Merck, Darmstadt, Germany)
- Tryptone-yeast extract-maltose (TYM) medium [173]

  composition:

  - 20 g Tryptone (OXOID, Altrincham, UK)
  - 10 g Yeast extract (OXOID, Altrincham, UK)
  - 5 g Maltose (Sigma, Kawasaki, Japan)
  - 22,8 mg Ammonium iron (III) citrate (Sigma, Kawasaki, Japan)
  - 0,2 g Ascorbic acid (Sigma, Kawasaki, Japan)
  - 100 mL Inactivated horse serum (Gibco® Life Technologies, Penrose, New Zealand)
  - 1 g L-Cysteine (Sigma, Kawasaki, Japan)
  - 0,8 g KH_2PO_4 (Sigma, Kawasaki, Japan)
  - 0,8 g K_2HPO_4 (Sigma, Kawasaki, Japan)
  - 900 mL Distilled H_2O
  - pH adjusted with 1M KOH to 6.2 and sterilized by autoclaving
  - 100 mL Inactivated horse serum (Gibco® Life Technologies, Penrose, New Zealand), added before use

- Trypsin (Sigma, Kawasaki, Japan)
- Tween^{TM}-20 (Sigma, Kawasaki, Japan)
- Zymo IIC spin column (RNA clean & Concentrator-25) (Zymo Research, Irvine, California)

6. Methods

6.1 Cells and cultivation

The *T. vaginalis* clone, TV79-49c1$^+$, and its TVV free isogenic clone, TV79-49c1$^-$, were used in this study. The TVV infection of TV79-49c1$^+$ was cured with 2CMC treatment as previously described.[9] PCR was conducted to check the absence of *M. hominis* as described earlier.[174] *T. vaginalis* was cultured in the TYM medium supplemented with the 10% inactivated horse serum at pH 6.2 and 37 °C.[173] The HaCaT cell line was cultured in the RPMI 1640 complete medium supplemented with the 10% fetal bovine serum, 2% $NaHCO_3$, penicillin (100 U/mL) and streptomycin (100 µL/mL).[170]

6.2 Isolation of small EVs

When isolating exosomes it is impossible to distinguish them from microvesicles of identical size and density.[125] Acknowledging this technical difficulty, our isolated vesicles will be henceforth referred to as small EVs.

To isolate the *T. vaginalis* small EVs, a culture of 1 x 10^9 *T. vaginalis* cells in the logarithmic phase of growth was harvested using a 15 minute centrifugation at 2000 x g and 25 °C. The cells were washed two times utilizing a serum-free TYM medium. Thereafter, a suspension of the washed *T. vaginalis* cells with total concentration of 1x10^6/mL was incubated for 2.5 hours at 37 °C in serum-free TYM medium. The integrity of *T. vaginalis* cells was inspected by the trypan blue exclusion test.[175] The cells were then harvested by centrifugation at 2000 x g and 25 °C. The supernatant containing distinct EVs was purified by filtering through a 0.22 µm pore size filter. To concentrate the filtered supernatant, tangential filtration using a Vivaflow 200 system with 100 000 MWCO PES membrane was used. The resulting ∼30 mL EV concentrate was centrifuged for 1 hour at 100 000 x g and 4 °C. The supernatant was subjected to protein extraction with methanol and chloroform (4:1) and analyzed by mass spectrometry to be later used as a contamination control. The small EV containing pellet was resuspended in a Sucrose-Tris (ST) buffer (pH 7.2) and fractionated on a linear gradient of 5% to 50% OptiPrep (pH 7.4) according to the OptiPrep^{TM} protocol on a Beckman SW 41 swing-out rotor at 100 000 x g and 4 °C for 15 hours. Fractionation of the gradient was performed using a Beckman Fraction recovery system connected to a FPLC pump, a UV-Vis flow spectrophotometer and a fraction collector. The result of the fractionation step were 24 fractions. Dilution of 1:10 of each gradient fraction in ST buffer were centrifuged at 100 000 x g and 4 °C for 1 hour. Immunoblotting of the resulting pellets of all fractions was conducted using the Tsp1 antibody (dilution 1:1000) to identify the small

EV fractions. The Tsp1 antibody was visualized by IgG anti-rat antibody conjugated with peroxidase (dilution 1:2000). Altogether, three independent parallel isolation experiments from TV79-49c1^{+} and TV79-49c1^{-} were performed (A, B and C).

6.3 Quantitative mass spectrometry

The extracted proteins from small EVs and soluble proteins from corresponding supernatants were subjected to a label-free quantitative mass spectrometry analysis as described previously.[57] Trypsin was used as a sample digestive agent. The digested samples were analysed by nano-liquid chromatography-mass spectrometry. The *T. vaginalis* database of annotated proteins and 92 TVV amino acid sequences from the NCBI non-redundant protein database were utilized to annotate the MS/MS spectra. The data were quantified with the label-free algorithms using MaxQuant LFQ. The raw MS data from the three independent experiments were deposited to the ProteomeXchange Consortium via the PRIDE partner repository under the data set identifier PXD031790 and 10.6019/PXD031790.[176]

6.4 Mass spectrometry data processing

To estimate the reproducibility of the independent biological experiments, the original MaxQuant data set was analysed using the artMS package to obtain the principle component analysis (PCA) graph of the proteomic data (Fig. 7; DEA_proteins.R, lines 589-607).

6.4.1 Protein differential expression analysis

Processing of the mass spectrometry data was performed via Rstudio. To process the MaxQuant output data, a function was written in Rstudio (DEA_proteins.R, lines 32-393). The MaxQuant output data were preprocessed (DEA_proteins.R, lines 14-30) to obtain the input parameters for the function (DEA_proteins.R, lines 32-41). To process the raw MaxQuant data set:

1. The column headings were changed for easier manipulation (DEA_proteins.R, lines 42-76).

2. Several proteins were removed if they were according to the MaxQuant data set potential contaminants or identified based on a single peptide (DEA_proteins.R, lines 98-101).

3. The LFQ intensities were log2-transformed (DEA_proteins.R, line 116) and imputation of all missing values (NAs) of all LFQ intensities was conducted by replacement

of the NAs with numbers randomly selected from the normal distribution around the mass spectrometer limit (DEA_proteins.R, lines 123-133).

4. The proteins, which were identified in less than two independent experiments, were assign p-value 1 and they were filtered out (DEA_proteins.R, lines 161-169). This was done to prevent any proteins being falsely assigned to either of the *T. vaginalis* clones.

5. The LFQ intensities of the remaining proteins were used for fold change and p-value calculation (DEA proteins.R, lines 170-198). The LFQ intensities of the supernatant (contamination) from small EVs were compared to the LFQ intensities of the small EV pellets and proteins with the following parameters were removed: fold change <1.5 and p-value >0.02 (DEA proteins.R, lines 199-200).

6. Lastly, since *T. vaginalis* possesses many paralogues of most of its proteins [46][53], the proteins IDs were filtered and only the first ID was taken into account for simpler manipulation (DEA_proteins.R, lines 203-219).

This procedure was done for both clones (TV79-49c1$^+$ and TV79-49c1$^-$) yielding two data sets (DEA_proteins.R, lines 221-224). The two data sets were compared with one another (DEA_proteins.R, lines 324-348) and significant differences between the two small EV data sets were shown in a vulcano plot (Fig. 9). The cut-off p-value was set to 0.01 to identify deferentially expressed small EV proteins (DEA_proteins.R, lines 454-544). Prior to the plotting, the proteins IDs were changed from Uniprot IDs to TVAG IDs (DEA_proteins.R, lines 405-452).

6.4.2 Annotation

The resulting data set from the differential expression analysis was annotated using the TrichDB database of annotated proteins and written into a tsv file (DEA_proteins.R, lines 547-576). To expand on the basic TrichDB annotation, a fasta file with all of the small EV protein sequences was extracted from the TrichDB database of annotated proteins (DEA_proteins.R, lines 577-587). The fasta file was used as an input into several programs to further annotate the small EV protein data set. The utilized locally installed programs were hhblits with the UniRef30_2020_06_hhsuite database and eggnog mapper with the inbuilt eukaryotic database.

6.4.3 Domain and signal peptide prediction

PfamScan with the Pfam database was utilized to identify all functional domains in our small EV protein data set. Furthermore, to predict protein cellular localization

and protein transmembrane helixes, the online services TargetP and TMHMM were used, respectively.

6.4.4 Processing of the annotation and prediction results

The results of all programs were loaded into Rstudio and parsed (Parsing.R, lines 6-190). During the parsing, the hhblits hits, which represented uncharacterized proteins, were filtered out (Parsing.R, lines 38-41). Further, the Uniref IDs were extracted (Parsing.R, lines 55-68) and mapped to their protein names and GO terms via the Uniprot mapping service. The Uniprot mapping results were loaded into Rstudio (Parsing.R, lines 79-80) to finish the hhblits parsing (Parsing.R, lines 82-109). The TMHMM results were combined with the TargetP results. When a predicted signal peptide overlapped with a predicted trans-membrane helix, this predicted trans-membrane helix was removed (Parsing.R, lines 145-177). The parsed annotation was combined with the TrichDB annotated protein data set (Parsing.R, lines 193-202). All of the programs' specifications and parameters are shown below.

- hhblits
  Parameters: -cpu 15 -d UniRef30_2020_06

- eggnog mapper
  Parameters: –cpu 15 -d euk –usemem –hmm_maxhits –evalue 0.05 –sensmode very-sensitive –outfmt_short

- PfamScan
  Parameters: -cpu 8 -dir location/of/the/pfam/database -e_seq 1e-5

- TargetP
  Parameters: Organism: Non-plant, Output format: Short output

- TMHMM
  Parameters: Output: one line per protein

Description: Parameters of the programs used for the protein data set annotation (hhblits and eggnog mapper) and domain (PfamScan), trans-membrane helix (TMHMM) and signal peptide prediction (TargetP)

6.4.5 Ortholog group distribution

The cluster of orthologous groups (COGs) from the eggnog mapper were utilized to plot the graph showing the groups percentage representation (Fig. 8A). The plotting was done in Excel.

6.4.6 Protein set enrichment analysis

The GO terms from the Uniref IDs mapping were transformed into three gmt files (PSEA.R, lines 12-104). Only the Uniref IDs with the hhblits probability >90 were transformed (PSEA.R, line 29). The gmt files were used to create personal libraries for protein set enrichment analysis (PSEA.R, lines 106-111). The protein set enrichment analysis was performed with the Rstudio package gprofiler2 (Fig. 11; PSEA.R, lines 113-182). The resulting enriched GO terms required mapping back to the corresponding TVAG IDs (PSEA.R, lines 184-269). The mapped GO terms were written into csv files and manually curated to get the final Table_S2_GO_term_PSEA.xlsx.

6.4.7 Identification of human immune related homologs

To look for distant immune related protein human homologs in our small EV data set, a databases of immune related molecules was obtained by filtering the human protein database from Uniprot with databases from InnateDB and ImmPort (ImmuneDB.R, lines 7-49). This database of immune related proteins was subsequently used to build a hhblits database (the specifications are listed below), which was used to search for immune related proteins in our small EV data set via hhblits. The parameters for the hhblits search were: -cpu 20, -d built_immune_database -blasttab -n 4. The results of the immune database search were parsed and written into a tsv file (ImmuneDB.R, lines 52-105), which was manually curated to get the final Table_S3_immune_database_hits.xlsx.

1. Indexing the fasta file
   Parameters: ffindex_from_fasta -s db_fas.ff(data,index) db.fasta

2. Building multiple sequence alignment (MSA) for every database sequence
   Parameters: hhblits_omp -i db -d UniRef30_2020_06 -oa3m db_a3m -n 2 -cpu 20 -v 2

3. Computing hidden markov models
   Parameters: ffindex_apply -d db_hmm.ffdata -i db_hmm.ffindex db_a3m.data
   db_a3m.ffindex – hhmake -i stdin -o stdout -v 2

4. Computing context states for pre-filtering (run for each a3m)
   Parameters: cstranslate -f -x 0.3 -c 4 -I a3m -i db_a3m -o db_cs219

5. Creating a helping sorting file
   Parameters: sort -k3 -n -r db_cs219.ffindex | cut -f1 > sorting.dat

6. Sorting the markov models
   Parameters: ffindex_order sorting.dat db_hhm.ff(data,index)
   db_hhm_ordered.ff(data,index)

7. Sorting the alignments
   Parameters: ffindex_order sorting.dat db_a3m.ff(data,index)
   db_a3m_ordered.ff(data,index)

8. Renaming all a3m and hmm files with the mv command (example is shown)
   Parameters: mv db_hhm_ordered.ffindex db_hhm.ffindex

Description: Sequence of codes used to build the immune database. The codes used are shown in the order how they were used. ff(data, index): both files should be written one after another with a space between them; db: database name

6.4.8 Venn Diagram construction

The annotated data set was compared with the publicly available *T. vaginalis* proteomic data in a Venn diagram using the Rstudio package VennDiagram (Fig. 8B; Venn.R, lines 102-150). For this purpose all of the suplementary data from four *T. vaginalis* proteomic analyses were downloaded.[42][47][48][101] The tables were loaded into R studio and parsed (Venn.R, lines 11-78). Subsequently, they were all merged together and written into a single csv file (Venn.R, lines 80-100). This csv file was manually curated to get the final Table_S1_Proteome_DEA_results.xlsx.

6.5 Real-time quantitative PCR

Total RNA from TV79-49c1^{+} and TV79-49c1^{-} was isolated by the Highpure RNA isolation kit as described in the manufacturer protocol. The RNA concentration was 50 ng/µL and for cDNA synthesis 100 ng of RNA was used. RT-qPCR was performed using the Kapa SYBR FAST one-step Universal kit. The selected gene for normalization was DNA topoisomerase II (TVAG_038880) as described earlier.[57] The experiment was conducted in triplicates and GraphPad Prism 7 was utilized to analyse the data (Fig. 10).

6.6 RNA extraction from small EVs

Trizol reagent was utilized to extract RNA from the small EVs. The extracted RNA was then purified on Zymo IIC spin column (RNA clean & Concentrator-25) yielding 25-40 ng/µL of the small EV RNA. From the three independent experiments (A, B and C), in which RNA was extracted from both isogenic clones (TV79-49c1^{+} and TV79-49c1^{-}), six libraries were constructed. Inspection of the RNA integrity was done using the RNA Nano 6000 Assay Kit of the Bioanalyzer 2100 system and determination of the RNA concentration was performed by Qubit® RNA Assay Kit in Qubit® 2.0 Flurometer. Using 200 ng of RNA, small RNA-Seq libraries were prepared by the NEXTFLEX® Small RNA-Seq Kit v3 for Illumina® Platforms. The libraries were pooled in equimolar amounts and the Illumina sequencer MiSeq was loaded with a 9 pM solution. The sequencing was unidirectional and produced 50 base long reads. Libraries construction and sequencing were conducted at GeneCore facility of the European Molecular Biology

Laboratory, Heidelberg, Germany. The raw reads were made available in the European Nucleotide Archive under the accession number PRJEB50674.

6.7 RNA data processing

6.7.1 Mapping

Raw RNA-seq data were processed with cutadapt to remove the adapter (sequence: TGGAATTCTCGGGTGCCAAGG), first 4 and last 4 nucleotides and to filter all reads with the length lower than 15 nt. This yielded a data set with the reads size from 15 to 42 nt. The sequences of TVV1-4 from GenBank and the reference genome of *T. vaginalis* G3 from TrichDB database were downloaded. The sequences were manually combined into a single fasta file, which was used to build Bowtie2 indexed database with the bowtie2-build command with default parameters apart from seed, which was set to 1. The trimmed RNA-seq reads were then mapped to the built database using Bowtie2 with the following parameters: –norc, –threads 20, –end-to-end, –very-sensitive and –seed 1. The Bowtie2 mapping results (sam files) were assigned to their respective *T. vaginalis* genes using FeatureCounts from the Rstudio package Rsubread (DESeg2.R, lines 13-33). The percentage of the mapped (Bowtie2 results) and assigned (FeatureCount results) genes were manually written into the Table_S4_RNA_DESeg.xlsx.

6.7.2 Differential expression analysis

The FeatureCounts results were parsed (DESeg2.R, lines 35-57) so they could serve as an input into the PCA (Fig. 12; DESeg2.R, lines 123-134) and the differential gene expression analysis (DESeg2.R, lines 59-121), which were both done by the DESeg2 Rstudio package. The DESeg2 results were annotated using the data set of annotated transcripts from the TrichDB database (DESeg2.R, lines 136-215). The number of reads of both clones was divided by their own per million scaling factor to get normalized number of reads (rpm). The scaling factor was the number of annotated reads divided by one million (DESeg2.R, lines 216-280). Then each gene was assigned either of the three main RNA categories (mRNA, tRNA or rRNA) according to its TrichDB annotation (DESeg2.R, lines 282-328). The resulting data set was written into a csv file (DESeg2.R, lines 330-340) and manually edited to obtain the Table_S4_RNA_DESeg.xlsx. The annotated normalized DESeg2 results were used for plotting of the volcano plot comparing the two *T. vaginalis* clones with the cut-off p-value 0.01 (Fig 17A; DESeg2.R, lines 342-455). Lastly, the DESeg2 results were used to plot the anticodon usage graph of the mapped tRNA genes (Fig. 18; DESeg2.R, lines 458-510).

6.7.3 RNA distribution

To analyse the distribution of the annotated normalized DESeg2 results, the results were divided into two data sets corresponding to the two clones (DistRNA.R, lines 46-94). From these data sets, genes with p-values higher than 0.01 were filtered out. As a result two more data sets were obtained (DistRNA, lines 96-145). The non-filtered data sets were than used to construct the distribution graph of the basic RNA types: mRNA, tRNA and rRNA (Fig. 13; DistRNA.R, lines 146-323). The tRNA group was further separated based on the tRNA type (tRNA-Gly, tRNA-Ala etc., DistRNA.R, lines 325-402) and likewise used for the plotting of distribution of the tRNA types (DistRNA, lines 406-445). The filtered data sets were used to construct the pie chart with significantly enriched tRNA types (Fig. 17B, DistRNA, lines 446-509).

6.7.4 Analysis of tRNA and rRNA reads

Gene coordinates for all tRNA and rRNA reads were extracted from the gff file of the reference genome of *T. vaginalis* from the TrichDB database (Position.R, lines 1-55). Using these gene coordinates and bowtie2 results, the specific tRNA and rRNA reads were extracted via commands from locally installed samtools (the sequence of samtools commands is shown below). From the samtools commands, reads for every extracted position were obtained. These reads were parsed into two data frames for further use (Position.R, lines 57-134). The data frames of the extracted tRNA and rRNA reads were used to plot the reads length distribution graphs of total tRNA reads (Fig. 20; RNA_coverage.R, lines 11-70), total 5.8S rRNA reads (Fig. 15; RNA_coverage.R, lines 72-128), specific tRNA types (Fig. 22; RNA_coverage.R, lines 129-203) and specific rRNA genes (Fig. 16A; RNA_coverage.R, lines 205-272).

1. Conversion of sam files into bam files (run for all sam files)
   Parameters: samtools view -b f.sam > f.bam

2. Sorting the bam files (run for all bam files)
   Parameters: samtools sort -o f_ordered.bam f.bam

3. Merging the bam files from the corresponding experiments (run for the experiments A, B and C for both clones)
   Parameters: samtools merge A_f_ordered.bam B_f_ordered.bam C_f_ordered.bam f_ordered_merged.bam

4. Indexing the merged files (run for both merged files)
   Parameters: samtools index f_ordered_merged.bam f_ordered_merged.bai

5. Filtering the merged bam files based on the extracted tRNA and rRNA positions (run for both merged files and all extracted positions)
   Parameters: samtools view pos f_ordered_merged.bam > pos.txt

Description: Sequence of samtool commands used to obtain the rRNA and tRNA genes. The commands used are shown in the order how they they need to be used to function. f: name of the file; pos: contig:from-to

Afterwards, the bam files containing all RNA reads from the combined RNA-seq experiments (created with the 3. command from the above listed commands) were divided to three bam files: the first with reads 15-26 nt long, the second with reads 27-39 nt long and the third with reads 42 nt long. This was done to separate the reads from the three peaks found in the legnth distribution graph of all tRNA reads (Fig. 19). To divide combined bam files, they were filtered via the reformat.sh script from locally installed BBmap with the following parameters: minlength = 15 and maxlength = 26 or minlength = 27 and maxlength = 39 or minlength = 42. The resulting files were used to obtain the coverage of the specific tRNA genes and the specific rRNA genes employing coverageBed with one parameter -d. The coverageBed command further required the gff file of the *T. vaginalis* genome used for the read mapping.

The coverageBed results were parsed (RNA_coverage.R, lines 327-463) and every nucleotide of every tRNA gene was assigned one of the following position: 5' end, anticodon and 3' end (RNA_coverage.R, lines 466-579). Then based on the signal from the coverageBed results, fragments from the tRNA genes were extracted. According to their length and the assigned position they were annotated as one of the tRF types. For a nucleotide to be included as part of a tRF, its signal had to be at least 70% of the most covered nucleotide (RNA_coverage.R, lines 581-691). The tRF types were defined as follows: 5' tRNA halves (starting at the 5' end and reaching all the way to the first nucleotide of the anticodon loop), 3' tRNA halves (the same as the 5' tRNA halves but starting at the 3' end), tRF-5 (starting anywhere near the 5' end and not overreaching the anticodon), tRF-3 (the same as the tRF-5 but starting at the 3' end) and internal tRF (starting either at the 5' end or the 3' end and overreaching the anticodon).

The assigned tRF types were processed into pie charts showing their distribution (Fig. 20; RNA_coverage.R, lines 693-725). The extracted sequences of the fragments were written into a tsv file (RNA_coverage.R, lines 727-832), which was used for the creation of the Table_S5_tRNA_fragments.xlsx. Then the graph showing the length distribution of all tRNA reads (Fig. 19) was split by the assigned tRF types, to obtain the length distribution of tRNA reads based on the tRF types (Fig. 21; RNA_coverage.R, lines 834-881). Lastly, the same coverageBed results, which were used for tRF assignment were parsed similarly as before (RNA_coverage.R, lines 883-1042) and these parsed results were used to plot the coverage of distinct tRNA types (Fig. 23A; RNA_coverage.R, lines 1044-1099).

To obtain the coverage graphs for rRNA genes, the rRNA coverageBed results were processed identically to the tRNA coverageBed results (RNA_coverage.R, lines 1101-1263). The coverage graphs of specific rRNA genes were plotted and enriched rRNA fragments were extracted (Fig, 14 and Fig. 16B; RNA_coverage.R, lines 1265-1391). The rRNA fragments were grouped based on sequence identity to identify the most frequent rRNA fragment (RNA_coverage.R, lines 1393-1421).

6.7.5 tRF sequence extraction

The most abundant peaks in the reads length distribution graphs of the specific tRNA types were extracted (Extraction.R, lines 1-37). As major peaks were considered the peaks with at least 60% signal of the highest peak. The combined bam files were filtered based on the determined lengths (the most abundant peaks) using BBmap with the corresponding minimum and maximum lengths as described above. Subsequently, these filtered bam files were used to get the length specific coverage of the specific tRNA types with coverageBed with the same parameter as described previously. The results were parsed (Extraction.R, lines 41-150) and from the the parsing results the sequences of the specific tRFs were extracted with the same condition for nucleotides inclusion into the tRF as mentioned above (Extraction.R, lines 152-283). The Extracted tRFs were highlighted in the tRNA structures of the corresponding tRNA molecules (Fig. 23B). The tRNA structures were predicted using tRNAscan-SE.

6.7.6 Target prediction

The extracted tRF sequences with the size between 20 and 30 nt and rpm higher than 500, were subjected to online BLASTN search against the human genome with parameters automatically corrected to small reads search. Furthermore, the seed regions (nucleotides 2-8 from the 5'end) were extracted from the downloaded miRbase database of mature miRNA and from the tRFs. These seed regions were compared and the miRNA molecules with matching seeds where extracted (Exctraction.T, lines 286-354). The resulting miRNA molecules from the miRbase seed search were further analysed by the miRabel online service.

De novo target prediction was done using locally installed miRanda and TargetScan. For both of them, the default parameters were used. For the TargetScan analysis, the tRFs needed to be processed to create a tsv file with tRFs names, seed regions and organism's numerical ID (9606) against which the scanning of targets would be done (TargetScan_miRanda.R, lines 8-58). For miRanda, the whole sequences of the fragments could be used without any changes. To allow comparison between miRanda and TargetScan results, the same 3' UTR database from the Targetscan server was used. For this purpose the downloaded UTRs needed to be adjusted so they could be used as

an input for miRanda. For both programs only the 3' UTRs from humans (ID: 9606) were used (TargetScan_miRanda.R, lines 60-96). The results from both programs were parsed (TargetScan_miRanda.R, lines 98-277). During this parsing miRanda results with the total score lower than 350 (TargetScan_miRanda.R, line 227) were filtered out and TargetScan results with only 6 nucleotide match within the seed region were filtered out (TargetScan_miRanda.R, lines 261-263). Both results were combined and filtered based on the InnateDB and ImmPort database to look for immune related targets (TargetScan_miRanda.R, lines 279-361). The results from TargetScan, miRanda, BLASTN and miRabel were merged into a single file (TargetScan_miRanda.R, lines 363-490) and manually edited to get the Table_S6_RNA_predicted_targets.xlsx

6.8 TVV1 and LRV1 RdRp modeling

The TVV1 and LRV1 RdRp models were based on the sequences with the accession numbers AAA62868.1 and APT68186.1, respectively. Prior to modeling, both sequences were subjected to BLASTP searches against the non-redundant protein sequence database. The homolog sequences were filtered as follows: coverage = 0-99 and e-value = 1e-05. The RdRp domains from all of the sequences acquired were extracted (Pfam.R, lines 7-83). The domains were identified via hmmscan command from locally installed HMMER with Pfam database with the following parameters: –domtblout and –cpu 4. The conserved domains of the two models were submitted into PHYRE2 online service utilizing the intensive mode. Two models with 90% confidence for 98% amino acids were obtained. The resulting models were further refined using locPREFMD online service with the default options. The refined models had molprobity scores ∼1,7 as calculated by the molprobity online service. The binding pockets of the TVV1 model was predicted with P2rank online service on PrankWeb. The final models were visualized using PyMOL. In PyMOL, CTP was superimposed into the binding pocket of the TVV1 RdRp model from the crystal structure of the poliovirus RdRp (Fig. 3A; PDB entry: 2IM1). Further, the LRV1 and TVV1 structures were aligned in PyMOL and the structural motives of RdRp [78] were identified and manually extracted from the models (Fig. 4).

Furthermore, both of the BLASTP results of LRV and TVV1 were manually combined and sequences from RdRps with known structures were added. The structures of RdRps used were those of *Caliciviridae*, *Totiviridae* and *Picornaviridae* from PDB (PDB IDs are listed in the materials under the PDB database). MSA of the combined data sets of the RdRps was constructed with the MAFFT online service. The following parameters were used: –thread 8, –threadtb 5, –threadit 0, –reorder, –maxiterate 1000, –retree 1, –localpair. The structures of all of the RdRps of the viruses were used to construct their structural alignment in PyMOL. This structural alignment was extracted from PyMOL and utilized for manual curation of the MSA (Fig. 3B).

6.9 Cytokine detection

6.9.1 HaCaT cells stimulation by small EVs

HaCaT cells were harvested at 80-90% confluency after incubation in 5 mL of RPMI 1640 medium. Then, the cells were inoculated in fresh RPMI 1640 medium and small EVs were added. The co-incubation with the small EVs lasted 24 h and was performed at 5% CO_2 atmosphere and 37 °C. The number of small EVs was calculated according to the load of *T. vaginalis* during a vaginal infection ($4x10^5$ trichomonads/mL, 27 µg small EVs per 1 mL of HaCaT cells). After 24 h the medium was collected and centrifuged for 10 min at 1000 x g and 4 °C. Subsequently, aliquots were prepared and stored at -80 °C. Small EV isolation was done in triplicates for both isogenic clones (TV79-49c1$^+$ and TV79-49c1$^-$). Samples from each small EV isolation (A, B and C) were incubated in biological triplicates of HaCaT cells yielding the samples A1-3, B1-3 and C1-3. As a negative control, HaCaT cell conditioned medium without small EV stimulation was used.

6.9.2 Human inflammation antibody array

Initially, the cytokines released into the medium were measured using the human inflammation antibody array. First, the basic Washing Buffers were prepared as described in the manufacturer protocol. Thus 25 mL of each of the 20X concentrated Wash Buffers I and II were diluted in 475 mL of deionized water to prepare the 1X working concentration.

With the reagents prepared, each membrane was placed into a well of the provided 8-well tray and it was immediately covered with 2 mL of the supplied 1X Blocking Buffer. The tray was then covered with a lid and placed on a shaker and gently rocked at 1 cycle/sec at room temperature for 30 min. After the incubation, the 1X Blocking Buffer was aspirated from each well and 1 mL of undiluted sample of small EVs from TV79-49c1$^+$, TV79-49c1$^-$ and non-stimulated control were added into their own well with one of the blocked membranes. The tray was covered and incubated at 4 °C on a shaker at 1 cycle/sec overnight.

After the overnight incubation, each membrane was removed from the tray and placed with the printed side up into clean containers. 30 mL of the 1X Wash Buffer I was added onto each membrane. The containers were covered and placed onto a shaker and incubated at room temperature at 1 cycle/sec for 45 min. During this washing step the provided 2000X Biotin-Conjugated Anti-Cytokines was centrifuged at 5000 x g for 30 s. Then, it was diluted in 2 mL of the supplied 1X Blocking Buffer to get the 1X working concentration. After the washing, the membranes were transferred back into their original emptied wells and 2 washing steps were performed. First, 2 mL of the 1X Wash Buffer I

was added into each well. The tray was covered and incubated for 5 minutes on a shaker at room temperature at 1 cycle/sec. Then, the 1X Wash Buffer I was aspirated and the washing was repeated 3 times. Second, 2 mL of the 1X Wash Buffer II was added into each well. After covering the tray, it was incubated for 5 minutes on a shaker at room temperature at 1 cycle/sec. This washing step was repeated 2 time. After the washing steps, 1 mL of the prepared 1X Biotin-Conjugated Anti-Cytokines was added into each well and the tray was incubated overnight at 4 °C on a shaker at 1 cycle/sec.

The next day, the membranes were washed as before. After the three washing steps, 2 mL of the prepared 1X HRP-Conjugated Streptavidin was added and the membranes were incubated overnight as described above.

After the incubation, the membranes were washed as before. The washed membranes were placed printed side up onto a piece of blotting paper and dried with a piece of another blotting paper. Then the membranes were placed onto the provided plastic sheet. In a tube, 1 mL of each of the provided Detection Buffer C and Detection Buffer D were mixed and immediately 500 µL were added onto each membrane. The membranes were incubated with the detection mixture for 2 minutes without rocking at room temperature. Exactly after 2 minutes, another plastic sheet was carefully placed onto the membranes to prevent any air bubbles. The sandwiched membranes were exposed to film for: 30 s, 60 s, 90 s and 120 s.

The exposure of 60 s was set up to have the highest signal to noice ratio. From this exposure time optical density (OD) was determined in the Fiji software. A circle of uniform size was drawn around each spot and the OD was written into a table in excel. From every spot, the negative control was subtracted and normalization was done by multiplying the OD of each spot by ratio of the positive control from non-stimulated HaCaT cells and the positive control from the respective membrane (see the equation below). The respective normalized ODs from both clones were subtracted and plotted in the bar chart of differentially secreted cytokines (Fig. 5).

$$OD^{+/-}_{norm} = OD^{+/-} * \frac{OD_{Pcon}}{OD^{+/-}_{Pcon}}$$

Description: The equation for the OD normalization. norm: normalized; Pcon: positive control

6.9.3 ELISA

Selected cytokines (IL-6, IL-8, CCL5, CCL2, and IL-1β) were analysed in triplicates with ELISA kits. The procedure was identical for IL-6, IL-8, CCL2, and IL-1β, but different for CCL5. The samples for measuring CCL2 and IL-6 were 2x diluted in the 1X ELISA/ELISPOT Diluent and CCL5 in the 1X Assay Buffer A prior to the ELISA. The

other samples for measuring IL-8 and IL-1β were not diluted.

The procedure for IL-6, IL-8, IL-1β and CCL2 was as follows. The first day, the 250X Capture Antibody was diluted in the 1X Coating Buffer to obtain the 1X working concentration. Each well of the provided ELISA plate was filled with 100 µL of the 1X Capture Antibody. The plate was sealed and incubated on a shaker at 250 rpm at 4 °C overnight.

The second day, the Coating Buffer was aspirated from the ELISA plate and the plate was washed 3 times with 250 µL of the Wash Buffer. Each washing, the Wash Buffer was allowed to soak for 1 minute. After the washing, the ELISA plate was blotted on absorbent paper. Afterwards, the 5X ELISA/ELISPOT Diluent was diluted in deionized water to obtain the 1X working concentration and each well was blocked with 200 µL of the 1X ELISA/ELISPOT Diluent. The plate was covered and incubated overnight under the same conditions as previously.

The third day, the standards were reconstituted in deionized water and swirled gently. After 30 min of reconstitution, the plate was washed 1 time as earlier. Two replicates of serial dilution of the reconstituted standards were prepared. First, into 14 wells, 100 µL of the 1X ELISA/ELISPOT Diluent was added. Then 200 µL of the standard was added into 2 empty wells. The serial dilutions were done by subsequent transferring of 100 µL, starting from the highest concentration (the 2 wells with the non-diluted standard) to the lowest. Each time when 100 µL was transferred, the well was mixed well by repeated aspirations. Then the empty wells were filled as follows: 3 wells were filed with 100 µL of the 1X ELISA/ELISPOT Diluent (blank), 3 wells were filled with 100 µL of the clean medium from the HaCaT cell cultivation (medium background), 3 wells were filled with 100 µL of the samples from non-stimulated HaCaT cells (control) and 27 wells were filled with 100 µL of the samples from the small EV stimulation (the samples for CCL2 and IL-6 were 2x diluted). Technical triplicates were made from each EV co-incubation sample A1-3, B1-3 and C1-3. The plate was sealed and incubated overnight under the same conditions as previously.

The forth day, the 250X Detection Antibody was diluted in the 1X ELISA/ELISPOT Diluent to obtain the 1X working concentration. Then the plate was washed 5 times as described earlier and afterwards 100 µL of the 1X Detection Antibody was added into each well and the plate was incubated at room temperature on a shaker at 250 rpm for 1 hour. During the incubation the 100X Streptavidin-HRP was diluted in the 1X ELISA/ELISPOT Diluent to obtain the 1X working concentration. After the one-hour incubation, the plate was washed 3 times as previously and 100 µL of the 1X Streptavidin-HRP was added into each well. The plate was covered and incubated at room temperature on a shaker at 250 rpm for 30 min. Next the plate was washed 7 times as described earlier and 100 µL of the substrate was added into each well. The plate was sealed, incubated on a shaker at 250 rpm for 15 min and after the the incubation, the

stop solution was added.

The procedure for the CCL5 was similar but with the following differences:

- 1X Assay Buffer A was used instead of the 1X ELISA/ELISPOT Diluent
- The second day, the Blocking buffer was 2X Assay Buffer A
- The third day, the sample was diluted 2 times in the 1X Assay Buffer A; The ELISA plate was washed 3 times after the overnight incubation; After the serial dilution all empty wells were filled with 80 µL of the 1X Assay Buffer A and then 3 wells were filled with 20 µL 1X Assay Buffer A (blank), 3 wells with 20 µL the of clean medium from the HaCaT cell cultivation (medium background), 3 wells with 20 µL of the samples from non-stimulated HaCaT cells (control) and 27 wells with 20 µL of the diluted sample from the small EV stimulation

There was no overnight incubation step after the addition of the CCL5 samples. Instead, the 1X Detection Antibody was prepared and 50 µL was added into each well. Then, the plate was incubated on a shaker at room temperature at 250 rpm for 2 hours.

Shortly before the end of the incubation, the 100X Streptavidin-HRP was diluted in the 1X Assay Buffer A to prepare the 1X Streptavidin-HRP. The Detection Antibody was aspirated and the plate was washed 5 times as previously. Each well was filled with 100 µL of the 1X Streptavidin-HRP and the covered plate was incubated 15 minutes at room temperature at 250 rpm. After 15 min, the Streptavidin-HRP was aspirated and the washing was done 5 times as described earlier. Subsequently, 100 µL of the substrate was added and the plate was covered and incubated at room temperature at 250 rpm for 15 minutes. Immediately after the incubation, 100 mL of stop solution was added.

For all cytokines the signal was detected at 450 nm and 570 nm wavelengths. The raw intensities from the 570 nm measurement were subtracted from the 450 nm measurement. The standard curves were plotted in excel and used for quantification of cytokines in samples in pg/mL. Using Outlier calculator, outliers were calculated with the alpha option set to 0.05. The results were visualized in GraphPad prism 7 (Fig. 6).

7. Results

The effect of TVV on *T. vaginalis* infection is unclear. Some studies reported positive correlation with symptoms [11], while other did not observe this correlation.[89] As exosomes were shown to play an important role in the *T. vaginalis* virulence, we were interested whether and how the presence of TVV endosymbiont affects the exosomal cargo. To address this issue, we have derived the TVV free isogenic clone, TV79-49c1- (henceforth TVV-), by 2CMC treatment from the TVV-positive TV79-49c1+ clone (henceforth TVV+) [9] and compared proteomes and RNA cargo between these clones.

7.1 RdRp models

Our experiments revealed that 2CMC inhibits the RdRp of TVV, but the same nucleoside analog derived from adenine, 2CMA, does not. Conversely, LRV1 is inhibited by 2CMA, but not 2CMC.[80] To understand this difference, the sequences of the RdRps of TVV1 and LRV1 were analysed. First, they were scanned against the Pfam database to identify the conserved RdRp domains. The domains were separated from the variable parts of the proteins and submitted to PHYRE2 for homology modelling.

The resulting TVV1 model was analyzed via P2rank online service to identify the nucleotide binding pocket (Fig. 3A). The binding pocket was spanning large part of the model. This binding pocket accommodates an RNA molecule and a nucleotide, which is ligated to the RNA molecule. The nucleotides' precursors are nucleosides, which must be phosphorylated to become substrates for RdRps. The same is true for nucleoside analogs.[177] Thus to mimic 2CMC accommodation, CTP was superimposed into the structure and amino acid residues within 4 Å were identified to find, which amino acid residues may directly interact with the nucleoside analogs (Fig. 3A and B).

Subsequently, MSA of our models and most similar RdRps from *Caliciviridae* and *Picornaviridae* was produced by MAFFT to see the conservation of the potentially interacting amino acid residues (Fig. 3B). Within the MSA seven partially conserved sequential motives A-G were identified. Inside these motives only one likely interacting amino acid residue was not well conserved and contained different amino acid residue between the two models (Fig. 3A and B). Namely, it was Q320 for TVV and T387 for LRV. All other nucleotide binding amino acid residues were highly conserved and identical in both TVV and LRV models (Fig. 3B).

In order to inspect the possibly interacting amino acid residues further, the two models were structurally aligned. Six of the identified sequential motives A-F were also found in the models (Fig. 4). The motif G was not modelled because it was not part of the conserved RdRp domain identified via Pfam. Motives A and B form mainly α-helixes

and motives C and F consists of two anti-parallel β-sheets. In comparison, motives D and E appear to be mostly disordered (Fig. 4).

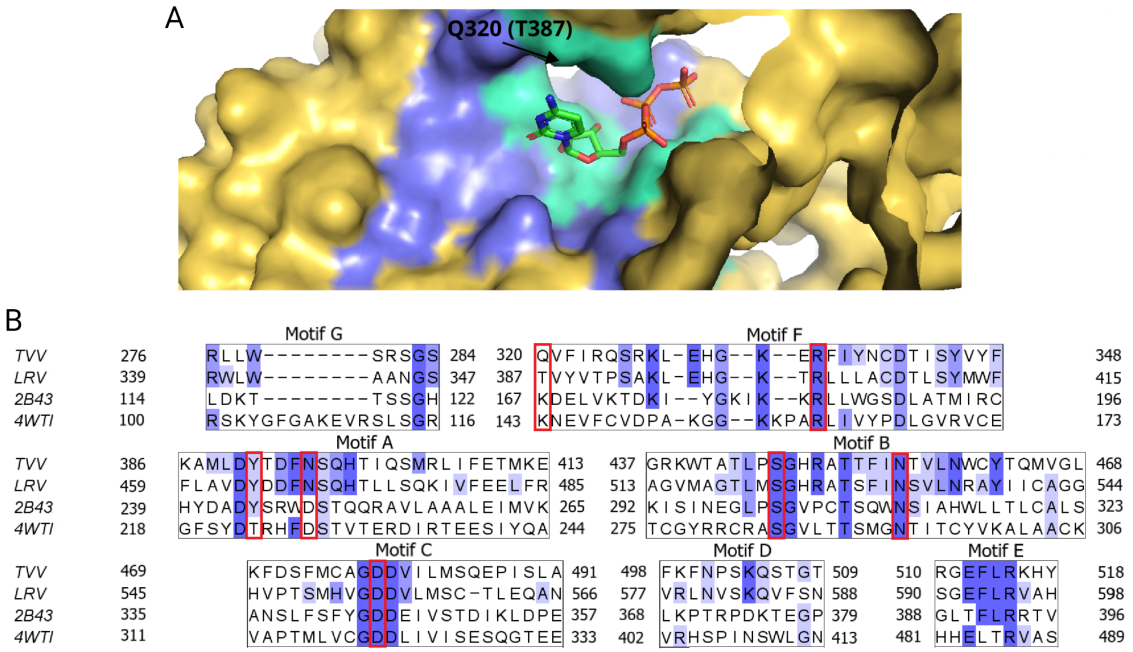

Figure 3: The TVV1 RdRp model with the predicted interacting amino acid residues. A. The model of the TVV1 RdRp binding pocket with the superimposed CTP from poliovirus (PDB entry: 2IM1; red, blue, green and orange indicating O, N, C and P, respectively). Light blue represents the predicted binding pocket and turquoise the amino acid residues, which are within the 4 Å reach. **B.** MSA of the conserved RdRp motives. The blue colour represents conservation levels of given amino acid residues. The deeper the colour the higher the conservation level. The amino acid residues marked with the red rectangles are the turquoise amino acid residues showed in A.

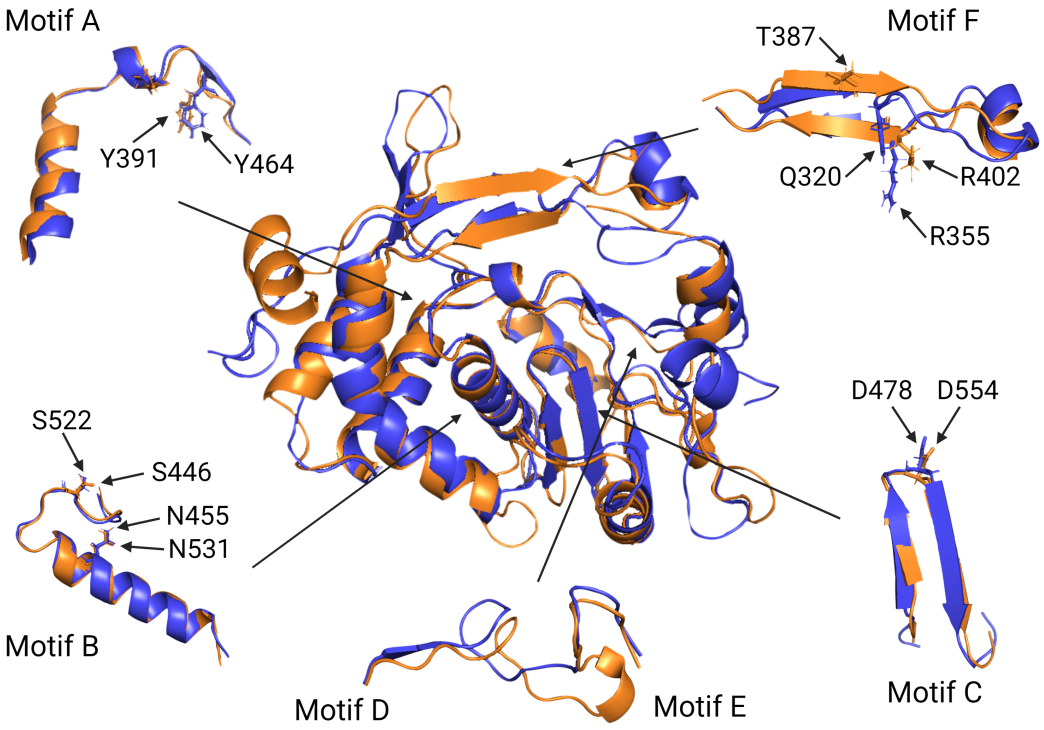

Figure 4: Conserved structural motives of the TVV1 and LRV1 RdRp model. A Structural alignment of the TVV1 (blue) and LRV1 model (orange). Arrows indicate the six identified structural motives and the amino acid residues within the 4 Å reach from the superimposed CTP.

From the six motives, A-C and F may interact with the superimposed nucleotide (Fig. 3B). These motives appear to be highly conserved in structure and the predicted interacting amino acid residues seem to be at identical positions. Exception is the motif F, which is the most variable of these four potentially interacting motives. Of note, the amino acid residues Q320 and T387 are not aligned in the structures (Fig. 4) like they are in the MSA (Fig. 3B).

7.2 Effect of small EVs on cytokine secretion

First, we decided to screen the the changes in cytokine secretion using a membrane multiplex with antibodies against 40 different cytokines and immune modulating molecules. For this purpose, HaCaT cells were stimulated with small EVs from the TVV- and TVV+ clone and their conditioned medium was collected. Conditioned medium of unstimulated HaCaT cells was used as a control.

The results showed that CCL2 and IL8 were markedly up-regulated upon the exposition of the HaCaT cells to the TVV- small EVs, whereas CCL5, IL-6, soluble TNF receptor I (sTNF RI) and dimeric platelet-derived growth factor-BB (PRGF-BB) were prominent after the TVV+ stimulation (Fig. 5).

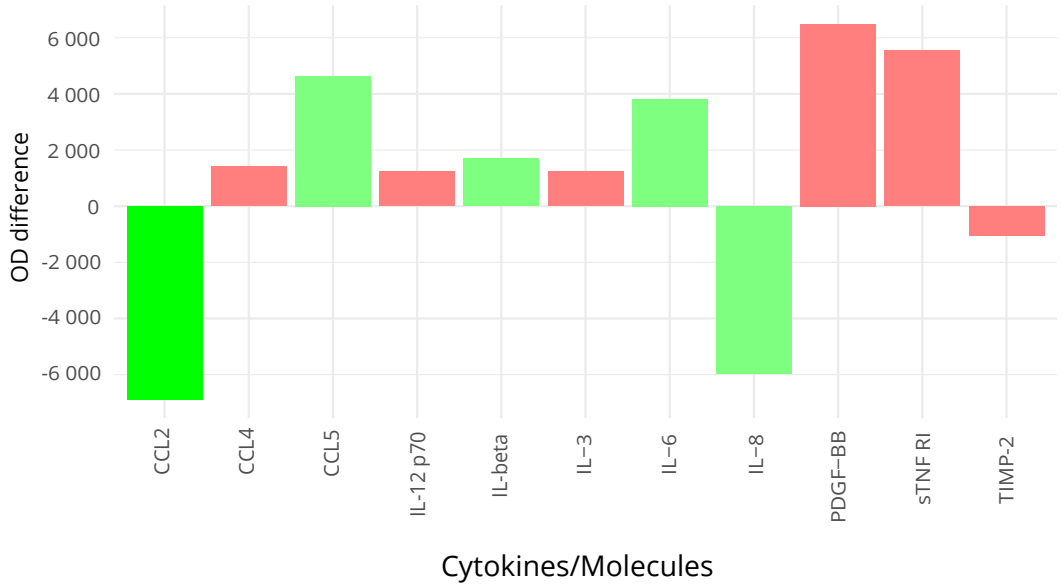

Figure 5: The difference of OD (TVV+ OD minus TVV- OD) of the most secreted inflammatory molecules by HaCaT cells upon 24h stimulation with small EVs detected by the human inflammation antibody array. Subtraction of the normalized TVV+ OD from the normalized TVV- OD is represented as the OD difference. The green bars represent cytokines/molecules, which were selected for further analysis with ELISA. The red bars show cytokines/molecules, which were not selected for further analysis. Only the cytokines/molecules with the OD difference higher than 1 000 are shown.

Based on their function and OD difference, five of the effected cytokines were selected for further experiments. IL-6 and CCL5 were chosen for their prominent role

in viral infections and their previous detection after stimulation of cells with exosomes from *T. vaginalis*.[7][42] Furthermore, IL-8, as probably the most important cytokine in *T. vaginalis* infection, was also included.[34] Lastly, two members both with high and low OD were chosen to confirm the multiplex results. As such CCL2, a monocyte attracting cytokine, and IL-1β, a caspase-1 dependent cytokine, were selected for having the highest and one of the lowest OD difference, respectively (Fig. 5).

The production of selected cytokines was analysed with ELISA. The results showed significant increase in CCL5, IL6 and IL-1β after HaCaT cells stimulation with the TVV+ small EVs (Fig. 6). These results were comparable with the multiplex analysis, in which these cytokines were elevated after the stimulation with the TVV+ small EVs (Fig. 5). Additionally, CCL2 and IL-8 were also both increased after the stimulation with the TVV+ small EVs, although CCL2 up-regulation was not significant (Fig. 6). These results were contradictory to the multiplex analysis, in which CCL2 and IL-8 were increased after the stimulation with the TVV- small EVs (Fig. 5).

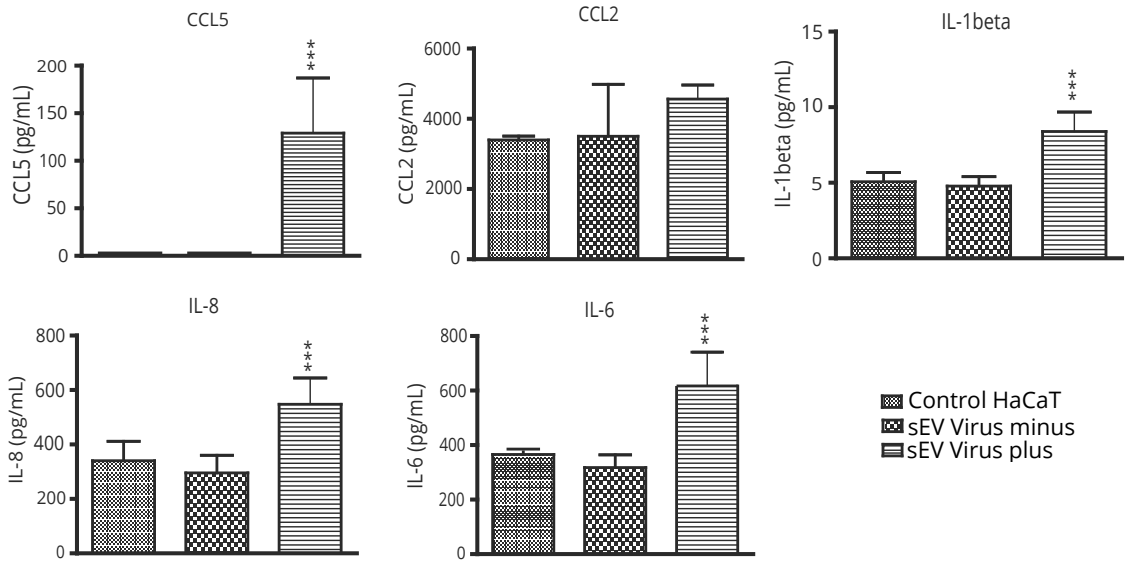

Figure 6: ELISA detection of the selected cytokines secreted by HaCaT cells upon 24h stimulation with small EVs. The bar plots represent the amounts of different cytokines in pg/mL in not stimulated control (left), TVV- small EVs stimulated HaCaT cells (middle) and TVV+ small EVs stimulated HaCaT cells (right). *** p-value < 0.0001.

7.3 Proteomic analysis

7.3.1 Principal component analysis (PCA)

Proteomic analyses often includes large number of proteins, which makes the interpretation challenging. This issue has been solved by methods, which reduce dimensionality of large data sets into just two dimensions and at the same time preserve as much variability as possible. One of these methods is PCA, which calculates so called

principle component (PC) variables from the original variables. The best PCs capturing as much variation (information) as possible are used for the construction of a PCA graph. These best PC are usually denoted as PC1 and PC2.[178] In our case this analysis is useful to see the reproducibility of the mass spectrometry experiments. Thus, PCA for all of the twelve proteomic experiments was conducted. In the PCA graph, the small EV experiments form a small cluster. The close clustering suggests high reproducibility of our small EV protemic experiments (Fig. 7).

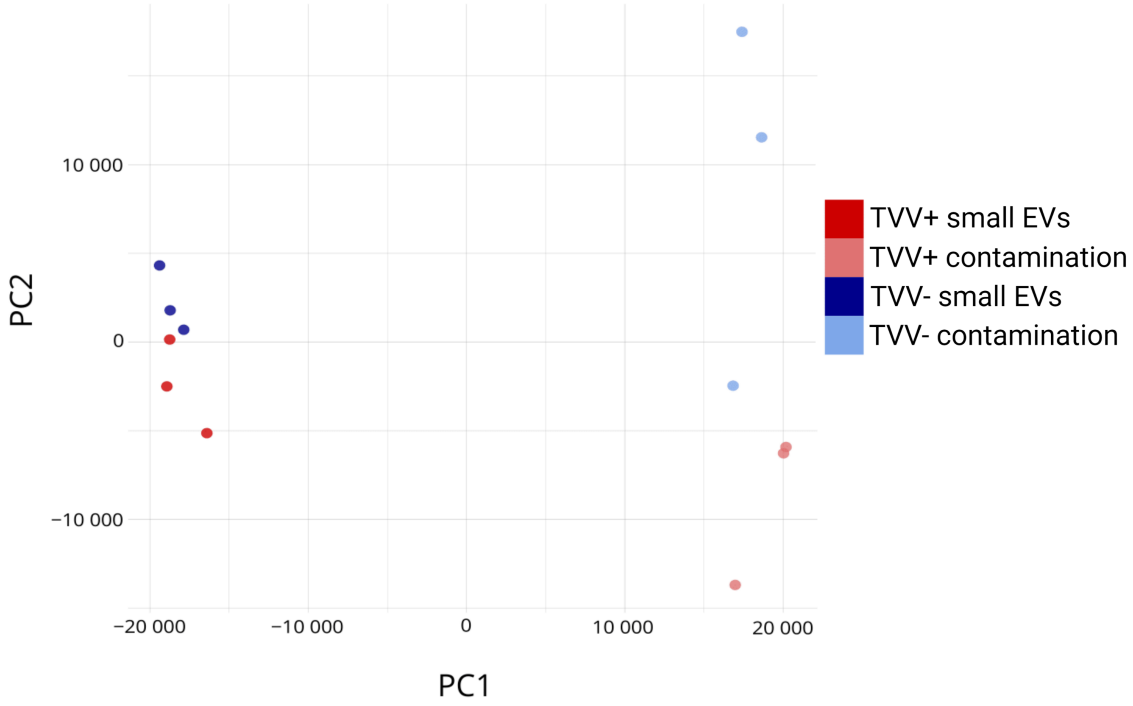

Figure 7: PCA of the detected proteins from all of the mass spectrometry experiments. A PCA plot of all proteomic experiments. Every dot represents a single experiment. The dots of different colours represent mass spectrometry experiments of TVV+ small EVs (deep red), TVV+ contamination (light red), TVV- small EVs (deep blue) and TVV- contamination (light blue).

7.3.2 Annotation and comparison with publicly available data

Altogether 1633 proteins were identified in all six small EV experiments. As a next step, we wanted to annotate these proteins and compare our results to available proteomic analyses of *T. vaginalis*. Thus the proteins were annotated using basic annotation from the TrichDB database and programs hhblits, PfamScan and eggnog mapper. Additionally, signal peptides and transmembrane domains were predicted using TargetP and TMHMM, respectively.

According to the annotation from eggnog mapper, the proteins were assigned to cluster of orthologous group (COG) categories. These categories were manually curated using the annotation from the other programs and a graph representing the percentage distribution of these COG categories was plotted (Fig. 8A).

These categories showed that 35% of the identified proteins were uncharacterized hypothetical proteins. The biggest functional group was made of proteins controlling intracellular trafficking (COG category U; 17%). Among these, there were an expanded group of Rab proteins (110 paralogues) and other proteins involved in trafficking or EV biogenesis exemplified by soluble NSF (N-ethylmaleimide-sensitive factor) attachment protein receptors (SNAREs; 15 proteins) and vacuolar protein sorting-associated proteins (VPSs; 20 proteins). The second largest COG category O (post-translational modification, protein turnover, chaperones; 14%) consisted of many peptidases. These involved membrane-bound serine peptidases (10 paralogues), GP63-like peptidases (11 paralogues) and various soluble cysteine proteases (CPs; 18 paralogues). The third largest COG category was involved in signal transduction (COG category T; 9%) with the largest protein family being protein kinases (35 proteins). All of the mentioned groups covered together 75% of the small EV data set (Fig. 8A).

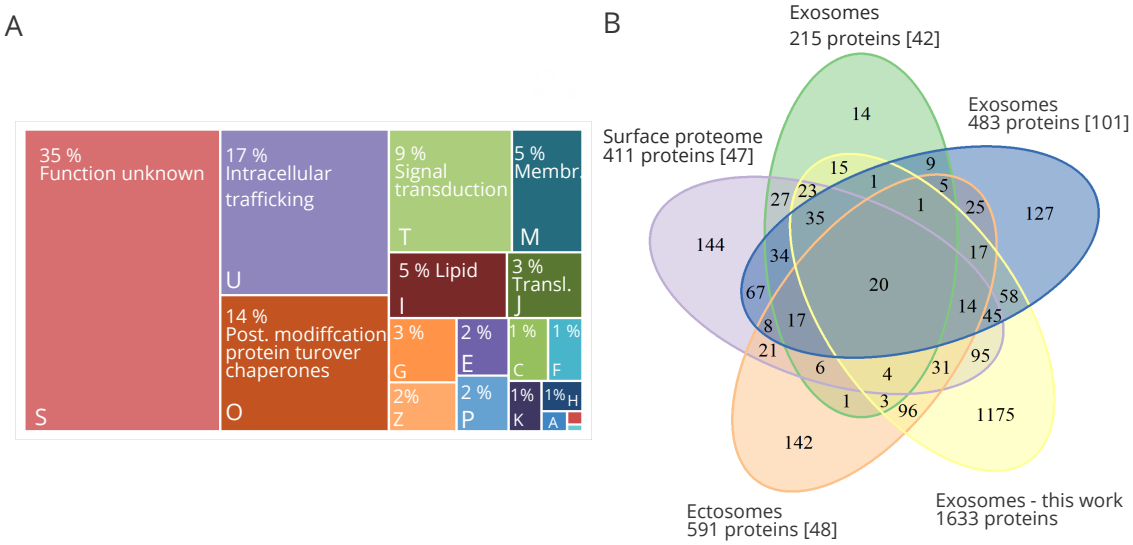

Figure 8: Distribution of the assigned COG categories and comparison with publicly available data. A. Distribution of the COG categories assigned using eggnog. The COG categories are represented with rectangles with the COG category acronym and its percentage representation. The size corresponds to the number of proteins in the COG category. **B.** A Venn diagram showing the overlaps of *T. vaginalis* proteins identified in different proteomic experiments. Descriptions at each ellipse indicate the compartment tested in the given proteomic analysis. Coresponding references are shown in rectangular brackets.

The studies, which focused on exosomal [42][101], ectosomal [48] or surface proteins [47] are compared in a Venn diagram with our results (Fig. 8B). In comparison with the available proteomic data of *T. vaginalis*, our small EV proteome is the largest. The second largest proteome is from microvesicles and consists of 591 proteins (Fig. 8B). All of the proteomic data sets are compared in the supplementary Table 1. Comparison with the proteomic analysis performed by Govender et al. was problematic, due to the identified proteins being first scanned against a human database. The proteins, which had homologs in the human database, were named after the human proteins and only those proteins

that did not have any human homologs, were assigned an unambiguous TVAG ID (45 out of 192).[7] Since TVAG IDs are used for the comparison of the proteomic data sets, only the proteins with a TVAG ID from this study [7] are shown in the supplementary Table 1.

From the two exosomal studies ∼47% [42] and ∼40% [101] of the proteins are common with our small EV proteome. Furthermore, ∼31% of the ectosomal proteins [48] are present in our data set as well. Lastly, ∼60% of the surface proteins [47] are part of our EV proteome (Fig. 8B).

7.3.3 Detection of immune protein homologs

T. vaginalis possesses a human homolog TvMIF (*T. vaginalis* macrophage migration inhibitory factor), which has similar functions like the human MIF.[69] Thus we have decided to search for more potentially important immune homolog in *T. vaginalis*. For this purpose, a database of immune related proteins based on the data from InnateDB and ImmPort was constructed. The small EV proteins were screened against this database with hhblits. This screening confirmed the annotation of the known functional human homolog TvMIF (TVAG_219770) [69], which showed the database functionality.

Furthermore, among the most significant hits, there were homologs of endoplasmic reticulum aminopeptidase 1 (ERAP1, TVAG_311790), SH2 domain-containing inositol 5'-phosphatase 1 (SHIP1, TVAG_373240) and phosphatidylinositol 3-kinases (PI3K, TVAG_236630; Table 1). SHIP1 and PI3K homologs are of interest as they control the phosphorylation of inositol rings, which serve as a binding structure for pleckstrin homology domains.[179] ERAP1 is an endoplasmatic reticulum protein, which cleaves peptides for MHCI loading. Interestingly, it can be also present on the cell surface where it facilitates cleavage of the TNF RI, effectively decreasing the signaling through TNF-α.[180] Further hits can bee seen in the Table 1.

TVAG ID	Uniprot ID	Hits	E value	Pfam domains	TrichDB annotation
TVAG_464010	P27824; P27797; Q96L12	CALX; CALR; CALR3	3.66e-145; 5.9e-105; 4.78e-90	Calreticulin (Family)	calreticulin, putative
TVAG_122020	P27797; P27824; Q96L12	CALR; CALX; CALR3	6.29e-109; 2.58e-108; 1.36e-95	Calreticulin (Family); Calreticulin (Family)	calreticulin, putative
TVAG_174100	P27797; P27824; Q96L12	CALR; CALX; CALR3	5.02e-105; 3.18e-102; 5.49e-92	Calreticulin (Family); Calreticulin (Family)	calnexin, putative
TVAG_236630	P48736; O00329; P42338; P42336	PK3CG; PK3CD; PK3CB; PK3CA	3.82e-97; 8.45e-97; 4.51e-96; 7.57e-95	PI3Ka (Repeat); PI3_PI4_kinase (Family)	phosphatidylinositol kinase, putative
TVAG_311790	Q6P179; Q9NZ08	ERAP2; ERAP1	2.5e-97; 2.72e-95	Peptidase_M1_N (Domain); Peptidase_M1 (Domain); ERAP1_C (Domain)	Clan MA, family M1, aminopeptidase N-like metallopeptidase
TVAG_373240	Q92835	SHIP1	2.1e-94	Exo_endo_phos (Domain)	skeletal muscle/kidney enriched inositol 5-phosphatase, putative
TVAG_030810	P08238; P07900	HS90B; HS90A	1.39e-90; 1.12e-88	HATPase_c_3 (Domain); HSP90 (Family)	heat shock protein, putative
TVAG_378910	P08238; P07900	HS90B; HS90A	2.57e-90; 4.42e-89	HATPase_c_3 (Domain); HSP90 (Family)	heat shock protein, putative
TVAG_028010	P20592; P20591	MX2; MX1	5.04e-86; 2.75e-74	Dynamin_N (Domain); Dynamin_M (Family); GED (Family)	dynamin, putative
TVAG_350040	P20592; P20591	MX2; MX1	1.78e-85; 2.85e-74	Dynamin_N (Domain); Dynamin_M (Family); GED (Family)	dynamin, putative
TVAG_099180	Q8WVP7; Q6UX01	LMBR1; LMBRL	6.26e-83; 1.85e-81	LMBR1 (Family); LMBR1 (Family)	conserved hypothetical protein
TVAG_062360	P20592; P20591	MX2; MX1	3.01e-82; 1.97e-71	Dynamin_N (Domain); Dynamin_M (Family); GED (Family)	dynamin, putative
TVAG_161600	Q16549; Q6UW60; P29120; P09958; P29122; Q92824; P16519	PCSK7; PCSK4; NEC1; FURIN; PCSK6; PCSK5; NEC2	1.16e-70; 2.79e-68; 4.56e-67; 9.15e-61; 2.3e-58; 4.74e-55; 3.12e-50	Peptidase_S8 (Domain); P_proprotein (Family)	Clan SB, family S8, subtilisin-like serine peptidase
TVAG_298300	P20592; P20591	MX2; MX1	8.83e-81; 5.31e-70	Dynamin_N (Domain); Dynamin_M (Family); GED (Family)	dynamin, putative
TVAG_123140	P20592; P20591	MX2; MX1	6.48e-80; 2.29e-69	Dynamin_N (Domain); Dynamin_M (Family); GED (Family)	interferon-induced GTP-binding protein mx, putative

Table 1: The first 15 most significant results from the immune database screening. The table shows the hits from the built immune database together with the hits' Uniprot ID and E value. Pfam domain annotation and TrichDB annotation of the *T. vaginalis* proteins are shown. More details are shown in the Table_S3_immune_database_hits.xlsx. CALX: calnexin; CALR: calreticulin; GED: GTPase effector domain; PK3: phosphatidylinositol 3-kinases; HS: heat shock protein; LMBR: limb development membrane protein; MX: MX dynamin like GTPase; NEC = PCSK; PCSK: proprotein convertase subtilisin/kexin

7.3.4 Comparison of small EV proteomes

After the general analysis of the small EV data set, we investigated, whether there is any significant difference in proteome between the TVV+ and TVV- clone. For this

reason differential expression analysis was conducted in Rstudio. The p-value 0.01 was set as a cut-off for significance.

The first striking difference between the two data sets is the absence of TVV RdRps and capsid proteins in the TVV- clone confirming that the 2CMC treatment was successful. More up-regulated and unique proteins were observed in the TVV- clones with 12 unique and 42 enriched proteins. Of these, the most prominent were proteins involved in intracellular trafficking (11 proteins, 20%) and hydrolases (8 proteins, 15%). In the latter group, there is an important *T. vaginalis* virulence factor GP63-like peptidase (TVAG_064330), present only in the TVV- clone (Fig. 9). In comparison, the TVV+ small EVs had lower number of differentially expressed proteins, as only 8 unique proteins were present and 12 were significantly enriched. Of the enriched proteins the most interesting is the BspA protein (TVAG_268070, Fig. 9) due to the role of the BspA proteins in *T. vaginalis* adherence.[49] However, 18 other BspA paralogues are found in our data set and these were not significantly increased in the TVV+ nor TVV- small EVs. Of the unique proteins the one worth mentioning is the repair of iron centres 2 (RIC2) protein (TVAG_167830, Fig. 9), which has been recently shown to be located in the *T. vaginalis* nucleus, where it binds DNA by its leucine zipper domain.[181]

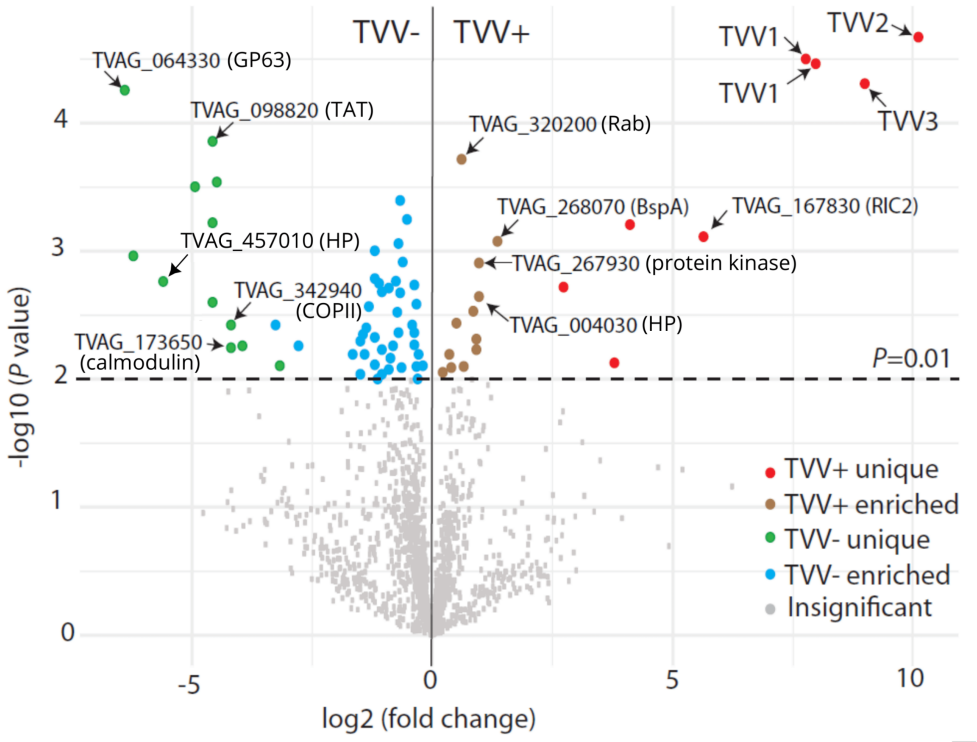

Figure 9: Differential expression analysis of the small EV proteins from the TVV- and TVV+ clone. A volcano plot showing the comparison of the TVV- (left) and TVV+ (right) clone. The dashed line indicates the p-value cut-off 0.01. Arrows indicate *T. vaginalis* proteins, whose expression was further analysed via RT-qPCR, and TVV proteins. TAT: aminotransferase; HP: hypothetical protein.

7.3.5 RT-qPCR

Further, we wanted to assess whether the change in protein abundance in the small EVs is also reflected in the mRNA levels in *T. vaginalis* cells. To evaluate this, several genes were selected based on their proteins significance in the differential expression analysis and RT-qPCR was conducted.

The results of RT-qPCR partially correlated with the quantitative proteomic data. The relative expression of mRNA of both RIC2 and BspA were significantly increased in the TVV+ clone. Similarly, a hypothetical protein (TVAG_457010) had higher relative gene expression in the TVV- clone (Fig 10). Conversely to the proteomic results, the relative mRNA levels of the GP63-like peptidase and aminotransferase (TAT, TVAG_098820) were both decreased in the TVV- clone (Fig 10). In the TVV+ clone, the mRNA level of a protein kinase (TVAG_267930) was significantly lower in contrast to its protein levels (Fig 10).

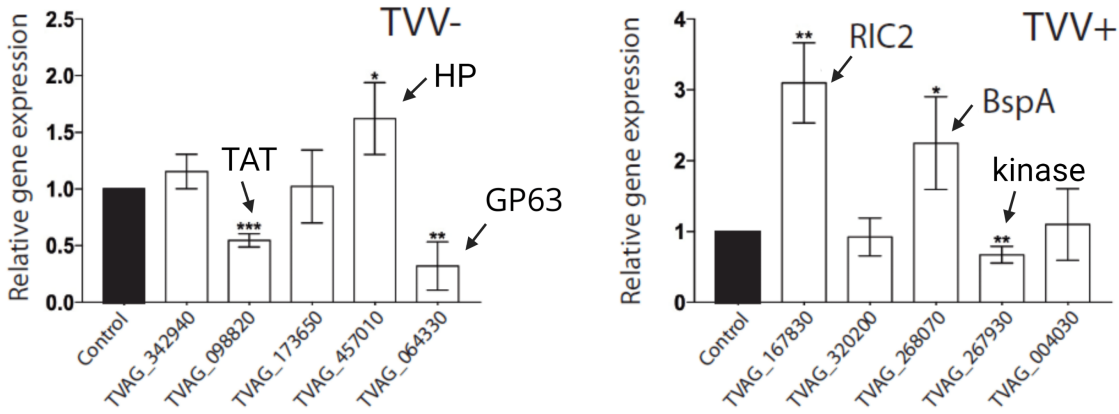

Figure 10: RT-qPCR analysis comparing the levels of mRNA in cells of the TVV+ and TVV- clone. The bar charts indicate the relative expression (normalized to TVAG_038880) of mRNA extracted from the cells of the TVV- or TVV+ clone. Asterisks represent distinct p-values as follows: * p-value <0.05, ** p-value <0.005, *** p-value <0.0005. HP: hypothetical protein

7.3.6 Protein set enrichment analysis

As a next step, every hhblits annotation with at least 90% degree of confidence was converted into its appropriate gene ontology (GO) term of biological process (BP), molecular function (MF) and cellular compartment (CC). GO term annotation allows to identify if any of the annotated GO terms or its parental or child terms are significantly over-represented. This permits the identification of groups of proteins involved in similar processes, functions or found in a similar cell compartment.

GO term enrichment analysis is best fitted for large protein data sets, in which interconnections between the protein functions are too demanding to be identified by visually inspecting annotation of every single protein. Since our cut-off p-value 0.01 was meant to identified the most differently expressed proteins, many potentially important

proteins were under the selected cut-off. Therefore, for the GO term enrichment analysis comparing the TVV- and TVV+ small EV proteome, the total of 200 proteins with the p-value cut-off 0.05 from the differential expression analysis were used. The analysis was conducted separately for CC, MF and BP GO terms.

The GO term enrichment analysis results for the TVV- small EV proteins showed specific enrichment of proteins involved in intracellular protein transport. Among these are adaptor proteins associated with clathrins, SNAREs, VPS and Rab proteins (Fig. 11A-C). In contrast, GO term enrichment analysis results of the TVV+ small EVs identified increase of proteins involved in proton transport coupled with ATPase activity (Fig. 11A-C). After mapping these GO terms to the individual proteins, we identified that they were all sub-units of a V-type proton ATPase. Altogether 11 *T. vaginalis* proteins corresponding to the V-type proton ATPase subunits B, C, D, E and H were enriched in the TVV+ small EV proteome.

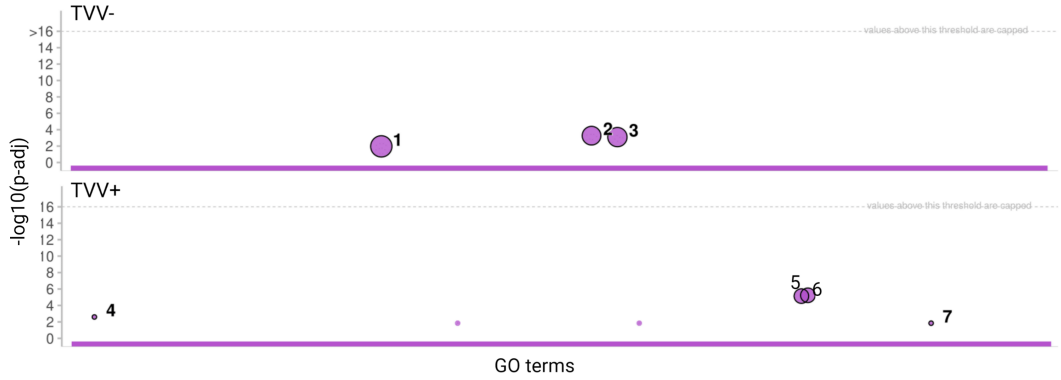

id	source	term_id	term_name	term_size	p_value TVV−	p_value TVV+
1	CC_TVV	GO:0005887	integral component of plasma membrane	14	1.1e−02	NA
2	CC_TVV	GO:0030117	membrane coat	8	5.4e−04	NA
3	CC_TVV	GO:0030131	clathrin adaptor complex	9	8.0e−04	NA
4	CC_TVV	GO:0000221	vacuolar proton−transporting V−type ATPase, V1 domain	2	NA	2.5e−03
5	CC_TVV	GO:0033178	proton−transporting two−sector ATPase complex, catalytic domain	4	NA	7.3e−06
6	CC_TVV	GO:0033180	proton−transporting V−type ATPase, V1 domain	4	NA	5.8e−06
7	CC_TVV	GO:0045261	proton−transporting ATP synthase complex, catalytic core F(1)	2	NA	1.4e−02

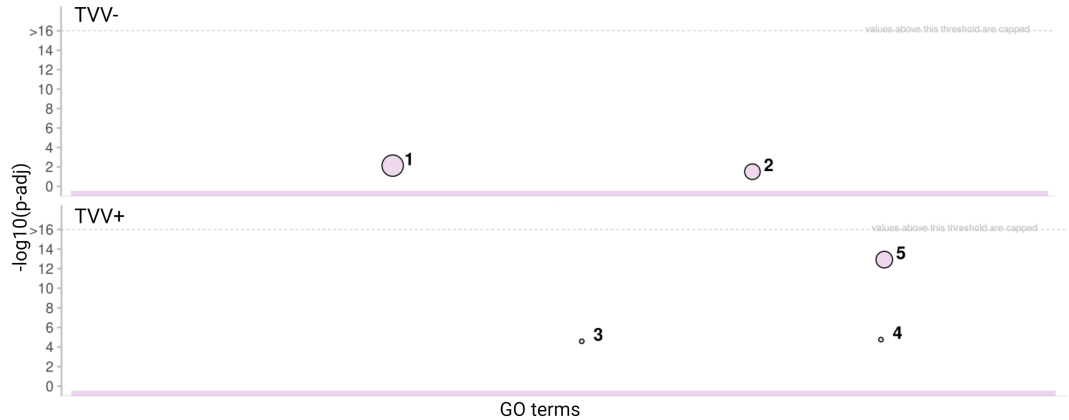

id	source	term_id	term_name	term_size	p_value TVV−	p_value TVV+
1	MF_TVV	GO:0004843	thiol−dependent deubiquitinase	20	7.4e−03	NA
2	MF_TVV	GO:0030276	clathrin binding	8	3.1e−02	NA
3	MF_TVV	GO:0008900	P−type potassium:proton transporter activity	4	NA	2.6e−05
4	MF_TVV	GO:0046933	proton−transporting ATP synthase activity, rotational mechanism	4	NA	1.8e−05
5	MF_TVV	GO:0046961	proton−transporting ATPase activity, rotational mechanism	9	NA	1.2e−13

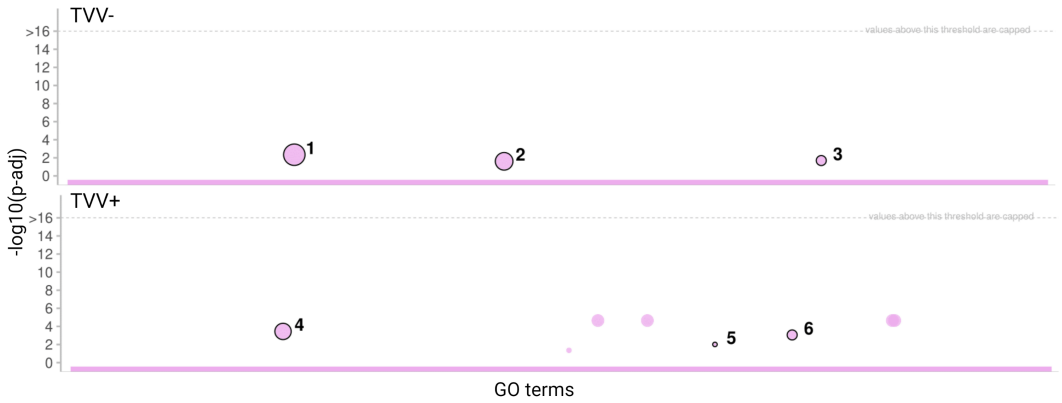

id	source	term_id	term_name	term_size	p_value TVV−	p_value TVV+
1	BP_TVV	GO:0006886	intracellular protein transport	93	4.6e−03	NA
2	BP_TVV	GO:0016579	protein deubiquitination	20	2.4e−02	NA
3	BP_TVV	GO:0048280	vesicle fusion with Golgi apparatus	3	2.0e−02	NA
4	BP_TVV	GO:0006811	ion transport	13	NA	3.6e−04
5	BP_TVV	GO:0042777	plasma membrane ATP synthesis coupled proton transport	2	NA	9.8e−03
6	BP_TVV	GO:0046034	ATP metabolic process	3	NA	8.7e−04

Figure 11: GO term enrichment analysis conducted on the proteins with the p-value $<$ 0.05 from the differential expression analysis. A. A graphical representation of the significantly over-represented GO terms of CC. **B.** A graphical representation of the significantly over-represented GO terms of MF. **C.** A graphical representation of the significantly over-represented GO terms of BP. The GO terms are depicted as filled circles, whose size indicate the number of proteins belonging into this GO term. Under each graph, there is a table with descriptions of the GO terms, which are indicated with numbers in the graphs.

7.4 RNA analysis

7.4.1 Data set evaluation using PCA

As the first step, the RNA reads were mapped to the *T. vaginalis* genome and assigned to their respective genes using the FeatureCounts function from the Rstudio package Rsubread. Then PCA of the detected reads from every RNA extraction was performed, to see the variation among the experimental replicates. In the graph, RNA extraction replicates from the TVV- clone form a small cluster, whereas the replicates from the TVV+ clone do not. This suggests higher reproducibility of the RNA extraction replicates from the TVV- clone and low reproducibility of the TVV+ RNA extraction (Fig 12).

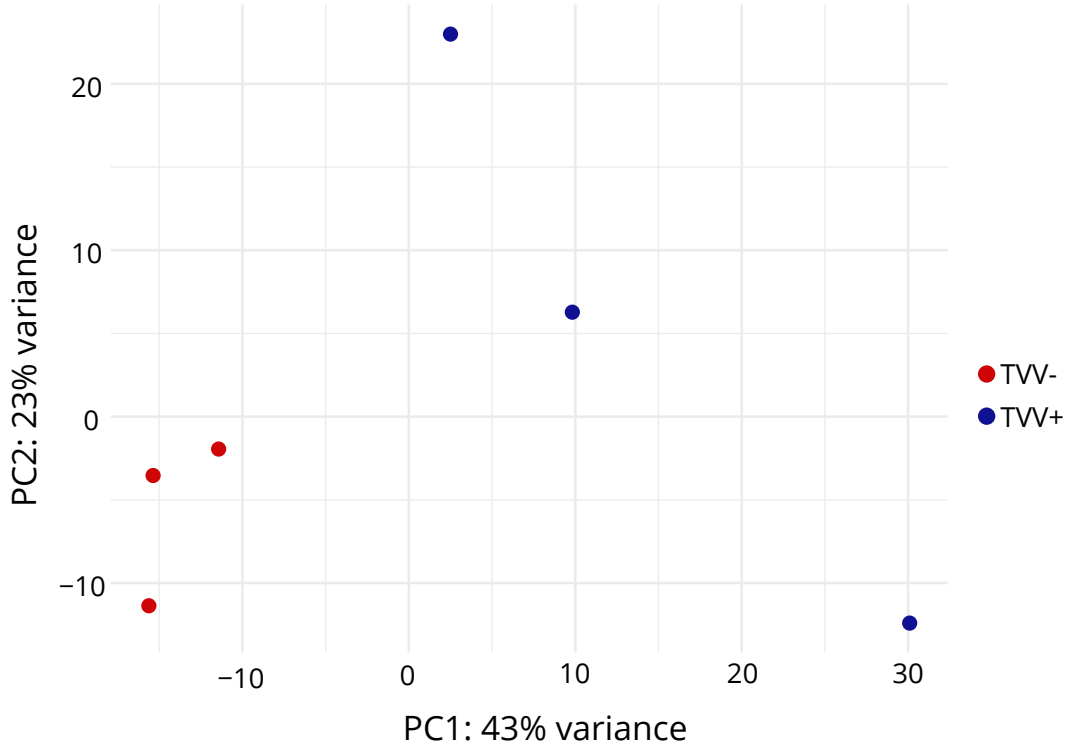

Figure 12: PCA of the reads mapped to their genes via FeatureCounts A PCA graph comparing the reads assigned to their respective genes in the three RNA extraction replicates from TVV+ (blue) and the three RNA extraction replicates from TVV- (red).

7.4.2 RNA distribution

The identified sequences were annotated according to the TrichDB database and based on this annotation they were assigned to one of the three RNA types: mRNA, rRNA or tRNA. Then, the read numbers obtained for both TVV- and TVV+ clones were normalized as reads per million (rpm). This normalization allowed comparison between the TVV- and TVV+ data set.

The rpm values for the three RNA types were summed for both clones and the percentage distribution of the three RNA types was calculated and plotted. This revealed that rRNA constituted ∼85% and ∼70% of the total small EV RNA for TVV- and TVV+, respectively. Conversely to rRNA, which was represented more in the TVV- clone, tRNA appeared to be enriched in the TVV+ clone, comprising ∼28% of its total RNA. In the TVV- clone, tRNA constituted only ∼12% of the total EV RNA (Fig 13).

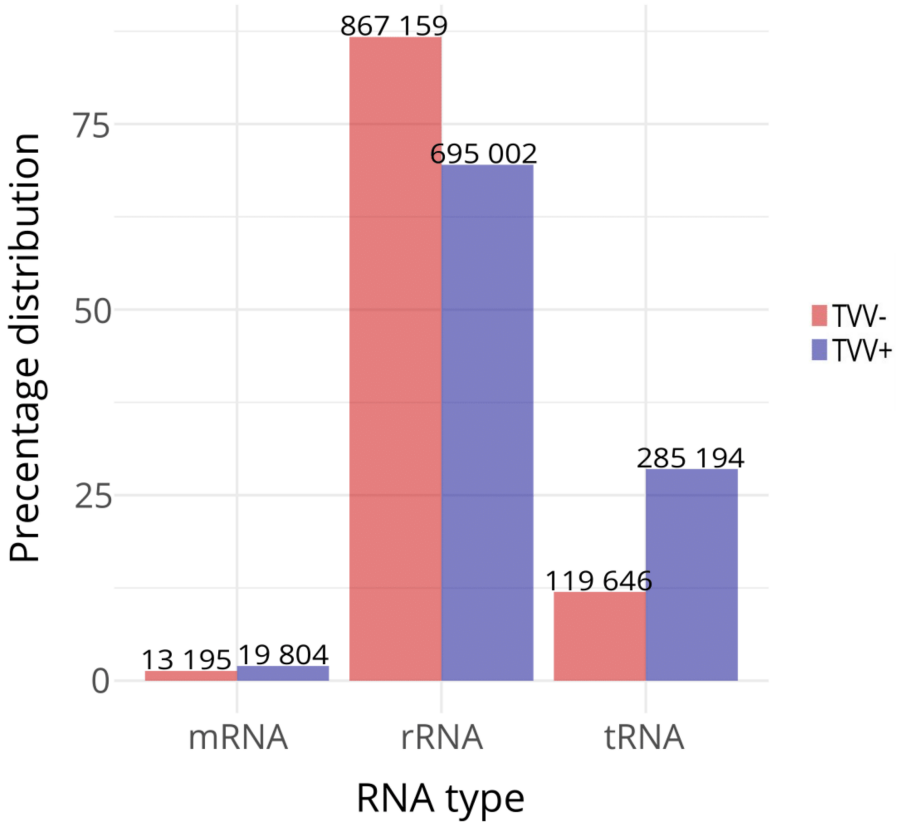

Figure 13: Comparison of the distribution of the small EV RNA reads identified in the TVV- and TVV+ clone. The bar chart depicts the total RNA percentage distribution divided into the three RNA types: mRNA, rRNA and tRNA. The numbers above the bars indicate rmp.

7.4.3 rRNA analysis

The high amount of rRNA prompted us to investigate the rRNA reads in more detail. Therefore, all reads mapping to rRNA genes were extracted from both TVV- and TVV+ clone and using the coverageBED program, the coverage of all rRNA genes was obtained.

There are three gene groups of rRNA in *T. vaginalis*: 5.8S, 16S and 28S. The genes of the respective groups have many paralogues and thus some reads map indistinguishably to multiple rRNA genes. Nevertheless, the patterns within the three types are similar hence the resolution of the groups is sufficient to estimate if specific fragments are enriched.

Due to the multi-mapping of the reads, only the representative examples of the coverageBED results are shown. Firstly, difference in the coverage between the two clones appears to be negligible (Fiq. 14). Secondly, all of the 28S and 16S rRNA genes seem to be the products of random degradation, since no clear flat peaks of >15 nt are visible in the coverage plots. Only short sharp peaks are present. These peaks are created, when many random reads originate from two positions, which do not overlap completely (Fiq. 14).

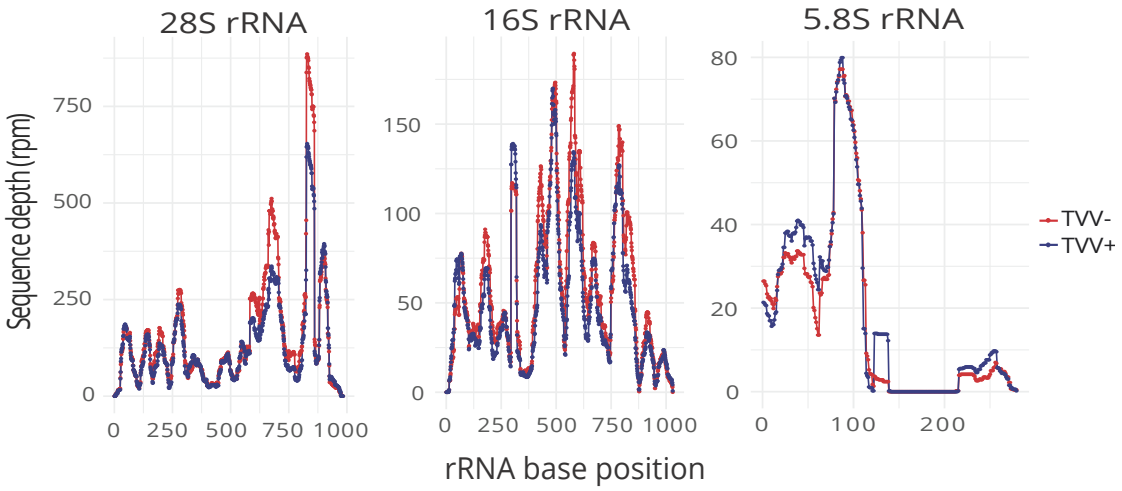

Figure 14: Representative examples of the coverage of rRNA genes indicate random degradation of the three rRNA types. Coverage graphs show rpm of every nucleotide position of representative genes of the 16S rRNA, 28S rRNA and 5.8S rRNA. Coverage of the genes for both TVV- (red) and TVV+ clone (blue) is shown.

In comparison, only a few 5.8S rRNA genes exhibited the degradation pattern and thus they were investigated further. Interestingly, plotting length distribution of the reads mapping to the 5.8S rRNA genes revealed two major peaks: 28 and 42 nt (Fig. 15).

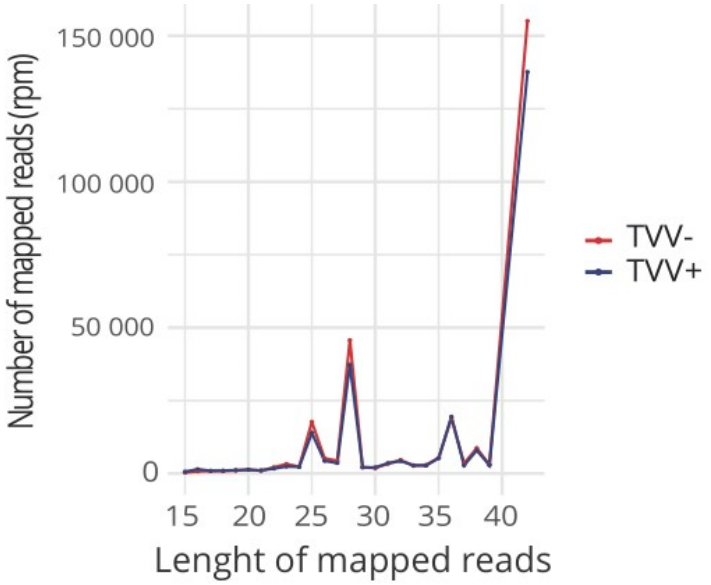

Figure 15: Length distribution of all of the reads mapping to 5.8S rRNA genes. A line graph showing rpm of the 5.8S rRNA reads grouped by their length. Red indicates the TVV- clone and blue the TVV+ clone.

The 42 nt peak consist of not fully sequenced reads, and, therefore, it is not possible to estimate, whether reads of specific lengths are enriched. In contrast, the 28 nt peak represents a possibly enriched rRNA fragment. To see if this fragment is uniformly found in the 5.8S rRNA genes, specific length distribution and coverage graphs of the genes were constructed. Indeed, there are three major coverage and read length distribution

patterns of the 5.8S rRNA genes, two of which exhibit the 28 nt peak (Fig. 16). Moreover, the nucleotide sequence of the 28 nt fragment is the same regardless of from which 5.8S rRNA it is extracted (CGAGAAGCAUGGGUGUGACAGUACUACA). Hence, there appears to be at least one short rRNA fragment enriched in the small EVs of *T. vaginalis*.

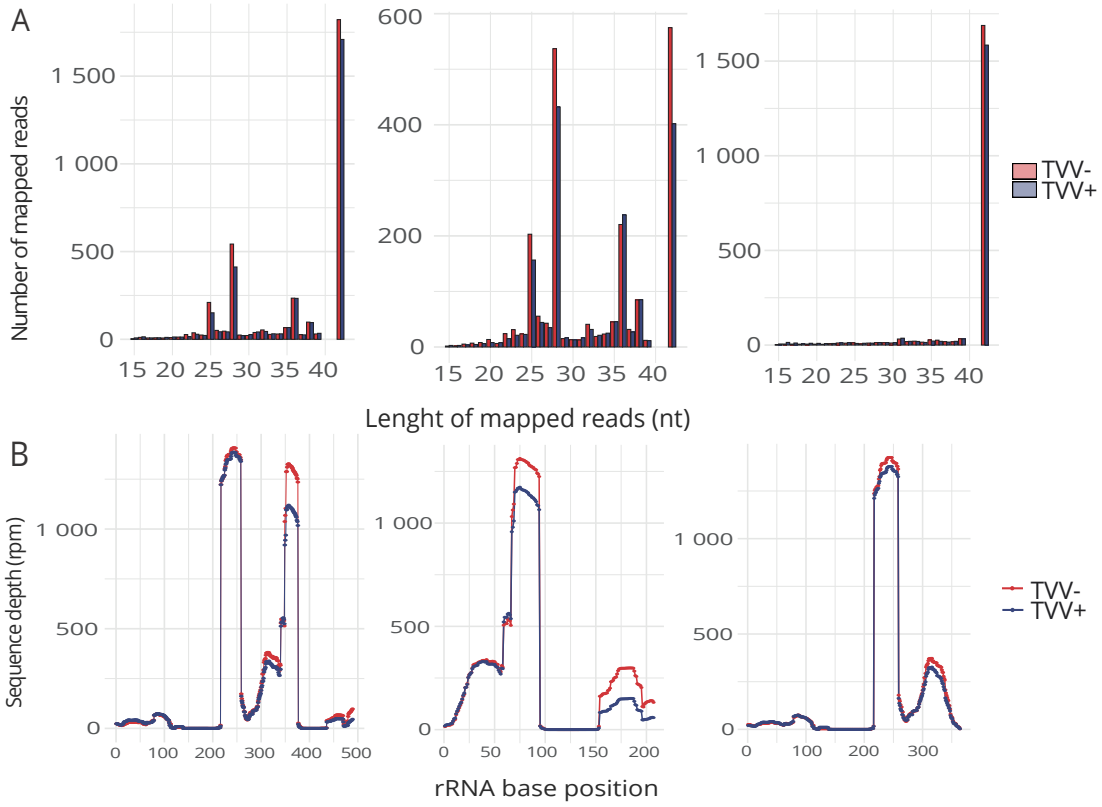

Figure 16: Length distribution and coverage graphs of representative examples of the 5.8S rRNA genes. A. Bar charts showing the number of reads in rpm of given length mapping to representative 5.8S rRNA genes. **B.** The coverage of every nucleotide in rpm of the same representative rRNA genes, which are presented in A. Red represents the TVV- clone and blue the TVV+ clone.

7.4.4 Differential expression analysis

Differential expression analysis of the detected RNA reads with the cut-off p-value 0.01 was performed to compare the RNA cargo between the TVV- and TVV+ small EVs in detail. The analysis showed that the RNA of TVV is found only in the TVV+ clone (Fig. 17A), which further confirms the successful derivation of the TVV- clone. Furthermore, we can observe a specific enrichment of reads mapping to tRNA genes in the TVV+ small EVs (Fig. 17A). In contrast, only few reads mapping to mRNA and rRNA genes are enriched in the TVV- clone. Specifically, all of the enriched rRNA genes belong to the 28S rRNA group. One of the mRNA genes encodes a myosin heavy chain and the rest are hypothetical proteins (Fig. 17A).

Similarly to the rRNA genes, tRNA genes have many paralogues in *T. vaginalis* genome. Unlike the rRNA genes, the tRNA prologues have the same length, which allows

grouping by their respective tRNA types (e.g. tRNA-Gly). Examples of these types are indicated in the volcano plot (Fig. 17A).

To determine the distribution of the enriched tRNA types, they were extracted from the volcano plot results, grouped by the respective types and their distribution based on rpm values was plotted in a pie chart. This analysis reveled that ∼50%, ∼20% and ∼20% belonged to the tRNA-Gly, tRNA-Val and tRNA-Glu, respectively (Fig. 17B).

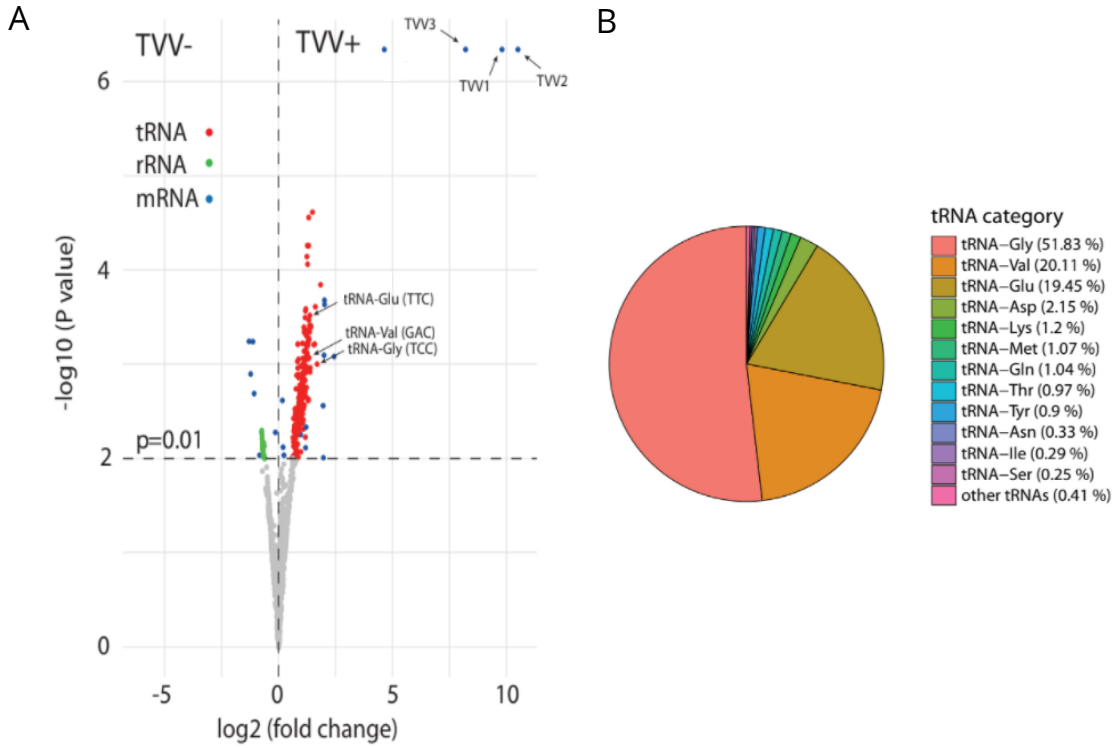

Figure 17: Analysis of the RNA reads from the TVV- and TVV+ clones. A. A volcano plot comparing mRNA (blue), tRNA (red) and rRNA (green) reads between the TVV- and TVV+ clone. Arrows indicate examples of the three most abundant tRNA types and TVV RNA. **B.** Distribution of the TVV+ enriched tRNA types from the volcano plot.

As a next step the enriched tRNA types were divided according to their anticodons to elucidate if there is an equal usage of the anticodons. This analysis revealed that for many tRNA types only a single anticodon is present. Furthermore, the three most abundant enriched tRNA types tRNA-Gly, tRNA-Val and tRNA-Glu are represented with a single anticodon by ∼99%, ∼80% and ∼75%, respectively (Fig. 18).

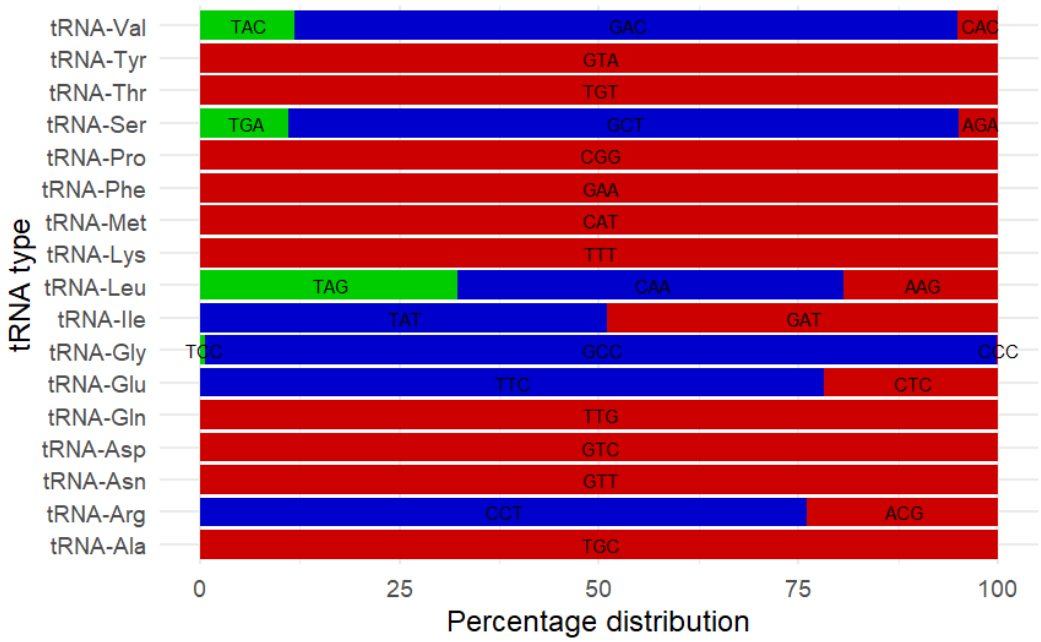

Figure 18: Anticodon usage of the enriched tRNA types A bar chart shows percentage usage of the enriched tRNA types anticodons. The anticodons are indicated in the respective bar charts of the tRNA types. They are coloured in alphabetic order, the first anticodon is red, the second blue and the third green.

7.4.5 Analysis of tRFs

All of the reads mapping to tRNA genes were extracted and grouped by their length to determine whether there are any enriched fragments (tRFs) of a given size. Indeed, two major peaks appeared at the length of 21 and 27-29 nt (Fig. 19). Importantly, the number of the reads is higher in the TVV+ clone (Fig. 19).

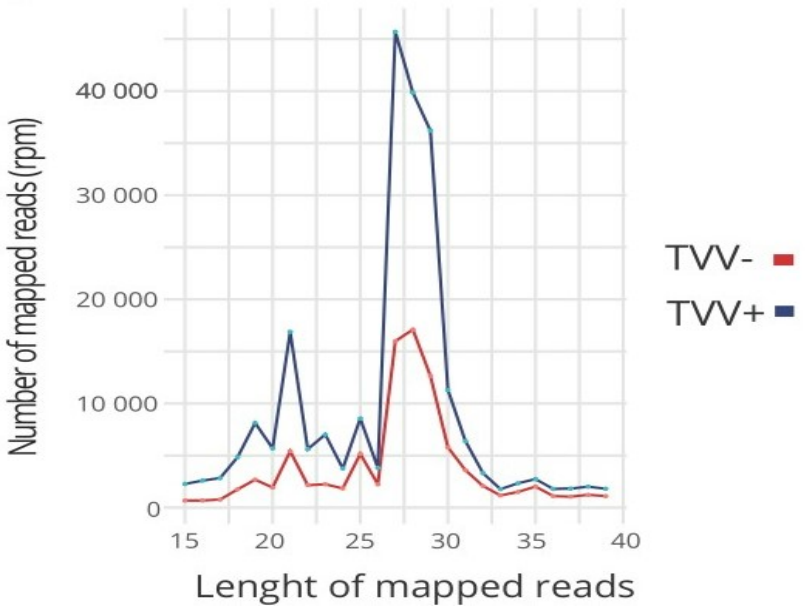

Figure 19: Length distribution of all of the reads mapping to tRNA genes. A line graph showing rpm of the tRNA reads grouped by their length. Red indicates the TVV- clone and blue the TVV+ clone.

The tRFs are part of the *T. vaginalis* exosomal cargo [119], therefore, we were interested to elucidate to which of the five tRF classes (5' tRNA halve, 3' tRNA halve, tRF-5, tRF-3 and internal tRF) our tRNA reads belong. For this purpose, the coverage of the tRNA types was obtained via the coverageBED function. Based on the position of the peak in the coverage graphs of the tRNA types, the tRFs were assigned one of the five tRF classes. The percentage distribution of the tRF classes is similar in the two clones. In both clones the most abundant are tRFs-5 with ∼87.5% and ∼89.5% in the TVV+ and TVV- clone, respectively. While tRFs-5 are more abundant in the TVV- clone, the internal tRFs are represented more in the TVV+ clone (∼8.5%) than in the TVV- clone (∼6%). The tRFs-3 are the most similar in abundance with ∼4% in both clones (Fig. 20).

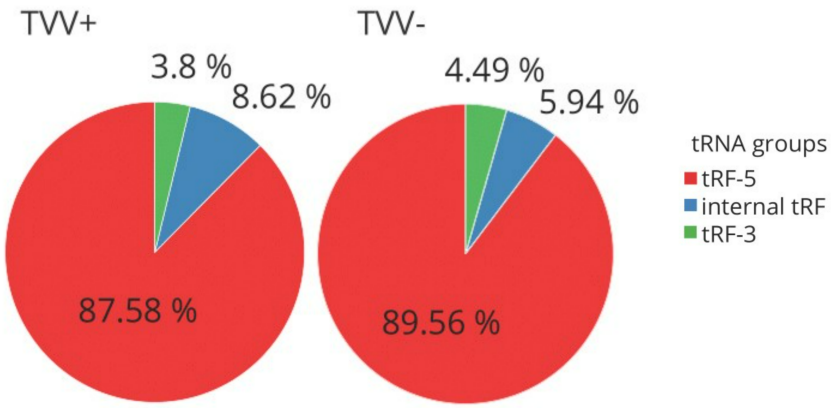

Figure 20: Distribution of the tRFs. Two pie charts show tRFs distribution in the small EV from the TVV- clone (right) and TVV+ clone (left).

Next we were interested, which tRF classes account for the 21 and 27-29 nt peaks (Fig. 19). Thus, the tRNA reads were separated according to the tRF classes and a graph was plotted based on the reads' lengths. Since there is only a minor difference in the distribution of the tRF classes between the two clones (Fig. 20), only the reads from the TVV+ clone were used. According to the graph, the tRF-5, tRF-3 and internal tRF appear to be preferentially processed into 27-29, 19 and 21 nt long fragments, respectively (Fig. 21).

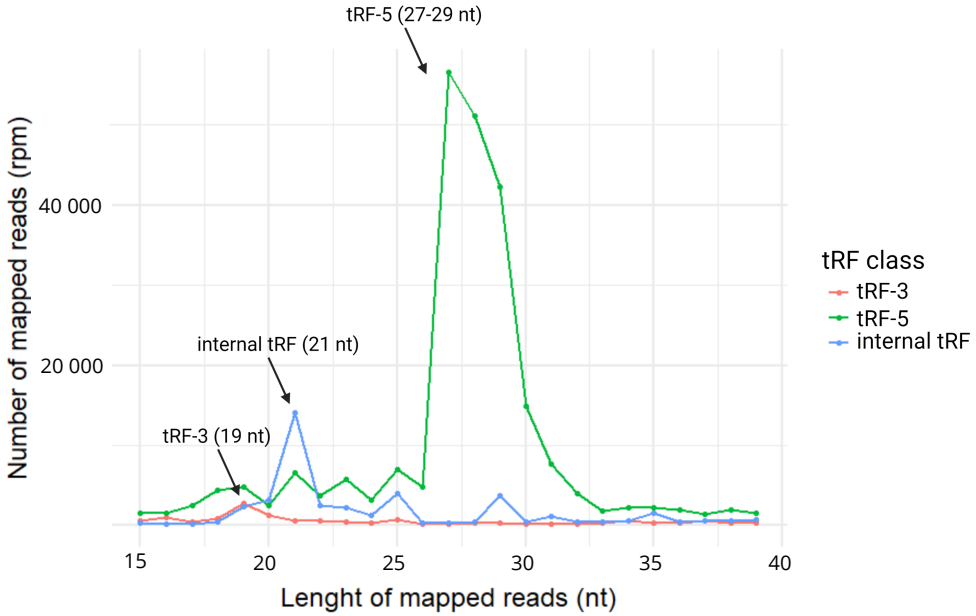

Figure 21: Length distribution of the reads mapping to tRNA genes sorted by tRF classes. A line graph shows number reads (rpm) mapped to the tRNA genes grouped by their length and tRF classes from the TVV+ clone.

As a next step, specific examples of the three detected tRFs classes were analyzed. The most abundant tRNA types were chosen and grouped by their anticodons: tRNA-Gly^{GCC} and tRNA-Glu^{TTC} (tRF-5), tRNA-Val^{GAC} (internal tRF) and tRNA-Thr^{TGT} (tRF-3). Sequences of these examples were extracted and their length distribution graphs were plotted (Fig. 22).

It is apparent that tRFs are more abundant in the TVV+ clone than the TVV- clone. Further, the tRNA-Gly^{GCC} reads are 27 and 28 nt long and have ∼44 000 and ∼32 000 rmp in the TVV+ clone, respectively. In comparison, the tRNA-Glu^{TTC} has only one major 29 nt peak with ∼22 000 rpm in the TVV+ clone. Reads mapping to the tRNA-Val^{GAC} are usually 21 nt long with ∼10 000 rpm in the TVV+ clone. Lastly, tRNA-Thr^{TGT} has two peaks of 19 and 25 nt, which have ∼600 and ∼400 rpm in the TVV+ clone, respectively (Fig. 22).

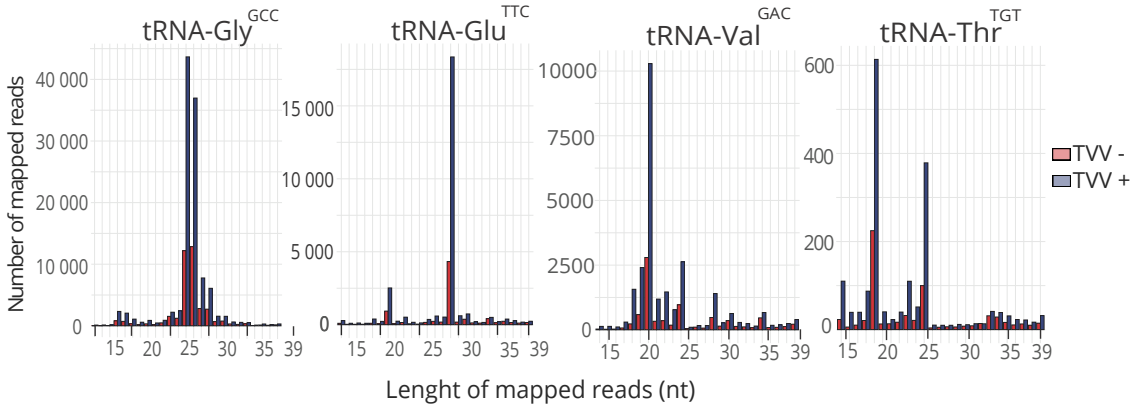

Figure 22: Length distribution of the selected tRFs. Abundance (rpm) of reads grouped by their length mapping to specific tRNA types

To determine from where the tRFs exactly originate, the coverage graphs of the selected tRFs were constructed from their extracted sequences (Fig. 23A). In the graphs, we can observe that the assignment of the tRF classes to these specific examples based on the data used to plot the pie charts of the tRF classes distribution (Fig. 20; supplementary Table 5) was conducted correctly. The tRNA-Gly^{GCC} and tRNA-Glu^{TTC} indeed originate from the 5' end. The major fragment of the tRNA-Val^{GAC} comes from the middle of its tRNA and the fragment from the tRNA-Thr^{TGT} is produced from the 3' end (Fig. 23A). Further, the structures of the tRNA molecules of the selected tRFs were predicted and the sequences of the tRFs were mapped onto the predicted structures to identify the cleavage positions of the tRFs (Fig. 23B). The structures showed that the cleavage of the tRNA-Gly^{GCC} and tRNA-Glu^{TTC} tRFs-5 occurs just before the anticodon loop. The tRF-3 of the tRNA-Thr^{TGT} is produced by cleaving its tRNA before the T loop. The internal tRF of the tRNA-Val^{GAC} is derived by cleavage of its tRNA before the anticodon loop and the T loop.

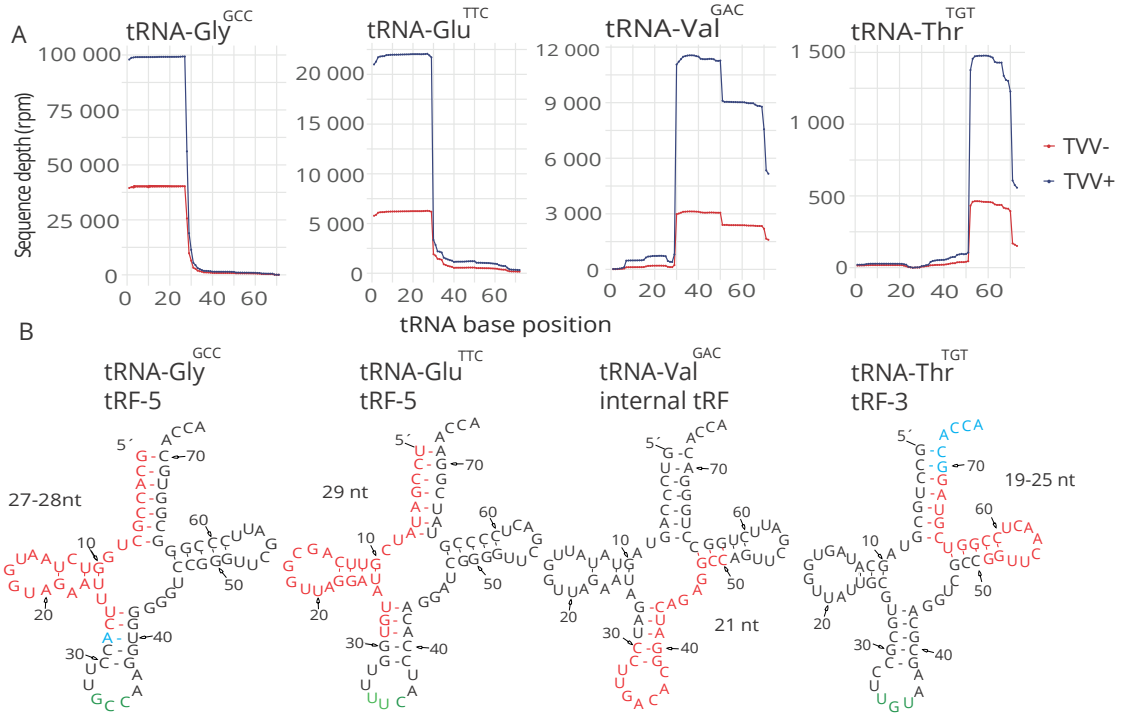

Figure 23: Coverage graphs and structures of tRNA molecules of the selected tRFs A. Represents coverage in rpm of the tRNA molecules of the selected tRFs. Red indicates the TVV- clone and blue the TVV+ clone. **B.** The predicted structures of the tRNA molecules of the selected tRFs. The colours represents the tRFs' sequences. Red stands for the first tRF variant and the combination of red and blue for the second variant.

7.4.6 Target prediction

It is well established that tRFs can influence gene expression of the host cells. AGO dependent gene silencing has been shown as one of the means, how tRFs affect the host.[116] There are two main targeting mechanisms of the AGO bound RNA molecules.

First, they are perfectly complementary with the target genes. Second, the RNA molecules do not match the targets' sequences completely, but they are complementary in the seed regions. This region consists of the nucleotides 2-8 from the 5' end of the AGO bound RNA molecule.[121]

To examine the possibility that the fragments target specific genes, they extracted sequences were first subjected to BLAST analysis against the human transcripts. This did not reveal any perfect matches. Thus, the seed regions were extracted from the sequences in Rstudio and compared to the seed regions extracted from the database of the mature miRNA molecules from the miRbase database. Using this approach, several tRFs were found to have the same seed regions as annotated miRNA molecules. To find the targets of the miRNA molecules with the complementary seeds, miRabel database was used. This database comprises of known miRNA molecules and their experimentally confirmed targets and *in silico* predicted targets. From the available targets only the experimentally confirmed were considered.

Using this database several targets were identified. From these the most interesting were for the 25 nt long tRF from tRNA-Phe^{AAA} whose seed region matched that of hsa-miR-365a-5p and hsa-miR-365b-5p. These miRNA molecules share the same targets and among those are for instance receptor for IL-7, signal transducer and activator of transcription 3 (STAT3) or spleen tyrosine kinase (SYK) (Table 2).

Apart from the BLAST search and the seed comparison, de novo target prediction for the tRFs and the single rRNA fragment was conducted with miRanda and TargetScan. The results of miRanda were filtered based on the total score, which had to be higher than 350. The total score of >350 meant that the given fragment had at least 3 seed matches with the target. The targets identified by the Targetscan analysis also must have had at least 3 seed matches and also full seed complememntarity. To achieve higher sensitivity and specificity, only the matching results from miRanda and TargetScan were considered potential targets.[182] Lastly, only those fragments with over 500 rpm were taken into account, as low abundant fragments cannot have any significant effect. With these condition several potential targets were identified (Table 2). Among those were, for instance, mothers against decapentaplegic homolog 2 (SMAD2), a target of the tRNA-Phe^{AAA} fragment, which regulates the generation of T helper 17 (Th17) cells [183], or thioredoxin reductase 3 (TXNRD3NB), a target of the tRNA-Val^{GAC} fragment, which plays a crucial role in redox homoeostasis.[184]

RNA type	Sequences	tRF type	rpm	complementary seed miRNA	miRabel targets	*de novo* target prediction
5.8rRNA	C*GAGAAGC*AUGGGUGUGACAGUACUACA	none	105728.5	bta-miR-2486-5p; cca-miR6108a; cca-miR6108g; cca-miR6108b; tca-miR-3858b-5p	none	none
tRNA-Asp^{GTC}	U*CGGUCAU*AGUGUGAUGGUUAUC	tRF-5	2562.24	none	none	QKI
tRNA-Glu^{CTC}	U*CCGACAU*CGUUCAUCGGUUAGGAUAAGC	tRF-5	3733.68	none	none	none
tRNA-Glu^{TTC}	U*CCGAUAU*CGUUCAGCGGUUAGGAUAUGU	tRF-5	18328.01	dme-miR-9370-3p	none	none
tRNA-Gly^{GCC}	G*CACCGCU*GGUCUACAUGGUAGAAUUU; G*CACCGCU*GGUCUACAUGGUAGAAUUUC	tRF-5; tRF-5	43601.73; 36932.81	none	none	RNF40; SUSD1
tRNA-Lys^{CTT}	G*CCUGUGU*AGCUCAACCGGAUAGAGCAUA	tRF-5	1432.57	ath-miR836	none	ANKRD11; HEATR6 and 33 more
tRNA-Phe^{AAA}	G*GGACUU*AGUUCAAUGGGAGAAUA	tRF-5	1423.07	miR-365 family (hsa-miR-365a-5p, hsa-miR-365b-5p etc.); mtr-miR5285a, b and c; dre-miR-193b-5p; mle-miR-12097-5p	CD99; IL7R; TNFSF10; TRPC4AP; TPM3; S1PR3; SEMA6B; SYK; TLR10; STAT3; SLC22A12; C3; CSRP1 and 113 more	TXNDC2; SMAD2 and 9 more
tRNA-Phe^{GAA}	G*GGACUUU*AGCUCACCUGGGAGAGCGUGC	tRF-5	999.57	tgu-miR-365-1-5p; mdo-miR-7263-3; ppt-miR1064-3p	none	PRX; SH3TC2 and 23 more
tRNA-Val^{CAC}	G*UCUCUGU*GUUCUAGCGGUUAGGAUCCA	tRF-5	677.54	efu-miR-9214	none	MUC19; KCNJ6 and 32 more
tRNA-Val^{GAC}	C*CUUGACA*CGGGAUCAGAGGCC	internal tRF	10066.36	none	none	GPR35; TXNRD3NB and 20 more
tRNA-Val^{TAC}	C*CUUUACA*CGGGAUAGAAGGCC	internal tRF	864.45	none	none	SOD2; ADAMTS5 and 37 more
tRNA-Val^{TAC}	G*CCCCAAU*AGUAUAUCGGUUAAAACAUAU	tRF-5	1320.45	bta-miR-2284h-3p; aca-miR-5395	none	GRIN2B; KCNJ6 and 12 more

Table 2: The predicted targets of the selected RNA fragments. The selected fragments with their specifications and potential targets are presented. The seed region is marked by italic in the fragments' sequences. Values of rpm are calculated as the mean rpm value from the coverageBed results of TVV+, from which the sequences were extracted. More details are shown in Table_S6_RNA_predicted_targets.xlsx. ADAMTS5: ADAM metallopeptidase with thrombospondin type 1 motif 5; ANKRD11: ankyrin repeat domain containing 11; CD: cluster of differentiation; GRIN2B: lutamate ionotropic receptor NMDA type subunit 2B; HEATR6: HEAT repeat containing 6; KCNJ6: potassium inwardly rectifying channel subfamily J member 6; MUC19: mucin 19; RX: retina and anterior neural fold homeobox; SEMA6B: semaphorin 6B; SH3TC2: SH3 domain and tetratricopeptide repeats 2; SOD2: superoxide dismutase 2; SUSD1: sushi domain containing 1; S1PR3: sphingosine-1-phosphate receptor 3; TNFSF10: TNF superfamily member 10; TRPC4AP: transient receptor potential cation channel subfamily C member 4 associated protein; TPM3: tropomyosin 3; TXNDC2: thioredoxin domain containing 2

8. Discussion

8.1 TVV RdRp structure

RdRps are structurally conserved proteins with 7 important structural/sequential motives [78], which were also identified in our TVV and LRV RdRp models. These RdRps are inhibited by similar 2'C methyl nucleoside analogs 2CMC and 2CMA, respectively. However, this inhibition is not interchangeable, despite the only difference between the two inhibitors being pyrimidine (cytosine) versus purine (adenine) base in the nucleoside structure.

To explain these differences in susceptibility, the TVV and LRV RdRp models were constructed. Within these models, amino acid residues important for nucleoside binding were identified. The identification was done by CTP superimposition into the TVV model, and the amino acid residues within the 4 Å range of the superimposed CTP were considered as the potentially interacting amino acid residues. From these, only a single amino acid residue inside the motif F was found to be different between the TVV and LRV models. The amino acid residues in this motif were Q and T for TVV and LRV, respectively. These amino acid residues were aligned in the MSA of the RdRp sequences, but after the structural superimposition of the two models, the two amino acid residues did not align. Actually, the T387 of the LRV model was too distant to even interact with the potential nucleoside analog. This could potentially influence the accommodation of 2CMA and 2CMC. In the case of LRV, the T387 is facing away from the binding pocket and thus the pocket could accommodate 2CMA with its larger purine base, whereas the TVV Q320 facing towards the pocket could hinder this accommodation. However, this can not explain why LRV is not susceptible to 2CMC with the smaller pirimidine ring. Moreover, hepatitis C virus (HCV) contains K, which is similar in size to Q, at the same position and it is susceptible both to 2CMC and 2CMA.[185][186] Hence, this difference probably does not explain the different susceptibility of LRV and TVV towards 2CMC and 2CMA.

Interestingly, S284T mutation in HCV conveys resistance to 2'C methyl nucleoside analogs due to the steric hindrance of the methyl moiety and the mutated threonine side chain.[187] However, this serine is conserved in both TVV and LRV RdRps. Thus, it appears there is not a single amino acid residue difference within the vicinity of the potential nucleoside analog that can explain the distinct susceptibilities towards 2CMC and 2CMA.

Virus RdRps are proteins, which change their structure substantially when an RNA and a nucleotide are bound. The degree of movement, of which the RdRp's motives are capable, dictates what can be accommodated within the binding pocket of the

RdRp.[188] Thus it is not a single amino acid residue difference that could explain the different susceptibility, but rather the entire amino acid composition of the important motives. An example could be motive B which changes its structure substantially when a nucleotide is bound.[188] Therefore, it is possible, that the observed difference between the susceptibility of TVV and LRV to 2CMC and 2CMA can be attributed to the different amino acid composition of the motives, which affects the dynamic capacity of the RdRps to accommodate nucleotides. Nevertheless, there could be a specific amino acid residue involved, which could explain the susceptibility of the two RdRps. However, X-Ray analysis of the RdRps with the respective nucleoside analogs is needed to elucidate the different sensitivity to the inhibitors.

Alternatively, 2CMA may not serve as a substrate for the purine salvage system of *T. vaginalis* constituted of purine nucleoside phosphorylase and purine nucleoside kinases.[189] Therefore, the 2CMA might not be phosphorylated in *T. vaginalis* and hence it is unable to serve as a substrate for the TVV RdRp.

8.2 TVV modulates the host immune response to *T. vaginalis*

Immune reaction to *T. vaginalis* is extremely complex as it can be influenced by the virulence of *T. vaginalis* [10][11], its endosymbionts [32][37] and the vaginal microbiome.[22] One of the endosymbionts of *T. vaginalis* is TVV, a non-segmented dsRNA virus, which has been considered a possible *T. vaginalis* virulence factor.[72] An important virulence factor of *T. vaginalis* is the secretion of exosomes, which are small single membrane vesicles with the potential to modulate the host immune response.[42] Importantly, the exosomal pathway can be hijacked by viruses, such as LRV, which belongs to the same *Totiviridae* family as TVV.[96][8] Thus we were interested in how the secretion of cytokines from HaCaT cells is affected, after stimulation with small EVs from the TVV+ or TVV- clone.

The HaCaT cells stimulation with small EVs from the TVV+ clone lead to a higher pro-inflammatory response as suggested by the increased secretion of IL-6 and 8 when compared to the stimulation with the TVV- small EVs. These results were in agreement with studies, in which co-incubation of *T. vaginalis* TVV-positive strains with Ect1/E6E7 cell line [32] and stimulation of the same cell line with *T. vaginalis* exosomes [42] led to increased levels of IL-6 and IL-8 secretion.[42] Similarly to our results, the study focusing on TVV also detected an increased level of CCL5 and IL-1β.[32] Importantly, all of these cytokines were secreted after the cell interaction with isolated TVV virion particles or by supernatant from metronidazole-treated *T. vaginalis*. The latter causes the release of virions due to the trichomonad disintegration in response to

the metronidazole drug.[32]

The detected chemokines CCL5 and IL-8 can be both induced by viral infections.[190] Furthermore, IL-6 is a cytokine also secreted during viral infections and it can either lead to the resolution of the infection or its exacerbation.[191] This viral-dependent cytokine secretion, together with our results and the results of the other study [32] implies that the TVV presence could be the main cause of the secreted cytokines. Surprisingly, the two most differentially expressed cytokines, CCL2 and IL-8, were originally elevated in the TVV- small EV stimulation as measured by the multiplex array. This inconsistency could be explained by saturation of the multiplex array, which led to false results as the membrane in the case of TVV- probably had more anti-cytokines antibodies against CCL2 and IL-8 than the TVV+ membrane.

There were several differences between our study and the above-mentioned studies.[32][42] The main difference was the cell lines used. In our study, the TVV effect on exosomal-induced cytokines was not assessed in Ect1/E6E7 cells, but in HaCaT cells. These keratinocytes express, among others, TLR2-4 [192], which are important in *T. vaginalis* sensing.[32][36] Furthermore, HaCaT cells are spontaneously immortalized keratinocytes [193], which makes them superior to the E6E7 cell lines in the assessment of the viral effect on the immune response. The reason is that these cell lines were immortalized using the papilomavirus oncoproteins E6 and E7 [194], which are known for interfering with the innate immune response.[195] Importantly, in the exosomal study, TVV presence was not assessed. However, some of the used *T. vaginalis* strains were TVV positive, for instance, the strain T1.[196] Nevertheless, it is not described which strains were used in which experiments.[42] Despite these differences, we acquired very similar results to the two mentioned studies.[32][42]

According to our results, the small EVs with TVV appear to be pro-inflammatory. However, exosomes are generally anti-inflammatory as has been shown in an experiment of the exosomal study.[42] In this experiment, the Ect1/E6E7 cells were preincubated with exosomes and trichomonads were added subsequently. Compared to controls, the preincubation led to lower IL-6 and IL-8 secretion after the Ect1/E6E7 were stimulated with trichomonads.[42]

Another study focused on the effect of *T. vaginalis* exosomes in End1/E6E7 cells and PBMCs. The results of this study showed that IL-8 and CCL5 are increased, but conversely to our results, upon the stimulation with exosomes from a TVV-negative *T. vaginalis* strain.[7] Furthermore, the stimulation of PBMCs with the TVV-negative strain led to higher secretion of IL-6, IL-8 and TNF-α when compared to the stimulation with a TVV-positive strain. The PBMCs were further stimulated with macrophage-activating lipopeptide-2 (MALP-2), a TLR2 and 6 agonist. This led to increased secretion of IL-8 and IL-10. However, when the conditioned medium from the End1/E6E7 cells was taken, the PBMCs reacted to MALP-2 by lower secretion of IL-8 and IL-10 when the

End1/E6E7 were incubated with exosomes from the TVV+ strain prior to the PBMC stimulation with the MALP-2.[7]

The study described above implies that exosomes from TVV+ *T. vaginalis* strains are immunosuppressive. However, this directly contradicts our results. There are four main differences between our and the other exosomal study.[7] First, in our study, small EVs were isolated from the medium after 2.5-hour incubation at 37 °C, while in the other study the incubation lasted 24 hours. An explanation for such long incubation was not provided. Second, we included two steps in our experiment to ensure as little contamination of the small EV proteins as possible: a fractionation step on OptiPrep and a contamination subtraction step based on the proteins found in the supernatant from the small EV isolation. No such steps were included in the EV extraction protocol of the other study. Third, we identified TVV proteins in our proteomic analysis indicating the presence of TVV. The TVV proteins were not identified in the analysis of the other study. Forth, the isogenic *T. vaginalis* clone used in the other study was derived through long-term cultivation, whereas in our experiments we used the TVV- clone derived through a short 2CMC treatment. Long-term cultivation is generally known to change the properties of the cultured organism. This all could potentially influence the results of the experiments.

TVV appears to influence the immune system similarly to LRV. LRV1 is the endosymbiont of leishmania and its presence has been connected to higher secretion of IL-6, CCL5, INF-β and TNF-α.[95] The secreted INF-β was shown to cause more severe leishmaniasis by lowering the caspase-1 activation in macrophages thus promoting leismania survival.[97] Importantly, LRV was found in exosomes and exosomes from an LRV-positive strain were shown to exacerbate leishmaniasis, when LRV-negative strains were co-injected with exosomes from LRV-positive strains into mice.[96] TVV causes similar cytokine secretion in HaCaT cells and End1/E6E7 cell line [32] like LRV1. Moreover, based on our proteomic, RNA-seq and electron microscopy results [172], we can confidently state that TVV is present in the *T. vaginalis* small EVs. Hence, continuous shedding of *T. vaginalis* exosomes could deliver TVV into different host cells and exacerbate inflammation by, so far, unknown means.

8.3 TVV influence on exosomal cargo

Several mRNA levels were shown to be altered by our RT-qPCR results in the whole cell of the TVV+ clone. However, these mRNA levels did not always correlate with the corresponding protein levels in small EVs, which suggests that not only expression but also packaging can be altered by TVV presence. It is known that many viruses, such as LRV and HCV, hijack the exosomal pathway for their spreading and that such hijacking alters the exosomal cargo.[96][8] The ESCRT machinery is indispensable for the

exosomal cargo sorting and release of exosomes.[98] Viruses often alter the expression of the ESCRT proteins [197] or other typical exosomal proteins like tetraspanins.[198] This alternation can be achieved via the viral proteins themselves or by the influence of the viral translation on mRNA translation in the cell. The first case is exemplified by the Ebola virus protein VP40, which increases the expression of several ESCRT proteins.[197] The latter one is the case of LRV, which appears to change the translation efficacy of several proteins by occupying the translation machinery.[96] Both LRV and TVV possess only two ORFs, which encode their RdRps and capsid proteins [199][76], thus TVV probably affects the exosomal cargo in a similar manner as LRV.

To study the effect of TVV on exosomal cargo, we have conducted mass spectrometry and RNA-seq experiments. Such experiments are sometimes difficult to replicate and thus to ensure that our proteomic and RNA-seq experimental replicates are reproducible, PCA analysis was conducted. PCA is a method of dimensionality reduction, which takes multidimensional data and creates two new dimensions (variables) from the original variables. These new variables represent as much information about the variation of the data as possible. Thus when these new variables are plotted against each other they show the overall variation of the data.[178] In our case, the PCA revealed that the protein detection in exosomes was highly reproducible, but the RNA detection in the TVV+ clone was not. The TVV+ clone is infected by TVV1, TVV2 and TVV3. However, it was not tested whether all the trichomonads from this clone are infected by all of the TVV species. Possible variability in the TVV infections may explain the high variability among the TVV+ RNA cargo replicates.

8.3.1 Proteins

Altogether we identified 1633 exosomal proteins. This number of proteins is similar to the findings in exosomes of some parasites, exemplified by leishmania (∼1000∼1500) [200][96], and of many human cell lines (∼2000∼2500).[201] However, previous *T. vaginalis* proteome analyses of exosomes reported 483 [101], 215 [42] and 241 proteins [7], which makes our proteome the largest one yet. This striking difference in the number of identified exosomal proteins could be explained by various methods used for exosomal extraction and mass-spectrometer sensitivity. Nevertheless, ∼40% of the proteins identified in the previous proteomes by Twu et al. [42] and Salas et al. [101] are common with our data set. The latest exosomal proteome analyzed by Govender et al. [7] was annotated using human databases, and only those proteins that did not have human homologs were assigned their unambiguous TVAG ID.[7] Therefore, a direct comparison between their and our data sets was impossible. Of note, Salas et al. [101] and Twu et al. proteome [42] share only 122 proteins, which is ∼56% and ∼25% of the respective proteomes. Strikingly, there is only a two-protein overlap between the Twu et al. [42] and Govender

et al. proteome.[7] Hence more studies with comparable methodologies and ideally with a larger set of well-characterized *T. vaginalis* strains are needed to truly ascertain, which proteins are part of the *T. vaginalis* exosomal cargo.

Among the 1633 proteins, there are the typical exosomal markers like tetraspanins (e.g. TVAG_019180) or heat shock proteins (e.g. TVAG_185750). Apart from these, we identified various adhesive proteins and protein peptidases involved in *T. vaginalis* virulence.

From the adhesins, the most intriguing are BspA proteins with ∼900 putative homologs found in the *T. vaginalis* genome. Of these, ∼190 possess a transmembrane domain [49] and 19 of these were found in our data set including the single BspA (TVAG_268070) enriched in the TVV+ small EVs. Importantly, the mRNA level corresponding to this protein was also increased in the *T. vaginalis* cell. It is tempting to speculate that, due to this enrichment, TVV might increase the adhesiveness of *T. vaginalis*. Indeed, in a surface proteome comparison of low adherent strains and high adherent strains of *T. vaginalis*, it has been found that expression of a single protein from a high adherent strain in a low adherent strain could increase its adhesiveness towards VECs.[47] Nevertheless, the BspA up-regulation and its consequences need to be further studied.

On the contrary, we observed the enrichment of *T. vaginalis* peptidases in the TVV- clone. Overall, two GP63-like and two serine peptidases were enriched in TVV-. Moreover, a single GP63-like peptidase was present only in the small EVs of the TVV- clone. However, the mRNA level of this GP63-like peptidase was significantly lower in the TVV- trichomonad cells. Thus the exosomal enrichment is not due to higher transcription but rather due to differential cargo selection. Both types of the mentioned proteases were implicated in *T. vaginalis* cytotoxicity [58], and, therefore, their enrichment in the small EVs could have a potential role in host-pathogen interactions. Nonetheless, similar to the enriched BspA, more studies are needed as, for instance, any host targets of these peptidases are yet to be identified.

Aside from the classical *T. vaginalis* virulence factors, a protein complex involved in proton transport, V-type proton ATPase, and a DNA binding protein, RIC2, were identified to be enriched in the TVV+ clone. RIC2 was also shown to have elevated mRNA levels in the whole trichomonads of the TVV+ clone. Yet very little is known about these proteins. Until now, RIC2 has been shown to localize in the cytosol and nucleus and bind the *T. vaginalis* DNA.[181] Interestingly, its leucine zipper-like motif resembles the one of the c-Fos/c-Jun heterodimer named activator protein 1 (AP-1). This protein is a crucial transcription factor in T cells, in which it is activated by co-stimulatory molecules engagement exemplified by CD28.[202] Due to this resemblance, the potential role of RIC2 as an exosomal protein needs to be investigated further. V-type ATPases were suggested to play a role in exosomal biogenesis [203], but any information about V-type ATPases and virus-containing exosomes are lacking.

Analyses of small EV proteins also revealed several noteworthy homologs of human immune-related proteins. Among those worth mentioning is the ERAP1 homolog (TVAG_311790). ERAP1 is usually found in the endoplasmic reticulum, where it processes peptides for MHCI loading. However, it has been also suggested to be involved in the shedding of the sTNF RI.[180] In our multiplex array, higher OD intensity of sTNF RI was detected in the TVV+ clone, in spite of the ERAP1 homolog not being enriched in either of the clones. However, the array's results may be inaccurate as in the case of CCL2 and IL-8. Therefore, an ELISA test is needed to confirm the results. Importantly, sTNF RI was found to be significantly increased in cervicovaginal lavage during symptomatic trichomoniasis.[29] Thus this potential ERAP1 homolog and its connection to the sTNF RI should be further investigated.

8.3.2 RNA fragments

Our RNA-seq analysis of small reads (50 nt long) showed that the major RNA type found in our small EVs is rRNA composing ∼85% and ∼70% of the small EV RNA cargo for the TVV- and TVV+ clone, respectively. The tRNA represented ∼12% and ∼28% in the small EVs of the TVV- and TVV+ clones, respectively, and mRNA constituted only ∼2% in both clones. The representation of rRNA is comparable to what was reported in leishmania or trypanosoma exosomes, in which rRNA constituted ∼90% of the total exosomal RNA.[102][120]

The amount of rRNA prompted us to investigate it in more detail. There are three types of rRNA in *T. vaginalis*: 5.8S, 16S and 28S. From these 16S and 28S rRNA appeared to be products of random degradation events. Conversely, 5.8S rRNA reads displayed 28 and 42 nt read enrichment, but the 42 nt reads are not fully sequenced. Thus, only the 28 nt read is of interest. Just like tRFs, rRNA fragments are being recognized as means of host-pathogen interaction with many potential targets.[121] Therefore, the single 28 nt long rRNA fragment found in our *T. vaginalis* small EVs warrants further investigation.

Interestingly, previous analysis of small RNA molecules in *T. vaginalis* exosomes showed that rRNA represents less than 1% of the RNA species and that ∼88% of the total RNA mapped to tRNA.[119] In this analysis, a different *T. vaginalis* strain was used, which may partially explain the observed difference between this and our study. There are also some differences in EV isolation, which may influence the results. Nevertheless, more studies on *T.vaginalis* exosomes focusing on small RNA composition are needed to clarify the observed differences in the RNA composition.

After the rRNA analysis, we were interested in whether the rRNA enrichment in the TVV- clone and the tRNA enrichment in the TVV+ clone are statistically significant. Therefore, differential expression analysis was conducted, which revealed that several

tRNA types are enriched in the TVV+ clone with the p-value <0.01. Interestingly, ∼50%, ∼20% and ∼20% of the enriched tRNA reads mapped to the tRNA-Gly, tRNA-Val and tRNA-Glu, respectively. The three main tRNA types also had a strong bias toward anticodon usage with tRNA-Gly^{GCC}, tRNA-Glu^{TTC} and tRNA-Val^{GAC} constituting ∼99%, ∼75% and ∼80% of the respective tRNA types. The tRNA types tRNA-Gly, tRNA-Val and tRNA-Glu are often representing the majority of reads in exosomes of *T. cruzi* [111][204] and *T. vaginalis*.[119] In the study focusing on tRFs in the *T. vaginalis* exosomes, the anticodon bias for the tRNA-Gly and tRNA-Glu is the same as in our study, with the GCC and TTC being the most represented anticodons for the respective tRNA types.[119]

Since tRFs are known as important gene regulators, we decided to study them further. We assigned our reads to the five tRF classes (5' tRNA halve, 3' tRNA halve, tRF-5, tRF-3 and internal tRF) based on the place of origin from a tRNA molecule. This revealed that ∼90% of all reads belonged to the tRF-5, while the rest ∼10% was divided between the tRF-3 and the internal tRF. For both clones, the percentage distribution was similar. The marked over-representation of tRF-5 is in agreement with what was reported in *T. vaginalis* exosomes, in which all major tRFs originated from the 5' end of tRNA molecules.[119] Similarly, the 5' end tRFs constituted ∼68% of all tRFs in the whole *T. vaginalis* cells.[118]

Further, we showed that there are three major nt peaks, one for each tRF class. The tRF-5, tRF-3 and internal tRF reads appear to be preferentially processed into 27-29, 19 and 21 nt long fragments, respectively. The 27-29 nt peak is mostly composed of the tRFs coming from tRNA-Gly^{GCC} and tRNA-Glu^{TTC}, and the 21 nt peak is mainly constituted of the tRFs from tRNA-Val^{GAC}. The length of our reads is mostly shorter than what has been reported in *T. vaginalis* cells [118] and in their exosomes [119], in which the tRFs were usually ∼3∼4 nt longer.[118][119] For instance, our sequences of the tRNA-Gly^{GCC} and tRNA-Glu^{TTC} are the same as those reported in the other study of *T. vaginalis* exosomes [119], although they are shorter by 2-3 and 1 nt, respectively. This difference could be explained by different *T. vaginalis* strains used.

tRFs are known to bind AGO proteins similarly to miRNA.[121] miRNA together with AGO and other proteins form the RISC complex, which is able to silence the target genes via various mechanisms. The targets are determined by the miRNA, which can be fully complementary to its target, or the complementarity can be restricted to a small portion of the miRNA called the seed region. The seed region is composed of the nucleotides 2-8 found at the 5' end of the miRNA. The miRNAs usually target the 3' UTRs of the target genes.[137]

Since tRFs have been shown to work in a similar manner to miRNA [116], we analyzed the most abundant tRFs by comparing their seed regions with known miRNAs from the miRbase database to identify whether any of the tRFs had the same seed as an

miRNA with known targets. One tRF from the tRNA-Phe^{AAA} had the same seed as the miR-365 family. Among the targets of this family were, for example, the transcription factor STAT3, the cytokine receptor of IL-7 and the tyrosine kinase SYK.

As a next step, we were looking for other targets of our tRFs by BLASTN analysis against the human transcripts. However, this analysis did not reveal any fully complementary targets. Further, TargetScan and miRanda were used to predict other potential tRF targets. These programs consider mainly the seed complementarity of the tRF with the target genes and various properties of the target genes.[137][154]

This analysis suggested two interesting immune system-related targets. The fragment from tRNA-Phe^{AAA} was predicted to interact with SMAD2. This could be of interest since SMAD2 regulates the generation of Th17 cells.[183] Furthermore, the prediction for tRNA-Val^{GAC} showed that G protein-coupled receptor 35 (GPR35) could be targeted by this fragment. GPR35 is a chemokine receptor, which facilitates the recruitment of neutrophils to inflamed tissues via sensing the serotonin metabolite 5-hydroxyindoleacetic acid.[205] From non-immune targets thioredoxin reductase 3, another predicted target of the tRNA-Val^{GAC} fragment, is worth mentioning due to its role in redox homoeostasis.[184]

Silencing of the identified targets could have a significant effect on the host cells. For instance, silencing of STAT3 could lead to impaired function of Th17 cells, since STAT3 is important for the expression of Th17 lineage-specific transcription factor retinoic acid receptor-related orphan receptors gamma (RORγ).[206] Nevertheless, there are other $\sim$130 potential targets of this specific tRF. Thus, the predictions of the potential targets of all of the tRFs should be taken into consideration for future research.

The miRNA, tRFs and rRNA fragments bound by AGO1 or AGO2 proteins are usually 20-25 nt long.[121] Moreover, only highly abundant RNA molecules can have a significant effect. As the tRNA-Val^{GAC} tRF is the most abundant and 21 nt long, it is the best candidate for further studies to test experimentally its interactions with the predicted targets. Further, it is possible that other tRFs longer than 25 nt, like the tRNA-Gly^{GCC} and tRNA-Glu^{TTC}, bind AGO3 and 4 and function in an miRNA-like manner. Alternatively, they do not bind AGO proteins and act in an AGO-independent manner.[116] Either way, due to their abundance in the *T. vaginalis* small EVs, their role in host-pathogen interactions should be further investigated. Importantly, the amount of tRFs is generally higher in the small EVs of the TVV+ clone, implying that the TVV presence may lead to a stronger regulation effect of the tRFs upon the tRFs delivery via small EVs into the host cells.

9. Conclusion

The main aim of this thesis was to elucidate the effect of dsRNA TVV on the characteristics of the small EVs of *T. vaginalis*. To investigate the TVV effect, we successfully derived the isogenic *T. vaginalis* clone without the viral infection (TVV-) from the clinical isolate TV79-49c1 (TVV+) harboring TVV1, TVV2 and TVV3. To remove the viruses, their RdRps were inhibited using the nucleoside analog 2CMC. [9] This inhibitor is specific for TVV, whereas it has no effect on related dsRNA virus LRV1 in leishmania. However, the modelling of RdRp-inhibitor interaction did not clarify this difference.

The investigations of the small EV effect on tissue culture of HaCaT cells showed that the cells' exposition to the TVV+ small EVs stimulated a proinflammatory response. This was indicated by higher secretion of IL-1β, IL-6, IL-8 and CCL5 when compared to the HaCaT cell stimulation with the EVs isolated from the TVV- clone.

Comparative proteomic analysis of small EVs from the TVV- and TVV+ clones revealed that BspA, RIC2 and several subunits of V-type proton ATPase were all significantly enriched in the TVV+ clone small EVs. In contrast, proteases, exemplified by GP63-like peptidase, were enriched in the TVV- clone. Additionally, screening for homologs related to the human immune system in our EVs, we identified several new potential research targets as, for instance, a homolog of ERAP1 (TVAG_311790).

Analysis of RNA cargo revealed that most of it is composed of rRNA. This rRNA is largely a product of random degradation, but a specific rRNA fragment from 5.8S rRNA was present in our small EVs. Furthermore, specific fragments of tRNA (tRFs) were present in the EV cargo and they mostly originated from the 5' end of tRNA molecules. Importantly, tRFs were significantly enriched in the TVV+ clone.

Using *in silico* approaches (miRanda, TargetScan etc.), we identified potential targets of the tRFs and of the one rRNA fragment. These targets should be considered for further research to elucidate the functions of the RNA fragments found in the *T. vaginalis* small EVs.

Identification of TVV capsid and RdRp proteins together with the virus RNA in the TVV+ small EVs strongly suggested that TVV is present in small EVs. This was directly confirmed by our electron microscopy results.[172] Therefore, it appears that TVV is present in the small EVs of *T. vaginalis* and causes changes to their cargo, which can potentially exacerbate trichomoniasis. Our results also brought further questions:

1. Are the distinct susceptibilities to 2CMC and 2CMA between LRV and TVV caused by differences in their RdRps or by differences upstream from the RdRps in the parasite's purine salvage system?

2. Do the cytokines induced by TVV in small EVs cause disease exacerbation *in vivo*?

3. Does the BspA enrichment improve adherence of the TVV+ clone?
4. What is the role of RIC2 in small EVs?
5. What is the role of the V-type proton ATPase in small EVs in relation to TVV infection of *T. vaginalis*?
6. Is TVAG_311790 a real homolog of ERAP1, and if so, what is its role in releasing sTNF-RI?
7. What is the function of tRFs in the small EVs of *T. vaginalis*?
8. What is the role of the single rRNA fragment?

References

1. ROWLEY, Jane et al. Chlamydia, gonorrhoea, trichomoniasis and syphilis: global prevalence and incidence estimates, 2016. *Bulletin of the World Health Organization*. 2019, vol. 97. Available from DOI: http://dx.doi.org/10.2471/BLT.18.228486.
2. *MERCER, Frances et al. Trichomonas vaginalis: pathogenesis, symbiont interactions, and host cell immune responses. *Trends in parasitology*. 2018, vol. 34. Available from DOI: https://doi.org/10.1016/j.pt.2018.05.006.
3. *LEITSCH, David et al. Recent advances in the molecular biology of the protist parasite Trichomonas vaginalis. *Faculty Reviews*. 2021, vol. 10. Available from DOI: https://doi.org/10.12703/r/10-26.
4. *GRAVES, K. J. et al. Trichomonas vaginalis virus: a review of the literature. *International journal of STD & AIDS*. 2019, vol. 30. Available from DOI: https://doi.org/10.1177/0956462418809767.
5. *MIELCZAREK, Ewelina et al. Trichomonas vaginalis: pathogenicity and potential role in human reproductive failure. *Infection*. 2016, vol. 44. Available from DOI: https://doi.org/10.1007/s15010-015-0860-0.
6. LI, Zhongyou et al. Transfer RNA-derived fragments, the underappreciated regulatory small RNAs in microbial pathogenesis. *Frontiers in Microbiology*. 2021, vol. 12. Available from DOI: https://doi.org/10.3389/fmicb.2021.687632.
7. GOVENDER, Yashini et al. The Role of Small Extracellular Vesicles in Viral-Protozoan Symbiosis: Lessons From Trichomonasvirus in an Isogenic Host Parasite Model. *Frontiers in cellular and infection microbiology*. 2020. Available from DOI: https://doi.org/10.3389/fcimb.2020.591172.
8. BUKONG, Terence N. et al. Exosomes from hepatitis C infected patients transmit HCV infection and contain replication competent viral RNA in complex with Ago2-miR122-HSP90. *PLoS pathogens*. 2014, vol. 10. Available from DOI: https://doi.org/10.1371/journal.ppat.1004424.
9. NARAYANASAMY, Ravi Kumar et al. Cytidine nucleoside analog is an effective antiviral drug against Trichomonasvirus. *Journal of Microbiology, Immunology and Infection*. 2021. Available from DOI: https://doi.org/10.1016/j.jmii.2021.08.008.
10. LUSTIG, Gila et al. Trichomonas vaginalis contact-dependent cytolysis of epithelial cells. *Infection and immunity*. 2013, vol. 81. Available from DOI: https://doi.org/10.1128/IAI.01244-12.
11. JEHEE, Ivo et al. Direct detection of Trichomonas vaginalis virus in Trichomonas vaginalis positive clinical samples from the Netherlands. *Journal of virological methods*. 2017, vol. 250. Available from DOI: https://doi.org/10.1016/j.jviromet.2017.09.007.
12. FRAGA, Jorge et al. Double-stranded RNA viral infection of Trichomonas vaginalis and association with clinical presentation. *Acta protozoologica*. 2007, vol. 46.
13. EL-GAYAR, Eman K. et al. Molecular characterization of double-stranded RNA virus in Trichomonas vaginalis Egyptian isolates and its association with pathogenicity. *Parasitology research*. 2016, vol. 115. Available from DOI: https://doi.org/10.1007/s00436-016-5174-3.
14. GRAVES, Keonte J. et al. A systematic review of the literature on mechanisms of 5-nitroimidazole resistance in Trichomonas vaginalis. *Parasitology*. 2020, vol. 147. Available from DOI: 10.1017/S0031182020001237.
15. HIRT, Robert P. Trichomonas vaginalis virulence factors: an integrative overview. *Sexually transmitted infections*. 2013, vol. 89. Available from DOI: http://dx.doi.org/10.1136/sextrans-2013-051105.
16. KUSDIAN, Gary et al. The actin-based machinery of T richomonas vaginalis mediates flagellate-amoeboid transition and migration across host tissue. *Cellular microbiology*. 2013, vol. 15. Available from DOI: https://doi.org/10.1111/cmi.12144.
17. NIEVAS, Yesica R. et al. Protein palmitoylation plays an important role in Trichomonas vaginalis adherence. *Molecular & Cellular Proteomics*. 2018, vol. 17. Available from DOI: https://doi.org/10.1074/mcp.RA117.000018.
18. BERI, Divya et al. Demonstration and characterization of cyst-like structures in the life cycle of Trichomonas vaginalis. *Frontiers in cellular and infection microbiology*. 2020. Available from DOI: https://doi.org/10.3389/fcimb.2019.00430.
19. DIAS-LOPES, Geovane et al. Morphologic study of the effect of iron on pseudocyst formation in Trichomonas vaginalis and its interaction with human epithelial cells. *Memórias do Instituto Oswaldo Cruz*. 2017, vol. 112. Available from DOI: https://doi.org/10.1590/0074-02760170032.
20. BROTMAN, Rebecca M. et al. Association between Trichomonas vaginalis and vaginal bacterial community composition among reproductive-age women. *Sexually transmitted diseases*. 2012, vol. 39. Available from DOI: https://doi.org/10.1097/OLQ.0b013e3182631c79.
21. RENDÓN-MALDONADO, José G. et al.o. Trichomonas vaginalis: in vitro phagocytosis of lactobacilli, vaginal epithelial cells, leukocytes, and erythrocytes. *Experimental parasitology*. 1998, vol. 89. Available from DOI: https://doi.org/10.1006/expr.1998.4297.
22. FICHOROVA, Raina N. et al. The villain team-up or how Trichomonas vaginalis and bacterial vaginosis alter innate immunity in concert. *Sexually transmitted infections*. 2013, vol. 89. Available from DOI: http://dx.doi.org/10.1136/sextrans-2013-051052.
23. PHUKAN, Niha et al. A cell surface aggregation-promoting factor from Lactobacillus gasseri contributes to inhibition of Trichomonas vaginalis adhesion to human vaginal ectocervical cells. *Infection and Immunity*. 2018, vol. 86. Available from DOI: https://doi.org/10.1128/IAI.00907-17.
24. HINDERFELD, Annabel S. et al. Cooperative interactions between Trichomonas vaginalis and associated bacteria enhance paracellular permeability of the cervicovaginal epithelium by dys-

regulating tight junctions. *Infection and immunity*. 2019, vol. 87. Available from DOI: https://doi.org/10.1128/IAI.00141-19.
25. HINDERFELD, Annabel S. et al. Vaginal dysbiotic bacteria act as pathobionts of the protozoal pathogen Trichomonas vaginalis. *Microbial pathogenesis*. 2020, vol. 138. Available from DOI: https://doi.org/10.1016/j.micpath.2019.103820.
26. JARRETT, Olamide D. et al. T. vaginalis Infection Is Associated with Increased IL-8 and TNFr1 Levels but with the Absence of CD38 and HLADR Activation in the Cervix of ESN. *PLOS one*. 2015, vol. 10. Available from DOI: https://doi.org/10.1371/journal.pone.0130146.
27. MERCER, Frances et al. Neutrophils kill the parasite Trichomonas vaginalis using trogocytosis. *PLoS biology*. 2018, vol. 16. Available from DOI: https://doi.org/10.1371/journal.pbio.2003885.
28. GAO, Yuhang et al. Trichomonas vaginalis induces extracellular trap release in mouse neutrophils in vitro. *Acta Biochimica et Biophysica Sinica*. 2021, vol. 53. Available from DOI: https://doi.org/10.1093/abbs/gmab139.
29. MAKINDE, Hadijat Moradekeet et al. IL-22 levels are associated with Trichomonas vaginalis infection in the lower genital tract. *American journal of reproductive immunology*. 2013, vol. 70. Available from DOI: https://doi.org/10.1111/aji.12100.
30. MASSON, Lindi et al. Relationship between female genital tract infections, mucosal interleukin-17 production and local T helper type 17 cells. *Immunology*. 2015, vol. 146. Available from DOI: https://doi.org/10.1111/imm.12527.
31. MALLA, N. et al. Kinetics of serum and local cytokine profile in experimental intravaginal trichomoniasis induced with Trichomonas vaginalis isolates from symptomatic and asymptomatic women. 2007, vol. 29. Available from DOI: https://doi.org/10.1111/j.1365-3024.2006.00914.x.
32. FICHOROVA, Raina N. et al. Endobiont viruses sensed by the human host–beyond conventional antiparasitic therapy. *PloS one*. 2012, vol. 7. Available from DOI: https://doi.org/10.1371/journal.pone.0048418.
33. LI, Ling et al. Trichomonas vaginalis induces production of proinflammatory cytokines in mouse macrophages through activation of MAPK and NF-κB pathways partially mediated by TLR2. *Frontiers in Microbiology*. 2018, vol. 9. Available from DOI: https://doi.org/10.3389/fmicb.2018.00712.
34. FICHOROVA, Raina N. et al. Trichomonas vaginalis lipophosphoglycan exploits binding to galectin-1 and-3 to modulate epithelial immunity. *Journal of Biological Chemistry*. 2016, vol. 291. Available from DOI: https://doi.org/10.1074/jbc.M115.651497.
35. FIORI, Pier Luigi et al. Association of Trichomonas vaginalis with its symbiont Mycoplasma hominis synergistically upregulates the in vitro proinflammatory response of human monocytes. *Sexually transmitted infections*. 2013, vol. 89. Available from DOI: https://doi.org/10.1136/sextrans-2012-051006.
36. HAN, I.H. et al. Signalling pathways associated with IL-6 production and epithelial–mesenchymal transition induction in prostate epithelial cells stimulated with Trichomonas vaginalis. *Parasite immunology*. 2016, vol. 38. Available from DOI: https://doi.org/10.1111/pim.12357.
37. MERCER, Frances et al. Leukocyte lysis and cytokine induction by the human sexually transmitted parasite Trichomonas vaginalis. *PLoS Neglected Tropical Diseases*. 2016, vol. 10. Available from DOI: https://doi.org/10.1371/journal.pntd.0004913.
38. RIESTRA, Angelica Montenegro et al. Trichomonas vaginalis induces NLRP3 inflammasome activation and pyroptotic cell death in human macrophages. *Journal of innate immunity*. 2019, vol. 11. Available from DOI: https://doi.org/10.1159/000493585.
39. TER KUILE, B. H. et al. Maltose utilization by extracellular hydrolysis followed by glucose transport in Trichomonas vaginalis. *Parasitology*. 1995, vol. 110. Available from DOI: https://doi.org/10.1017/S0031182000081026.
40. RIESTRA, Angelica M. et al. A Trichomonas vaginalis rhomboid protease and its substrate modulate parasite attachment and cytolysis of host cells. *PLoS pathogens*. 2015, vol. 11. Available from DOI: https://doi.org/10.1371/journal.ppat.1005294.
41. ŠTÁFKOVÁ, Jitka et al. Dynamic secretome of Trichomonas vaginalis: Case study of β-amylases. *Molecular & Cellular Proteomics*. 2018, vol. 17. Available from DOI: https://doi.org/10.1074/mcp.RA117.000434.
42. TWU, Olivia et al. Trichomonas vaginalis exosomes deliver cargo to host cells and mediate host parasite interactions. *PLoS pathogens*. 2013, vol. 9. Available from DOI: https://doi.org/10.1371/journal.ppat.1003482.
43. SONG, Hyun-Ouk et al. Trichomonas vaginalis: reactive oxygen species mediates caspase-3 dependent apoptosis of human neutrophils. *Experimental parasitology*. 2008, vol. 118. Available from DOI: https://doi.org/10.1016/j.exppara.2007.06.010.
44. GAO, Fei Fei et al. Trichomonas vaginalis induces apoptosis via ROS and ER stress response through ER–mitochondria crosstalk in SiHa cells. *Parasites & vectors*. 2021, vol. 14. Available from DOI: https://doi.org/10.1186/s13071-021-05098-2.
45. GOULD, Sven B. Deep sequencing of Trichomonas vaginalis during the early infection of vaginal epithelial cells and amoeboid transition. *International journal for parasitology*. 2013, vol. 43. Available from DOI: https://doi.org/10.1016/j.ijpara.2013.04.002.
46. HANDRICH, Maria R. et al. Characterization of the BspA and Pmp protein family of trichomonads. *Parasites & vectors*. 2019, vol. 12. Available from DOI: https://doi.org/10.1186/s13071-019-3660-z.
47. MIGUEL ET AL., de. Proteome analysis of the surface of Trichomonas vaginalis reveals novel proteins and strain-dependent differential expression. *Molecular & Cellular Proteomics*. 2010, vol. 9. Available from DOI: https://doi.org/10.1074/mcp.M000022-MCP201.

48. NIEVAS, Yesica R. aet al. Membrane-shed vesicles from the parasite Trichomonas vaginalis: characterization and their association with cell interaction. *Cellular and Molecular Life Sciences*. 2018, vol. 75. Available from DOI: https://doi.org/10.1007/s00018-017-2726-3.
49. NOËL, Christophe J. et al. Trichomonas vaginalis vast BspA-like gene family: evidence for functional diversity from structural organisation and transcriptomics. *BMC genomics*. 2010, vol. 11. Available from DOI: https://doi.org/10.1186/1471-2164-11-99.
50. CHEN, Yi-Pei; RIESTRA, Angelica M; RAI, Anand Kumar; JOHNSON, Patricia J. A novel cadherin-like protein mediates adherence to and killing of host cells by the parasite Trichomonas vaginalis. *MBio*. 2019, vol. 10. Available from DOI: https://doi.org/10.1128/mBio.00720-19.
51. MIRANDA-OZUNA, Jesús F. T. et al. The glycolytic enzyme triosephosphate isomerase of Trichomonas vaginalis is a surface-associated protein induced by glucose that functions as a laminin-and fibronectin-binding protein. *Infection and Immunity*. 2016, vol. 84. Available from DOI: https://doi.org/10.1128/IAI.00538-16.
52. MOLGORA, Brenda M. et al. A novel Trichomonas vaginalis surface protein modulates parasite attachment via protein: Host cell proteoglycan interaction. *MBio*. 2021, vol. 12. Available from DOI: https://doi.org/10.1128/mBio.03374-20.
53. HIRT, Robert P. et al. Trichomonas vaginalis pathobiology: new insights from the genome sequence. *Advances in parasitology*. 2011, vol. 77. Available from DOI: https://doi.org/10.1016/B978-0-12-391429-3.00006-X.
54. RENDÓN-GANDARILLA, Francisco Javier et al. The TvLEGU-1, a legumain-like cysteine proteinase, plays a key role in Trichomonas vaginalis cytoadherence. *BioMed Research International*. 2013, vol. 2013. Available from DOI: https://doi.org/10.1155/2013/561979.
55. PUENTE-RIVERA, Jonathan et al. The 50 kDa metalloproteinase TvMP50 is a zinc-mediated Trichomonas vaginalis virulence factor. *Molecular and biochemical parasitology*. 2017, vol. 217. Available from DOI: https://doi.org/10.1016/j.molbiopara.2017.09.001.
56. SOMMER, Ulf et al. Identification of Trichomonas vaginalis cysteine proteases that induce apoptosis in human vaginal epithelial cells. *Journal of Biological Chemistry*. 2005, vol. 280. Available from DOI: https://doi.org/10.1074/jbc.M501752200.
57. ZIMMANN, Nadine et al. Proteomic Analysis of Trichomonas vaginalis Phagolysosome, Lysosomal Targeting, and Unconventional Secretion of Cysteine Peptidases. *Molecular & Cellular Proteomics*. 2022, vol. 21. Available from DOI: https://doi.org/10.1016/j.mcpro.2021.100174.
58. MA, Lina et al. Involvement of the GP63 protease in infection of Trichomonas vaginalis. *Parasitology research*. 2011, vol. 109. Available from DOI: https://doi.org/10.1007/s00436-010-2222-2.
59. ÁNGELES RAMÓN-LUING, Lucero et al. de los. Identification and characterization of the immunogenic cytotoxic TvCP39 proteinase gene of Trichomonas vaginalis. *The International Journal of Biochemistry & Cell Biology*. 2011, vol. 43. Available from DOI: https://doi.org/10.1016/j.biocel.2011.07.001.
60. DIAZ, Nicia; AL., et. Production and functional characterization of a recombinant predicted pore-forming protein (TVSAPLIP12) of Trichomonas vaginalis in Nicotiana benthamiana Plants. *Frontiers in Cellular and Infection Microbiology*. 2020. Available from DOI: https://doi.org/10.3389/fcimb.2020.581066.
61. PROVENZANO, Daniele et al. Analysis of human immunoglobulin-degrading cysteine proteinases of Trichomonas vaginalis. *Infection and Immunity*. 1995, vol. 63. Available from DOI: https://doi.org/10.1128/iai.63.9.3388-3395.1995.
62. ALDERETE, John F. et al. Iron mediates Trichomonas vaginalis resistance to complement lysis. *Microbial pathogenesis*. 1995, vol. 19. Available from DOI: https://doi.org/10.1006/mpat.1995.0049.
63. IBÁÑEZ-ESCRIBANO, Alexandra et al. Sequestration of host-CD59 as potential immune evasion strategy of Trichomonas vaginalis. *Acta tropica*. 2015, vol. 149. Available from DOI: https://doi.org/10.1016/j.actatropica.2015.05.003.
64. SONG, Min-Ji et al. Modulation of dendritic cell function by Trichomonas vaginalis-derived secretory products. *BMB reports*. 2015, vol. 48. Available from DOI: 10.5483/BMBRep.2015.48.2.116.
65. LEE, Hye-Yeon et al. Trichomonas vaginalis α-actinin 2 modulates host immune responses by inducing tolerogenic dendritic cells via IL-10 production from regulatory T cells. *The Korean Journal of Parasitology*. 2017, vol. 55. Available from DOI: 10.3347/kjp.2017.55.4.375.
66. HAN, Ik-Hwan et al. IL-6 produced by prostate epithelial cells stimulated with Trichomonas vaginalis promotes proliferation of prostate cancer cells by inducing M2 polarization of THP-1-derived macrophages. 2020, vol. 14. Available from DOI: https://doi.org/10.1371/journal.pntd.0008126.
67. NAM, Young Hee et al. Leukotriene B4 receptors BLT1 and BLT2 are involved in interleukin-8 production in human neutrophils induced by Trichomonas vaginalis-derived secretory products. *Inflammation Research*. 2012, vol. 61. Available from DOI: https://doi.org/10.1007/s00011-011-0425-3.
68. TWU, Olivia et al. Trichomonas vaginalis homolog of macrophage migration inhibitory factor induces prostate cell growth, invasiveness, and inflammatory responses. *Proceedings of the National Academy of Sciences*. 2014, vol. 111. Available from DOI: 10.1073/pnas.1321884111.
69. CHEN, Yi-Pei et al. Trichomonas vaginalis macrophage migration inhibitory factor mediates parasite survival during nutrient stress. *Mbio*. 2018, vol. 9. Available from DOI: 10.1128/mBio.00910-18.
70. MANNY, Austin Reidet al. Discovery of a new species of trichomonasvirus in the human parasite Trichomonas vaginalis using transcriptome mining. *bioRxiv*. 2021. Available from DOI: https://doi.org/10.1101/2021.12.09.471948.

71. WANG, Alice L. el at. A linear double-stranded RNA in Trichomonas vaginalis. *Journal of Biological Chemistry*. 1985, vol. 260. Available from DOI: https://doi.org/10.1016/S0021-9258(19)83679-7.
72. BAHADORY, Saeed et al. A systematic review and meta-analysis on the global status of Trichomonas vaginalis virus in Trichomonas vaginalis. *Microbial Pathogenesis*. 2021, vol. 158. Available from DOI: https://doi.org/10.1016/j.micpath.2021.105058.
73. KHOSHNAN, Ali et al. Trichomonas vaginalis with a double-stranded RNA virus has upregulated levels of phenotypically variable immunogen mRNA. *Journal of virology*. 1994, vol. 68. Available from DOI: https://doi.org/10.1128/jvi.68.6.4035-4038.1994.
74. SNIPES, Lauren J. et al. Molecular epidemiology of metronidazole resistance in a population of Trichomonas vaginalis clinical isolates. *Journal of Clinical Microbiology*. 2000, vol. 38. Available from DOI: https://doi.org/10.1128/JCM.38.8.3004-3009.2000.
75. MALLA, N. et al. The presence of dsRNA virus in Trichomonas vaginalis isolates from symptomatic and asymptomatic Indian women and its correlation with in vitro metronidazole sensitivity. *Indian journal of medical microbiology*. 2011, vol. 29. Available from DOI: https://doi.org/10.4103/0255-0857.81801.
76. GOODMAN, Russell P. et al. Clinical isolates of Trichomonas vaginalis concurrently infected by strains of up to four Trichomonasvirus species (Family Totiviridae). *Journal of virology*. 2011, vol. 85. Available from DOI: https://doi.org/10.1128/JVI.00220-11.
77. BESSARAB, Irina N. et al. Identification and characterization of a type III Trichomonas vaginalis virus in the protozoan pathogen Trichomonas vaginalis. *Archives of virology*. 2011, vol. 156. Available from DOI: 10.1007/s00705-010-0858-y.
78. *VENKATARAMAN, Sangita et al. RNA dependent RNA polymerases: insights from structure, function and evolution. *Viruses*. 2018, vol. 10. Available from DOI: https://doi.org/10.3390/v10020076.
79. DULIN, David et al. Signatures of nucleotide analog incorporation by an RNA-dependent RNA polymerase revealed using high-throughput magnetic tweezers. *Cell reports*. 2017, vol. 21. Available from DOI: https://doi.org/10.1016/j.celrep.2017.10.005.
80. KUHLMANN, F. Matthew et al. Antiviral screening identifies adenosine analogs targeting the endogenous dsRNA Leishmania RNA virus 1 (LRV1) pathogenicity factor. *Proceedings of the National Academy of Sciences*. 2017, vol. 114. Available from DOI: https://doi.org/10.1073/pnas.1619114114.
81. HEIDARY, S. et al. Double-stranded RNA viral infection in Tehran Trichomonas vaginalis isolates. *Iranian Journal of Parasitology*. 2013, vol. 8.
82. ERTABAKLAR, Hatice et al. Microsatellite-Based Genotyping, Analysis of Population Structure, Presence of Trichomonas vaginalis Virus (TVV) and Mycoplasma hominis in T. vaginalis Isolates from Southwest of Turkey. *Iranian Journal of Parasitology*. 2021, vol. 16. Available from DOI: https://doi.org/10.18502/ijpa.v16i1.5515.
83. RIVERA, Windell L. et al. Detection and molecular characterization of double-stranded RNA viruses in Philippine Trichomonas vaginalis isolates. *Journal of microbiology, immunology and infection*. 2017, vol. 50. Available from DOI: https://doi.org/10.1016/j.jmii.2015.07.016.
84. LEZEAU, L. et al. The prevalence of Trichomonas vaginalis virus (TVV) in globally distributed Trichomonas vaginalis isolates. 2011, vol. 87. Available from DOI: http://dx.doi.org/10.1136/sextrans-2011-050108.524.
85. FRAGA, Jorge et al. Double-stranded RNA viral infection of Trichomonas vaginalis and correlation with genetic polymorphism of isolates. *Experimental parasitology*. 2011, vol. 127. Available from DOI: https://doi.org/10.1016/j.exppara.2010.09.005.
86. MARGARITA, Valentina et al. Prevalence of double-stranded RNA virus in Trichomonas vaginalis isolated in Italy and association with the symbiont Mycoplasma hominis. *Parasitology Research*. 2019, vol. 118. Available from DOI: https://doi.org/10.1007/s00436-019-06469-6.
87. MASHA, Simon C. et al. Molecular typing of Trichomonas vaginalis isolates by actin gene sequence analysis and carriage of T. vaginalis viruses. *Parasites & vectors*. 2017, vol. 10. Available from DOI: https://doi.org/10.1186/s13071-017-2496-7.
88. FRAGA, Jorge et al. Species typing of Cuban Trichomonas vaginalis virus by RT-PCR, and association of TVV-2 with high parasite adhesion levels and high pathogenicity in patients. *Archives of virology*. 2012, vol. 157. Available from DOI: https://doi.org/10.1007/s00705-012-1353-4.
89. GRAVES, Keonte J. et al. Trichomonas vaginalis virus among women with trichomoniasis and associations with demographics, clinical outcomes, and metronidazole resistance. *Clinical Infectious Diseases*. 2019, vol. 69. Available from DOI: https://doi.org/10.1093/cid/ciz146.
90. LUZ BECKER, et al. da. High rates of double-stranded RNA viruses and Mycoplasma hominis in Trichomonas vaginalis clinical isolates in South Brazil. *Infection, Genetics and Evolution*. 2015, vol. 34. Available from DOI: https://doi.org/10.1016/j.meegid.2015.07.005.
91. AL., Bokharaei-Salim et. The First Detection of Co-Infection of Double-Stranded RNA Virus 1, 2 and 3 in Iranian Isolates of Trichomonas vaginalis. *Iranian Journal of Parasitology*. 2020, vol. 15. Available from DOI: https://doi.org/10.18502/ijpa.v15i3.4200.
92. *MEADE, John C. Genetic diversity in Trichomonas vaginalis. *Sexually transmitted infections*. 2013, vol. 89. Available from DOI: http://dx.doi.org/10.1136/sextrans-2013-051098.
93. PROVENZANO, D. et al. Involvement of dsRNA virus in the protein compositionand growth kinetics of host Trichomonas vaginalis. *Archives of virology*. 1997, vol. 142. Available from DOI: https://doi.org/10.1007/s007050050130.
94. HE, Ding et al. Differential protein expressions in virus-infected and uninfected Trichomonas vaginalis. *The Korean Journal of Parasitology*. 2017, vol. 55. Available from DOI: 10.3347/kjp.2017.55.2.121.
95. IVES, Annette et al. Leishmania RNA virus controls the severity of mucocutaneous leishmaniasis. *Science*. 2011, vol. 331. Available from DOI: https://doi.org/10.1126/science.1199326.

96. ATAYDE, Vanessa Diniz et al. Exploitation of the Leishmania exosomal pathway by Leishmania RNA virus 1. *Nature Microbiology*. 2019, vol. 4. Available from DOI: https://doi.org/10.1038/s41564-018-0352-y.
97. CARVALHO, Renan V. H. et al. de. Leishmania RNA virus exacerbates Leishmaniasis by subverting innate immunity via TLR3-mediated NLRP3 inflammasome inhibition. *Nature communications*. 2019, vol. 10. Available from DOI: https://doi.org/10.1038/s41467-019-13356-2.
98. *MATHIEU, Mathilde et al. Specificities of secretion and uptake of exosomes and other extracellular vesicles for cell-to-cell communication. *Nature cell biology*. 2019, vol. 21. Available from DOI: https://doi.org/10.1038/s41556-018-0250-9.
99. ZHANG, Haiying et al. Identification of distinct nanoparticles and subsets of extracellular vesicles by asymmetric flow field-flow fractionation. *Nature cell biology*. 2018, vol. 20. Available from DOI: https://doi.org/10.1038/s41556-018-0040-4.
100. *SABATKE, Bruna et al. Unveiling the role of EVs in anaerobic parasitic protozoa. *Molecular Immunology*. 2021. Available from DOI: https://doi.org/10.1016/j.molimm.2021.02.007.
101. SALAS, Nehuén et al. VPS32, a member of the ESCRT complex, modulates adherence to host cells in the parasite Trichomonas vaginalis by affecting biogenesis and cargo sorting of released extracellular vesicles. *Cellular and Molecular Life Sciences*. 2022, vol. 79. Available from DOI: https://doi.org/10.1007/s00018-021-04083-3.
102. LAMBERTZ, Ulrike et al. Small RNAs derived from tRNAs and rRNAs are highly enriched in exosomes from both old and new world Leishmania providing evidence for conserved exosomal RNA Packaging. *BMC genomics*. 2015, vol. 16. Available from DOI: https://doi.org/10.1186/s12864-015-1260-7.
103. SHARMA, Manu et al. Characterization of extracellular vesicles from Entamoeba histolytica identifies roles in intercellular communication that regulates parasite growth and development. *Infection and immunity*. 2020, vol. 88. Available from DOI: https://doi.org/10.1128/IAI.00349-20.
104. EVANS-OSSES, Ingrid et al. Microvesicles released from Giardia intestinalis disturb host-pathogen response in vitro. *European journal of cell biology*. 2017, vol. 96. Available from DOI: https://doi.org/10.1016/j.ejcb.2017.01.005.
105. *JUAN, Thomas aet al. Biogenesis and function of ESCRT-dependent extracellular vesicles. In: *Seminars in cell & developmental biology*. 2018, vol. 74. Available from DOI: https://doi.org/10.1016/j.semcdb.2017.08.022.
106. MOYANO, Sofia et al. Exosome biogenesis in the protozoa parasite Giardia lamblia: a model of reduced interorganellar crosstalk. *Cells*. 2019, vol. 8. Available from DOI: https://doi.org/10.3390/cells8121600.
107. GAVINHO, Bruno; AL., et. Peptidylarginine deiminase inhibition abolishes the production of large extracellular vesicles from Giardia intestinalis, affecting host-pathogen interactions by hindering adhesion to host cells. *Frontiers in cellular and infection microbiology*. 2020, vol. 10. Available from DOI: https://doi.org/10.3389/fcimb.2020.00417.
108. SZEMPRUCH, Anthony J. et al. Extracellular vesicles from Trypanosoma brucei mediate virulence factor transfer and cause host anemia. *Cell*. [N.d.], vol. 164. Available from DOI: https://doi.org/10.1016/j.cell.2015.11.051.
109. ELIAZ, Dror et al. Exosome secretion affects social motility in Trypanosoma brucei. *PLoS pathogens*. 2017, vol. 13. Available from DOI: https://doi.org/10.1371/journal.ppat.1006245.
110. GARCIA-SILVA, Maria R.et al. Gene expression changes induced by Trypanosoma cruzi shed microvesicles in mammalian host cells: relevance of tRNA-derived halves. *BioMed research international*. 2014, vol. 2014. Available from DOI: https://doi.org/10.1155/2014/305239.
111. AL., Garcia-Silva et. Extracellular vesicles shed by Trypanosoma cruzi are linked to small RNA pathways, life cycle regulation, and susceptibility to infection of mammalian cells. *Parasitology research*. 2014, vol. 113. Available from DOI: https://doi.org/10.1007/s00436-013-3655-1.
112. ZHAO, Panpan et al. Extracellular vesicles secreted by Giardia duodenalis regulate host cell innate immunity via TLR2 and NLRP3 inflammasome signaling pathways. *PLoS neglected tropical diseases*. 2021, vol. 15. Available from DOI: https://doi.org/10.1371/journal.pntd.0009304.
113. RAI, Anand Kumaret et al. Trichomonas vaginalis extracellular vesicles are internalized by host cells using proteoglycans and caveolin-dependent endocytosis. *Proceedings of the National Academy of Sciences*. 2019, vol. 116. Available from DOI: https://doi.org/10.1073/pnas.1912356116.
114. LIN, Wei-Chen et al. Quantitative proteomic analysis and functional characterization of Acanthamoeba castellanii exosome-like vesicles. *Parasites & vectors*. 2019, vol. 12. Available from DOI: https://doi.org/10.1186/s13071-019-3725-z.
115. WOWK, Pryscilla Fanini et al. Proteomic profiling of extracellular vesicles secreted from Toxoplasma gondii. *Proteomics*. 2017, vol. 17. Available from DOI: https://doi.org/10.1002/pmic.201600477.
116. *DOU, Shengqian et al. Metazoan tsRNAs: biogenesis, evolution and regulatory functions. *Non-coding RNA*. 2019, vol. 5. Available from DOI: https://doi.org/10.3390/ncrna5010018.
117. HUANG, Po-Jung et al. Identification of putative miRNAs from the deep-branching unicellular flagellates. *Genomics*. 2012, vol. 99. Available from DOI: https://doi.org/10.1016/j.ygeno.2011.11.002.
118. WANG, Zhen-Sheng et al. Global survey of miRNAs and tRNA-derived small RNAs from the human parasitic protist Trichomonas vaginalis. *Parasites & vectors*. 2021, vol. 14. Available from DOI: https://doi.org/10.1186/s13071-020-04570-9.
119. ARTUYANTS, Anastasiia et al. Extracellular vesicles produced by the protozoan parasite Trichomonas vaginalis contain a preferential cargo of tRNA-derived small RNAs. *International Journal for Parasitology*. 2020, vol. 50. Available from DOI: https://doi.org/10.1016/j.ijpara.2020.07.003.

120. GARCIA-SILVA, Maria Rosa et al. A particular set of small non-coding RNAs is bound to the distinctive Argonaute protein of Trypanosoma cruzi: insights from RNA-interference deficient organisms. *Gene*. 2014, vol. 538. Available from DOI: https://doi.org/10.1016/j.gene.2014.01.023.
121. GUAN, Lingyu et al. Computational meta-analysis of ribosomal RNA fragments: potential targets and interaction mechanisms. *Nucleic acids research*. 2021, vol. 49. Available from DOI: https://doi.org/10.1093/nar/gkab190.
122. *PENG, Ruofan et al. Transfer RNA-Derived Small RNAs in the Pathogenesis of Parasitic Protozoa. *Genes*. 2022, vol. 13. Available from DOI: https://doi.org/10.3390/genes13020286.
123. WARRING, Sally D. et al. Small RNAs Are Implicated in Regulation of Gene and Transposable Element Expression in the Protist Trichomonas vaginalis. *Msphere*. 2021, vol. 6. Available from DOI: https://doi.org/10.1128/mSphere.01061-20.
124. *SOHEL, Mahmodul Hasan. Extracellular/circulating microRNAs: release mechanisms, functions and challenges. *Achievements in the Life Sciences*. 2016, vol. 10, no. 2. Available from DOI: https://doi.org/10.1016/j.als.2016.11.007.
125. *ABELS, Erik R. et al. Introduction to extracellular vesicles: biogenesis, RNA cargo selection, content, release, and uptake. *Cellular and molecular neurobiology*. 2016, vol. 36. Available from DOI: https://doi.org/10.1007/s10571-016-0366-z.
126. NEVES, Roberta F. C. et al. Trypanosoma cruzi-secreted vesicles have acid and alkaline phosphatase activities capable of increasing parasite adhesion and infection. *Parasitology research*. 2014, vol. 113. Available from DOI: https://doi.org/10.1007/s00436-014-3958-x.
127. GHOSH, June et al. Leishmania donovani targets Dicer1 to downregulate miR-122, lower serum cholesterol, and facilitate murine liver infection. *Cell host & microbe*. 2013, vol. 13. Available from DOI: https://doi.org/10.1016/j.chom.2013.02.005.
128. ZHANG, Hongxia et al. sncRNAs packaged by Helicobacter pylori outer membrane vesicles attenuate IL-8 secretion in human cells. *International Journal of Medical Microbiology*. 2020, vol. 310. Available from DOI: https://doi.org/10.1016/j.ijmm.2019.151356.
129. OLMOS-ORTIZ, L. M. et al. Trichomonas vaginalis exosome-like vesicles modify the cytokine profile and reduce inflammation in parasite-infected mice. *Parasite immunology*. 2017, vol. 39. Available from DOI: https://doi.org/10.1111/pim.12426.
130. BHATTACHARYA, Sanchita et al. ImmPort, toward repurposing of open access immunological assay data for translational and clinical research. *Scientific data*. 2018, vol. 5. Available from DOI: https://doi.org/10.1038/sdata.2018.15(2018)..
131. BREUER, Karin et al. InnateDB: systems biology of innate immunity and beyond—recent updates and continuing curation. *Nucleic acids research*. 2013, vol. 41. Available from DOI: https://doi.org/10.1093/nar/gks1147.
132. QUILLET, Aurélien et al. Improving bioinformatics prediction of microRNA targets by ranks aggregation. *Frontiers in Genetics*. 2020, vol. 10. Available from DOI: https://doi.org/10.3389/fgene.2019.01330.
133. KOZOMARA, Ana et al. miRBase: from microRNA sequences to function. *Nucleic acids research*. 2019, vol. 47. Available from DOI: https://doi.org/10.1093/nar/gky1141.
134. SAYERS, Eric W. et al. Database resources of the national center for biotechnology information. *Nucleic acids research*. 2021, vol. 49. Available from DOI: https://doi.org/10.1093/nar/gkaa892.
135. BERMAN, Helen M. et al. The protein data bank. *Nucleic acids research*. 2000, vol. 28. Available from DOI: https://doi.org/10.1093/nar/28.1.235.
136. MISTRY, Jaina et al. Pfam: The protein families database in 2021. *Nucleic acids research*. 2021, vol. 49. Available from DOI: https://doi.org/10.1093/nar/gkaa913.
137. LEWIS, Benjamin P. et al. Conserved seed pairing, often flanked by adenosines, indicates that thousands of human genes are microRNA targets. *cell*. 2005, vol. 120. Available from DOI: https://doi.org/10.1016/j.cell.2004.12.035.
138. AMOS, B. et al. VEuPathDB: the eukaryotic pathogen, vector and host bioinformatics resource center. *NUCLEIC ACIDS RESEARCH*. 2021, vol. 50. Available from DOI: http://dx.doi.org/10.1093/nar/gkab929.
139. UniProt: the universal protein knowledgebase in 2021. *Nucleic acids research*. 2021, vol. 49. Available from DOI: https://doi.org/10.1093/nar/gkaa1100.
140. MIRDITA, Milot et al. Uniclust databases of clustered and deeply annotated protein sequences and alignments. *Nucleic acids research*. 2017, vol. 45. Available from DOI: https://doi.org/10.1093/nar/gkw1081.
141. BUSHNELL, Brian. *BBMap: a fast, accurate, splice-aware aligner*. 2014. Tech. rep. Lawrence Berkeley National Lab.(LBNL), Berkeley, CA (United States).
142. ALTSCHUL, Stephen F. et al. Basic local alignment search tool. *Journal of molecular biology*. 1990, vol. 215. Available from DOI: https://doi.org/10.1016/S0022-2836(05)80360-2.
143. LANGMEAD, Ben et al. Fast gapped-read alignment with Bowtie 2. *Nature methods*. 2012, vol. 9. Available from DOI: https://doi.org/10.1038/nmeth.1923.
144. QUINLAN, Aaron R. et al. BEDTools: a flexible suite of utilities for comparing genomic features. *Bioinformatics*. 2010, vol. 26. Available from DOI: https://doi.org/10.1093/bioinformatics/btq033.
145. MARTIN, Marcel. Cutadapt removes adapter sequences from high-throughput sequencing reads. *EMBnet. journal*. 2011, vol. 17. Available from DOI: https://doi.org/10.14806/ej.17.1.200.
146. CANTALAPIEDRA, Carlos P. et al. eggNOG-mapper v2: functional annotation, orthology assignments, and domain prediction at the metagenomic scale. *Molecular biology and evolution*. 2021, vol. 38. Available from DOI: https://doi.org/10.1093/molbev/msab293.
147. SCHINDELIN, Johannes et al. Fiji: an open-source platform for biological-image analysis. *Nature methods*. 2012, vol. 9. Available from DOI: https://doi.org/10.1038/nmeth.2019.

148. STEINEGGER, Martin et al. HH-suite3 for fast remote homology detection and deep protein annotation. *BMC bioinformatics*. 2019, vol. 20. Available from DOI: https://doi.org/10.1186/s12859-019-3019-7.
149. FINN, Robert D. et al. HMMER web server: interactive sequence similarity searching. *Nucleic acids research*. 2011, vol. 39. Available from DOI: https://doi.org/10.1093/nar/gkr367.
150. FEIG, Michael. Local protein structure refinement via molecular dynamics simulations with locPREFMD. *Journal of chemical information and modeling*. 2016, vol. 56. Available from DOI: https://doi.org/10.1021/acs.jcim.6b00222.
151. KATOH, Kazutaka et al. MAFFT: a novel method for rapid multiple sequence alignment based on fast Fourier transform. *Nucleic acids research*. 2002, vol. 30. Available from DOI: https://doi.org/10.1093/nar/gkf436.
152. COX, Jürgen et al. Accurate proteome-wide label-free quantification by delayed normalization and maximal peptide ratio extraction, termed MaxLFQ. *Molecular & cellular proteomics*. 2014, vol. 13. Available from DOI: https://doi.org/10.1074/mcp.M113.031591.
153. MICROSOFT CORPORATION. *Microsoft Excel*. 2018. 2019 (16.0). Available also from: https://office.microsoft.com/excel.
154. ENRIGHT, Anton et al. MicroRNA targets in Drosophila. *Genome biology*. 2003, vol. 4. Available from DOI: https://doi.org/10.1186/gb-2003-4-11-p8.
155. CHEN, Vincent B. et al. MolProbity: all-atom structure validation for macromolecular crystallography. *Acta Crystallographica Section D: Biological Crystallography*. 2010, vol. 66. Available from DOI: https://doi.org/10.1107/S0907444909042073.
156. KELLEY, Lawrence A. et al. The Phyre2 web portal for protein modeling, prediction and analysis. *Nature protocols*. 2015, vol. 10. Available from DOI: https://doi.org/10.1038/nprot.2015.053.
157. SCHRÖDINGER, LLC; DELANO, Warren. *PyMOL*. 2020. Version 2.4.0. Available also from: http://www.pymol.org/pymol.
158. KRIVÁK, Radoslav et al. P2Rank: machine learning based tool for rapid and accurate prediction of ligand binding sites from protein structure. *Journal of cheminformatics*. 2018, vol. 10. Available from DOI: https://doi.org/10.1186/s13321-018-0285-8.
159. RSTUDIO TEAM. *RStudio: Integrated Development Environment for R*. Boston, MA, 2022. Available also from: http://www.rstudio.com/.
160. AL., David Jimenez-Morales et. *artMS: Analytical R tools for Mass Spectrometry*. 2022. Available also from: http://artms.org.
161. LOVE, Michael I. et al. Moderated estimation of fold change and dispersion for RNA-seq data with DESeq2. *Genome biology*. 2014, vol. 15. Available from DOI: https://doi.org/10.1186/s13059-014-0550-8.
162. AL, Liis Kolberg aet. gprofiler2– an R package for gene list functional enrichment analysis and namespace conversion toolset g:Profiler. *F1000Research*. 2020, vol. 9 (ELIXIR). Available from DOI: https://doi.org/10.12688/f1000research.24956.2.
163. CHOI, Meena et al. MSstats: an R package for statistical analysis of quantitative mass spectrometry-based proteomic experiments. *Bioinformatics*. 2014, vol. 30. Available from DOI: https://doi.org/10.1093/bioinformatics/btu305.
164. LIAO, Yanget al. The R package Rsubread is easier, faster, cheaper and better for alignment and quantification of RNA sequencing reads. *Nucleic acids research*. 2019, vol. 47. Available from DOI: https://doi.org/10.1093/nar/gkz114.
165. CHEN, Hanbo; BOUTROS, Paul C. VennDiagram: a package for the generation of highly-customizable Venn and Euler diagrams in R. *BMC bioinformatics*. 2011, vol. 12. Available from DOI: https://doi.org/10.1186/1471-2105-12-35.
166. LI, Heng et al. The sequence alignment/map format and SAMtools. *Bioinformatics*. 2009, vol. 25. Available from DOI: https://doi.org/10.1093/bioinformatics/btp352.
167. EMANUELSSON, Olof et al. Predicting subcellular localization of proteins based on their N-terminal amino acid sequence. *Journal of molecular biology*. 2000, vol. 300. Available from DOI: https://doi.org/10.1006/jmbi.2000.3903.
168. KROGH, Anders et al. Predicting transmembrane protein topology with a hidden Markov model: application to complete genomes. *Journal of molecular biology*. 2001, vol. 305. Available from DOI: https://doi.org/10.1006/jmbi.2000.4315.
169. LOWE, Todd M. et al. tRNAscan-SE On-line: integrating search and context for analysis of transfer RNA genes. *Nucleic acids research*. 2016, vol. 44. Available from DOI: https://doi.org/10.1093/nar/gkw413.
170. VONKA, V. et al. Increased effects of topically applied interferon on herpes simplex virus-induced lesions by caffeine. *Acta Virologica*. 1995, vol. 39.
171. FLEGR, J. et al. The dsRNA ofTrichomonas vaginalis is associated with virus-like particles and does not correlate with metornidazole resistance. *Folia microbiologica*. 1987, vol. 32. Available from DOI: https://doi.org/10.1007/BF02877224.
172. RADA, Petr et al. Double-Stranded RNA Viruses Are Released From Trichomonas vaginalis Inside Small Extracellular Vesicles and Modulate the Exosomal Cargo. *Frontiers in microbiology*. 2022, vol. 13. Available from DOI: https://doi.org/10.3389/fmicb.2022.893692.
173. DIAMOND, Louis S. The establishment of various trichomonads of animals and man in axenic cultures. *The Journal of parasitology*. 1957, vol. 43. Available from DOI: https://doi.org/10.2307/3274682.
174. AL., Van Kuppeveld et. Detection of mycoplasma contamination in cell cultures by a mycoplasma group-specific PCR. *Applied and environmental microbiology*. 1994, vol. 60.
175. STROBER, Warren. Trypan blue exclusion test of cell viability. *Current protocols in immunology*. 2015, vol. 111. Available from DOI: https://doi.org/10.1002/0471142735.ima03bs111.

176. AL., Perez-Riverolet. The PRIDE database and related tools and resources in 2019: improving support for quantification data. *Nucleic acids research*. 2019, vol. 47. Available from DOI: https://doi.org/10.1093/nar/gky1106.
177. NATTO, Manal J. et al. Comprehensive characterization of purine and pyrimidine transport activities in Trichomonas vaginalis and functional cloning of a trichomonad nucleoside transporter. *Molecular Microbiology*. 2021, vol. 116. Available from DOI: https://doi.org/10.1111/mmi.14840.
178. *JOLLIFFE, Ian T; CADIMA, Jorge. Principal component analysis: a review and recent developments. *Philosophical Transactions of the Royal Society A: Mathematical, Physical and Engineering Sciences*. 2016, vol. 374. Available from DOI: https://doi.org/10.1098/rsta.2015.0202.
179. *HIBBS, Margaret L. et al. Regulation of hematopoietic cell signaling by SHIP-1 inositol phosphatase: growth factors and beyond. *Growth Factors*. 2018, vol. 36. Available from DOI: https://doi.org/10.1080/08977194.2019.1569649.
180. *REEVES, Emma et al. The role of polymorphic ERAP1 in autoinflammatory disease. *Bioscience reports*. 2018, vol. 38. Available from DOI: https://doi.org/10.1042/BSR20171503.
181. NOBRE, Lıgia S. et al. Trichomonas vaginalis repair of iron centres proteins: the different role of two paralogs. *Protist*. 2016, vol. 167. Available from DOI: https://doi.org/10.1016/j.protis.2016.03.001.
182. OLIVEIRA, Arthur C. et al. Combining results from distinct microRNA target prediction tools enhances the performance of analyses. *Frontiers in genetics*. 2017, vol. 8. Available from DOI: https://doi.org/10.3389/fgene.2017.00059.
183. TANAKA, Shinya et al. Trim33 mediates the proinflammatory function of Th17 cells. *Journal of Experimental Medicine*. 2018, vol. 215. Available from DOI: https://doi.org/10.1084/jem.20170779.
184. LIU, Qi et al. Thioredoxin reductase 3 suppression promotes colitis and carcinogenesis via activating pyroptosis and necrosis. *Cellular and Molecular Life Sciences*. 2022, vol. 79. Available from DOI: https://doi.org/10.1007/s00018-022-04155-y.
185. MURAKAMI, Eisuke et al. Mechanism of activation of β-d-2-deoxy-2-fluoro-2-C-methylcytidine and inhibition of hepatitis C virus NS5B RNA polymerase. *Antimicrobial Agents and Chemotherapy*. 2007, vol. 51.
186. HECKER, Scott J. et al. Liver-Targeted Prodrugs of 2 '-C-Methyladenosine for Therapy of Hepatitis C Virus Infection. *Journal of medicinal chemistry*. 2007, vol. 50. Available from DOI: https://doi.org/10.1021/jm0701021.
187. CARROLL, Steven S. et al. Nucleoside analog inhibitors of hepatitis C virus replication. *Infectious Disorders-Drug Targets (Formerly Current Drug Targets-Infectious Disorders)*. 2006, vol. 6. Available from DOI: https://doi.org/10.2174/187152606776056698.
188. *SELISKO, Barbara et al. Structural and functional basis of the fidelity of nucleotide selection by flavivirus RNA-dependent RNA polymerases. *Viruses*. 2018, vol. 10. Available from DOI: https://doi.org/10.3390/v10020059.
189. MUNAGALA, Narsimha Rao et al. Adenosine is the primary precursor of all purine nucleotides in Trichomonas vaginalis. *Molecular and biochemical parasitology*. 2003, vol. 127. Available from DOI: https://doi.org/10.1016/S0166-6851(02)00330-4.
190. *SOKOL, Caroline L. et al. The chemokine system in innate immunity. *Cold Spring Harbor perspectives in biology*. 2015, vol. 7. Available from DOI: 10.1101/cshperspect.a016303.
191. AL., *Velazquez-Salinaset. The role of interleukin 6 during viral infections. *Frontiers in microbiology*. 2019, vol. 10. Available from DOI: https://doi.org/10.3389/fmicb.2019.01057.
192. OLARU, Florina et al. Chemokine expression by human keratinocyte cell lines after activation of Toll-like receptors. *Experimental dermatology*. 2010, vol. 19. Available from DOI: https://doi.org/10.1111/j.1600-0625.2009.01026.x.
193. BOUKAMP, Petra et al. Normal keratinization in a spontaneously immortalized aneuploid human keratinocyte cell line. *The Journal of cell biology*. 1988, vol. 106. Available from DOI: https://doi.org/10.1083/jcb.106.3.761.
194. FICHOROVA, Raina N. et al. Generation of papillomavirus-immortalized cell lines from normal human ectocervical, endocervical, and vaginal epithelium that maintain expression of tissue-specific differentiation proteins. *Biology of reproduction*. 1997, vol. 57. Available from DOI: https://doi.org/10.1095/biolreprod57.4.847.
195. REISER, Jeanette et al. High-risk human papillomaviruses repress constitutive kappa interferon transcription via E6 to prevent pathogen recognition receptor and antiviral-gene expression. *Journal of virology*. 2011, vol. 85. Available from DOI: https://doi.org/10.1128/JVI.05279-11.
196. LIU, H-W; AL., Chuet. Characterization of Trichomonas vaginalis virus proteins in the pathogenic protozoan T. vaginalis. *Archives of virology*. 1998, vol. 143.
197. PLEET, Michelle L. et al. Ebola VP40 in exosomes can cause immune cell dysfunction. *Frontiers in microbiology*. 2016, vol. 7. Available from DOI: https://doi.org/10.3389/fmicb.2016.01765.
198. CHAHAR, Harendra Singh et al. Respiratory syncytial virus infection changes cargo composition of exosome released from airway epithelial cells. *Scientific reports*. 2018, vol. 8. Available from DOI: 10.1038/s41598-017-18672-5.
199. *CANTANHÊDE, Lilian Motta et al. The maze pathway of coevolution: A critical review over the Leishmania and its endosymbiotic history. *Genes*. 2021, vol. 12. Available from DOI: https://doi.org/10.3390/genes12050657.
200. FORREST, David M. et al. Proteomic analysis of exosomes derived from procyclic and metacyclic-like cultured Leishmania infantum chagasi. *Journal of Proteomics*. 2020, vol. 227. Available from DOI: https://doi.org/10.1016/j.jprot.2020.103902.
201. KUGERATSKI, Fernanda G. et al. Quantitative proteomics identifies the core proteome of exosomes with syntenin-1 as the highest abundant protein and a putative universal biomarker.

Nature cell biology. 2021, vol. 23. Available from DOI: https://doi.org/10.1038/s41556-021-00693-y.
202. YUKAWA, Masashi et al. AP-1 activity induced by co-stimulation is required for chromatin opening during T cell activation. *Journal of Experimental Medicine*. 2020, vol. 217. Available from DOI: https://doi.org/10.1084/jem.20182009.
203. *JAN, Arif Tasleem et al. Expedition into exosome biology: A perspective of progress from discovery to therapeutic development. *Cancers*. 2021, vol. 13. Available from DOI: https://doi.org/10.3390/cancers13051157.
204. FERNANDEZ-CALERO, Tamara et al. Profiling of small RNA cargo of extracellular vesicles shed by Trypanosoma cruzi reveals a specific extracellular signature. *Molecular and biochemical parasitology*. 2015, vol. 199. Available from DOI: https://doi.org/10.1016/j.molbiopara.2015.03.003.
205. DE GIOVANNI, Marco et al. GPR35 promotes neutrophil recruitment in response to serotonin metabolite 5-HIAA. *Cell*. 2022, vol. 185. Available from DOI: https://doi.org/10.1016/j.cell.2022.01.010.
206. *HILLMER, Emily J. et al. STAT3 signaling in immunity. *Cytokine & growth factor reviews*. 2016, vol. 31. Available from DOI: 10.1016/j.cytogfr.2016.05.001.

Supplementary data

A flash drive with supplementary data is included in this thesis. It contains:

• Supplementary tables

- **Table_S1_Proteome_DEA_results.xlsx** – Differential expression analysis comparing the identified proteins (annotated) in our small EVs from the TVV- and TVV+ clones; Comparison with publicly available *T. vaginalis* proteomic data sets

- **Table_S2_GO_term_PSEA.xlsx** – Protein set enrichment analysis of identified proteins in the small EVs of the TVV- and TVV+ clones

- **Table_S3_immune_database_hits.xlsx** – The human immune related homologs of *T. vaginalis* proteins found in our small EV proteomic data set

- **Table_S4_RNA_DESeg.xlsx** – Number of mapped and annotated RNA reads; Differential expression analysis comparing the RNA in our small EVs from the TVV- and TVV+ clones

- **Table_S5_tRNA_fragments.xlsx** – Assignment of tRFs to their respective tRNA groups, together with the fragments' sequence

- **Table_S6_RNA_predicted_targets.xlsx** – The *in silico* predicted targets of the RNA fragments found in our small EV data set

- **Table_S7_PCR_primers.xlsx** – PCR primers

• Input files for all of the R script

• R scripts

- **TargetScan_miRanda.R** – Preparation of the inputs for the TargetScan and miRanda; Processing of the TargetScan and miRanda results

- **DEA_proteins.R** – Differential expression analysis of the small EV proteins; Plotting of the volcano plot of the small EV proteins; PCA of the small EV proteins

- **DESeg2.R** – Differential expression analysis of the small EV RNA; PCA of the small EV RNA content

- **DistRNA.R** – Plotting of the RNA distributions

- **Pfam.R** – Extraction of the RdRp domains identified via Pfam

- **Extraction.R** – Extraction of the tRF sequences; The comparison of tRF seeds with the miRBase database

- **ImmuneDB.R** – Combining of the InnateDB and ImmPort databases; Parsing of the hhblits results from the screen against the combined InnateDB and ImmPort databse

- **Parsing.R** – Parsing of the results from PfamScan, hhblits, eggnog mapper, TMHMM and TargetP

- **PSEA.R** – Protein set enrichment analysis of the proteins identified in the TVV+ and TVV- small EVs

- **Position.R** – Retrieving of the genome coordinates of the rRNA and tRNA from the *T. vaginalis* genome

- **RNA_coverage.R** – Plotting of the length distribution graphs, coverage graphs and pie chart showing tRF distribution

- **Venn.R** – Plotting of the Venn diagram comparing the publicly available *T. vaginalis* proteomic data sets